Smartphone-readable barcode assays for quantitative analysis

by

Jessica Xing Hua Wong

B.Sc., Simon Fraser University, 2012

Thesis Submitted in Partial Fulfillment of the
Requirements for the Degree of
Master of Science

in the
Department of Chemistry
Faculty of Science

SIMON FRASER UNIVERSITY

Summer 2016

Approval

Name:	**Jessica Xing Hua Wong**
Degree:	**Master of Science (Chemistry)**
Title:	***Smartphone-readable barcode assays for quantitative analysis***
Examining Committee:	**Chair:** Dr. David Vocadlo Professor

Dr. Hua-Zhong Yu
Senior Supervisor
Professor

Dr. Gary W. Leach
Supervisor
Associate Professor

Dr. Peter J. Unrau
Supervisor
Professor
Department of Molecular Biology and Biochemistry

Dr. Russ Algar
External Examiner
Assistant Professor
Department of Chemistry
University of British Columbia

Date Defended/Approved: July 25, 2016

Abstract

In the literature, there has been a recent surge in smartphone-based bioanalytical techniques, particularly for point-of-care and medical diagnostics. These devices aim to have certain characteristics such as affordability, sensitivity, be user friendly and equipment-free. To add to the growing field, a smartphone-readable, *bona fide* barcode assay is demonstrated; the work performed to develop the app to read colorimetric assays and the design of the barcode assay is discussed. Paper-printed tests and direct biotin-streptavidin assay were used to test the initial app. Barcode reading abilities in the app allowed for the validation of the barcode assay (for the pregnancy hormone, hCG), which proved to be both qualitative and quantitative when scanned and imaged using a smartphone-app combination. No external accessories are required, thereby highlighting its potential to boost the research and development of POC devices, particularly by minimizing the need for specialized instrumentation and providing instant testing results on-site.

Keywords: Smartphone; silver enhancement; scanometry; mobile app, optical darkness ratio; immunoassays.

To my family and friends

Acknowledgements

First and foremost, I would like to express my sincere gratefulness to my senior supervisor, Dr. Hua-Zhong (Hogan) Yu, for the support and guidance throughout the years. Without him, I would have never had this experience; he has bestowed upon me many opportunities that I would have never imagined, from attending conferences, to conducting research both in his lab and overseas. His willingness to help and his constructive suggestions are invaluable. Dr. Yu has shown patience and greater confidence in me than I have for myself and for that, I am truly appreciative.

Secondly, I give thanks to Dr. Gary W. Leach and Dr. Peter. J. Unrau for being my committee members – their advice, suggestions, and useful critiques has helped me greatly in my studies. I would also like to thank Dr. W. Russ Algar for taking the time to serve as the examiner of this thesis.

I would like to offer my special thanks to Dr. Bixia Ge, Dr. Xiaochun Li and Dr. Yunchao Li, for their assistance and support. I give additional thanks to past and present members of the Yu group, notably Clayton Schultz who aided me in obtaining the SEM images. I very much appreciate the friendship, help and encouragement they have given me.

I also acknowledge the Natural Sciences and Engineering Research Council, Mitacs Canada, and Simon Fraser University for their financial assistance.

Lastly, I express my deepest thankfulness to my family, particularly my mother and sister, for their unconditional love and support in all aspects of my life.

Table of Contents

List of Figures

List of Acronyms

AChE	Acetylcholinesterase
AFP	Alpha-fetoprotein
App	Application
ATCh	Acetylthiocholine iodide
B	Blue
BSA	Bovine serum albumin
C	Cyan
CMOS	Complementary metal-oxide semiconductor
DBAE	2-(Dibutylamino)-ethanol
DNA	Deoxyribonucleic acid
dpi	Dots per inch
DTNB	5,5’-dithio-bis-2-nitrobenzoate
EAN	International Article Number
ECL	Electrochemiluminescence
EDC	*N*-(3-dimethylaminopropyl)-*N*′-ethylcarbodiimide hydrochloride
ELISA	Enzyme-linked immunosorbent assay
FAO	Food and Agriculture Organization of the United Nations
FSH	Follicle-stimulating hormone
G	Green
GC	Gas chromatography
hCG	Human chorionic gonadotropin
HE4	Human epididymis protein 4
HIV	Human immunodeficiency virus
HPLC	High performance liquid chromatography
HRP	Horseradish peroxidase
K	Key
LED	Light-emitting diode
M	Magenta
Mab	Monoclonal antibody
MES	2-(*N*-morpholino) ethanesulfonic acid

mIU	Milli-international unit
MS	Mass spectrometry
NHS	N-hydroxysuccinimide
ODR	Optical darkness ratio
OP	Organophosphorus pesticide
PBS	Phosphate-buffered saline
PC	Polycarbonate
PDMS	Polydimethylsiloxane
PEG	Polyethylene glycol
PMMA	Poly(methyl methacrylate)
POC	Point-of-care
R	Red
TB	Tuberculosis
TMB	3,3′,5,5′-Tetramethylbenzidine
TNB	2-Nitro-5-thiobenzoate
TSH	Thyroid-stimulating hormone
uE_3	Unconjugated estriol
UPC	Universal Product Code
UV	Ultraviolet
VIS	Visible
WHO	World Health Organization
Y	Yellow

Chapter 1.

Mobile phones for bioanalytical sciences

The trend in any technologies, whether they are for consumer electronic or scientific purposes, is to move towards making future technologies smaller, faster, cheaper, and more readily available. One such example is the mobile phone, from the first commercially available phone in 1983, with its brick-like structure, to the modern day, flat screen and multi-functional abilities, albeit the latter has bucked the trend of becoming smaller in favor of larger screens and computing capabilities in the form of a smartphone (Figure 1.1). Nonetheless, it is exactly these functions that researchers have tried to exploit in recent years, working to develop mobile phone-based devices or methods that are capable of more than simply making a call; many areas of a phones hardware have been explored, such as the camera, to available ports (audio jack/port and microUSB port), as well as processing abilities as shown through applications (apps).

Figure 1.1. Mobile phones from the 1980s to present.
Note. Adapted from “Mobile phone evolution” By Jojhnjoy (Own work, based on the work of Anders) [Public Domain, https://commons.wikimedia.org/w/index.php?curid=36271517], via Wikimedia Commons.

At the same time, rising healthcare costs around the world have prompted many researchers to seek ways to reduce costs and some have done so by taking advantage of readily available, existing tools. Already owned by the majority of the population in the western world and increasingly in developing nations where healthcare sees the greatest limitations, smartphones have a great potential to be used in medical diagnostics and long term monitoring of patients for diseases and illnesses. In a survey of 40 countries, as expected, it has been reported that western countries such as the United States and Europe have more smartphone users than those in Africa and south eastern Asia (Figure 1.2).[1] However, even in the developing countries, usage rates have increased from 21% in 2013 to 37% in 2015 (global median of 43%), with no signs of decline.[1]

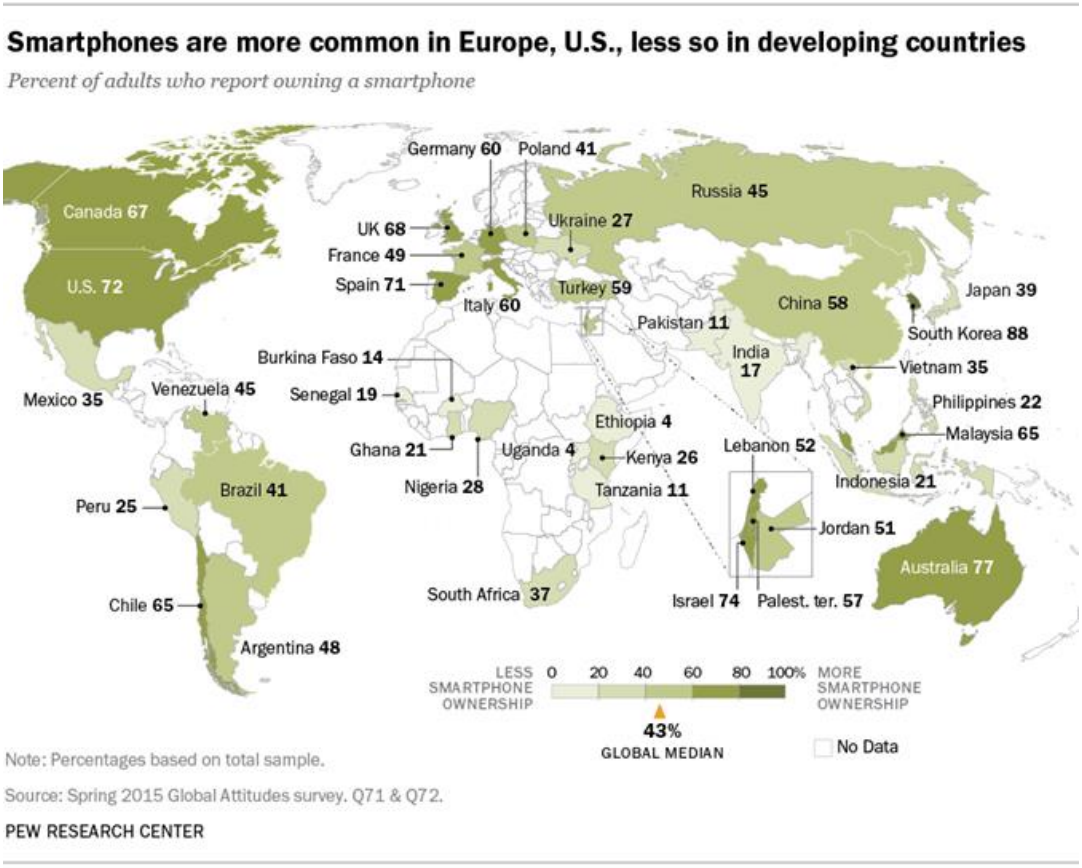

Figure 1.2. Smartphone usage in the world.
Note. "Smartphone Ownership and Internet Usage Continues to Climb in Emerging Economies." Pew Research Centre, Washington, D.C. (http://www.pewglobal.org/2016/02/22/smartphone-ownership-and-internet-usage-continues-to-climb-in-emerging-economies/).

The main area that mobile phones have shown great promise in aiding bioanalytical purposes is primarily in point-of-care medical diagnostics and monitoring of illnesses or diseases.

1.1. **Imaging using mobile phones**

Off-site diagnosis entails that the analysis of a test that is performed at a location other than the test site. For medically-related tests, this becomes difficult as trained personnel are typically required to analyze data. With the rise in today's technologies however, particularly in mobile phones (first with cellphones and later smartphones, of which the latter contains mobile operating systems that enable them to act as "mini computers") and their related hardware (e.g. cameras, antennas for networking), this has led to a boom in mobile-related research that takes advantages of the capabilities of the mobile phones. Early research primarily centered on imaging and the first off-site diagnosis facilitated by a mobile phone was first demonstrated by Martinez et al.[2] who showed that by using the camera equipped on the phone, an image of the assay could be captured and the image would be transferred to qualified medical personnel to interpret (Figure 1.3). Patterned paper-based assays for glucose and protein were prepared and tested with artificial urine. In the two colorimetric assays, the glucose test was enzyme-based, while the protein assay was based on the nonspecific binding of the dye to proteins. The quantification of each assay was subsequently done using image editing software such as Adobe Photoshop (or ImageJ) by digitalizing the assay, conversion to a suitable color space (either grayscale or CMYK), and selection of the test zone on the assay.[2] The mean color intensity within the test zone was determined to correlate with the concentration of the analyte; having previously obtained the calibration plots for each analyte tested, or if the calibration is generated along with test assay, the medical professional can use this information to determine the results and the appropriate course of action without the requirement of their physical presence at the test site.[2] The method relies primarily on the imaging capabilities of the mobile phone as analysis is to be done after remotely transmitting the data. Other devices including scanners (both desktop and portable) and digital cameras were shown to be adequate

alternatives to the mobile phone however, these particular alternatives do not have the ability to transmit data and therefore require a secondary device to do so. Even so, this demonstration of the method has paved the way for other researchers and mobile imaging for off-site quantitative analysis has been reported extensively in the literature, both in the same manner[3,4] and advancing the method further as will be discussed below.

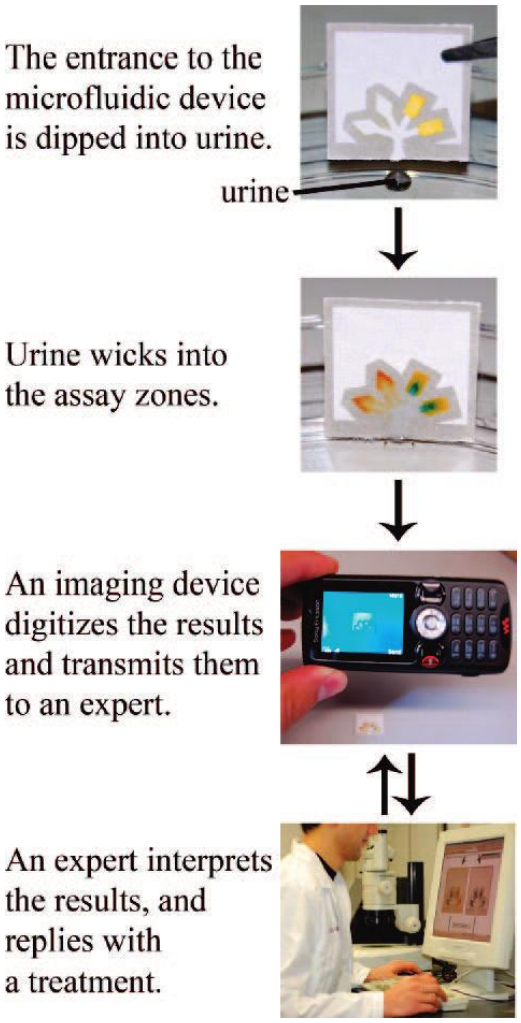

Figure 1.3. General principle for off-site bioassay testing and data transfer to medical personnel for interpretation.

Note. Reprinted with permission from Martinez, A. W.; Phillips, S. T.; Carrilho, E.; Thomas III, S. W.; Sindi, H.; Whitesides, G. M. Simple Telemedicine for Developing Regions: Camera Phones and Paper-Based Microfluidic Devices for Real-Time, Off-Site Diagnosis. *Anal. Chem*. 2008, 80, 3699–3707. Copyright 2008 American Chemical Society.

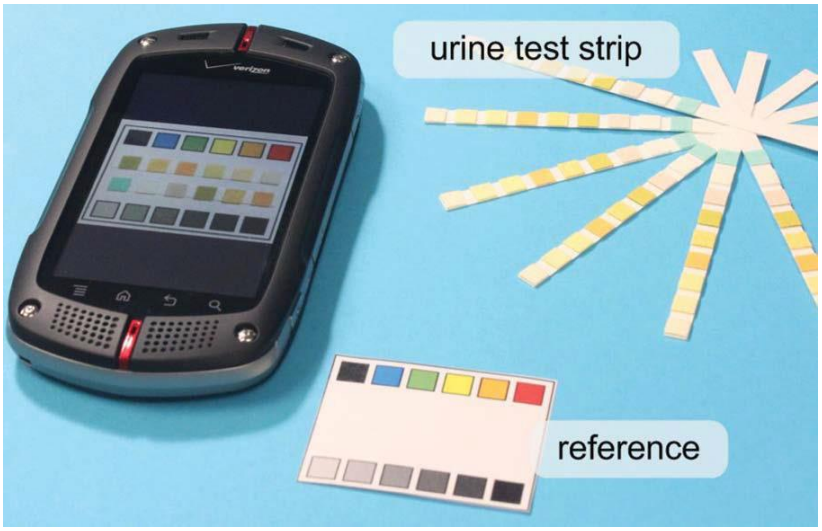

Figure 1.4. Smartphone imaging of commercially available test strips using a color reference chart of known intensities.

Note. Reprinted with permission from Shen, L.; Hagen, J. A.; Papautsky, I. Point-of-Care Colorimetric Detection with a Smartphone. *Lab Chip* 2012, 12, 4240–4243. Copyright 2012 The Royal Society of Chemistry.

In using the phone as a camera, Shen et al.[5] found that an improvement could be made, noting that calibration of the colorimetric tests would yield more accurate results as images generated under different lighting conditions could skew the results, particularly if the conditions used to obtain the calibration curve were different that those of the test images. The researchers showed that they could implement a color correction or compensation element to account for variability in imaging conditions by placing a reference chart with 12 colors of known intensity into the same frame of the mobile phone when imaging the colorimetric test.[5] The differences in the intensity caused by ambient lightning dependence could therefore be compensated for in the data processing steps. As a proof of concept, the authors used commercially available colorimetric pH test strips to study the correlation between the color intensity in various color spaces and the pH value.[5] Measurements of pH tests strips and color correction of the strips were achieved by imaging the strips in view of the reference chart; at the various lighting conditions tested, the degree of skewing in colors and the color correction required were determined by comparing the imaged intensity to the known intensity values.[5] In this case, the authors opted to implement the CIE 1931 color space over the conventional RGB values and other color spaces because a parameter of this

particular color space, chromaticity values, were found to better describe changes in pH, despite having the values been converted from the RGB values This differs from the method by Martinez et al.[2] where grayscale and the CMYK values were employed and the intensity changes correlated well with those assays. Images of the test strips were obtained under various lighting conditions, including 3500 K fluorescent lighting, in the sunshine, and in the shade, and calibrated against 5000K fluorescent lighting to determine the linear relationship between each condition and the standard.[5] The method is highly accurate in quantitating pH and could potentially be applied to an assortment of colorimetric-based tests and immunoassays. Like Martinez et al.,[2] images are transferred to a computer for post-imaging data processing and analysis (here, via MATLAB), although Shen et al. have noted that an app on smartphones to automate the imaging and data processes is in development.[5]

As demonstrated, the initial use of mobile cameras centered on using the device as a means of obtaining an image for the detection of analytes using the colorimetric signal that was exhibited by the presence of the target. Colorimetric responses are a result of color change in the presence (or absence) of a target and these types of tests are limited in their multiplexing capabilities. For example, in the commonly used sandwich enzyme-linked immunosorbent assays (ELISA), an enzyme (typically a peroxidase such as horseradish peroxidase, HRP) conjugated to a detection antibody that binds the analyte of interest with high specificity, catalyzes a reaction between a substrate (a chromogen, such as 3,3',5,5'-tetramthylbenzidine, TMB) and reagent (hydrogen peroxide) to yield a colored signal whose absorbance is then measured. However, since the color change is due to the enzymatic reaction as opposed to the binding event of the analyte, multiple analyte detection in a single test is not possible, even with the use of several target-specific antibody-HRP conjugates. Some researchers have sought to solve this is by exploring smartphone-based camera imaging for other responses such as fluorescence from fluorophores, dyes, and quantum dots.

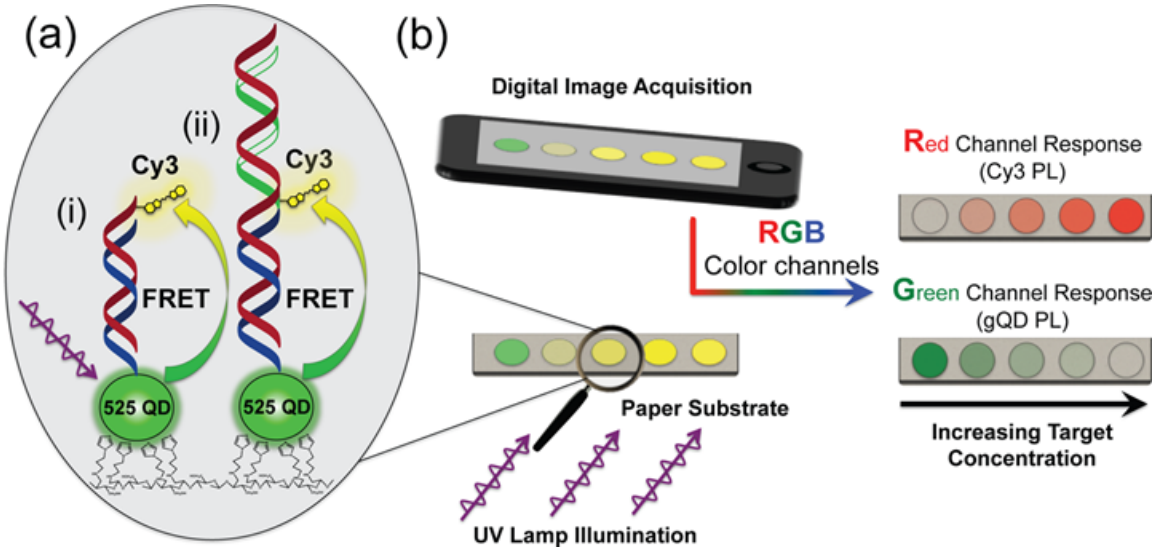

Figure 1.5. (a) Paper-based QD-FRET hybridization assays in (i) direct and (ii) sandwich format. (b) Imaging of the assays using a camera-equipped phone and analysis by splitting of RGB color channels to calculate R/G intensity ratio.

Note. Reprinted with permission from Noor, M. O.; Krull, U. J. Camera-Based Ratiometric Fluorescence Transduction of Nucleic Acid Hybridization with Reagentless Signal Amplification on a Paper-Based Platform Using Immobilized Quantum Dots as Donors. *Anal. Chem*. 2014, 86, 10331–10339. Copyright 2014 American Chemical Society.

Noor et al. showed that the phone could be used to obtain images of fluorescence resonance energy transfer (FRET) from quantum dots (QDs) to dye molecules in DNA hybridization assays, which could subsequently be used to quantitate target oligonucleotide concentration.[6,7] In the simplest example presented in their work, using a direct assay, two sets of oligonucleotides were used; quantum dots were conjugated with oligonucleotide probes, while dye molecules were conjugated to oligonucleotide targets whose sequence was complementary to the probes. The particular QD donors and dye acceptors were chosen because their photoluminescence intensities corresponded well to the RGB (red, green blue) color channels. Immobilized QDs were immobilized on the surface of a treated paper substrate and upon addition of the dye-oligonucleotide conjugate, DNA hybridization between the two strands brought the dye molecule in close proximity to the QD, such that when an excitation source was provided to the QD, FRET was observed with the emission from the acceptor dye. Images of the assay acquired by the phone were transferred to a computer, where

ImageJ software was used to split the images into their respective RGB color channels. A ratio of the R and G channel intensities, where R corresponds to the dye color and G for the luminescence of the QD, was used to correlate to the target concentration. This method is advantageous as it sets the stage for multiplexing abilities through specific quantum dots whose excitation could be done at any particular wavelength. Filters could then be used to isolate for a target of interested to be analyzed, provided that the QD donor and dye acceptor emission wavelengths be known.

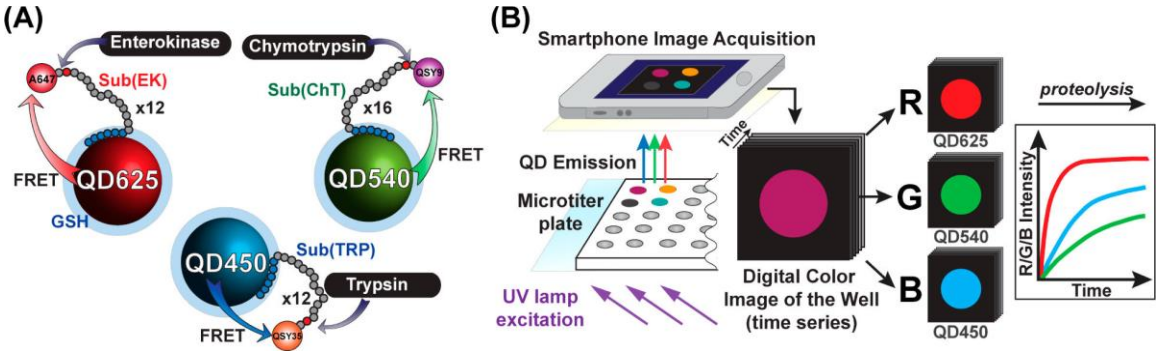

Figure 1.6. (a) FRET-based homogenous multiplexed assay with QDs to monitor protease activity. (b) Smartphone imaging, digitization, and RGB channel intensity analysis.

Reprinted with permission from Petryayeva, E.; Algar, W. R. Multiplexed Homogeneous Assays of Proteolytic Activity Using a Smartphone and Quantum Dots. *Anal. Chem*. 2014, 86, 3195–3202. Copyright 2014 American Chemical Society.

Petryayeva and Algar[8] have shown a similar approach to this FRET-based technique, successfully demonstrating the multiplexing capabilities by further improving the previous methods. In this case, assays to measure the activity of three proteases were conducted in a single spot using three different QDs, QD450, QD540, and QD625, chosen because their emission spectra correlates with the red, green, and blue regions such that their respective RGB intensities channels could be used for quantitation purposes (Fig. 1.6) as in the previous case. Dye-labeled peptides conjugated to the QDs, in the absence of the proteases, allowed energy transfer from the QDs to the dye, thereby quenching the fluorescence from the QD. However, in the presence of the proteases, the peptides were cleaved by the proteases; no FRET occurs between the QD and dye and its activity is therefore measured by the intensity of the QD emission.

Using long-pass and short-pass filters in front of a smartphone camera and a UV light as an excitation source, images of the assays were captured and transferred to a computer for additional processing. The images were split into the RGB channels; by taking advantage of each QD-dye pair and the luminescence at particular RGB wavelength regions, particularly in triplex assays, each target could be quantified based on the intensity of the channel to which the QD emits in, with minimal crosstalk as demonstrated by the authors.[8] In many instances of protein analyses, multiplex tests are accomplished with high-throughput arrays, where a large number of singular protein tests are conducted in parallel.[9] The research is significant in that it is the first to demonstrate homogenous multiplexing capabilities (multiplexing within a single test, rather than an array) could be accomplished via a smartphone.

Other multiplexed assays in the literature, while not demonstrated for use with smartphone-based techniques, have too utilized one signal-producing component per detection element. In other words, each analyte has its own signal component, such as in the above case of one protease per QD-dye pair. One multiplexed assay already in use for flow cytometric assays uses antibodies conjugated to FlowMetrix™ microsphere beads, which is a system of bead sets and software that quantitates the red, orange, and green dyes within the beads; a distinct proportion of red and orange fluorescent dyes are used to identify the different beads, while the green fluorescence is use to determine the amount of target that is bound to each set.[10] Here, the number of analytes performed in the assay is determined by the number of distinct bead types used. Nonetheless, in the phone-based methods, the limitation is not in the signal-inducing component directly, but rather the ability to differentiate between colors as they appear in the digital reproduction. In the simplest of forms, the RGB color space, an additive color model, lends itself to be split into 3 separate channels with no overlapping of the analysis regions, although a multitude of color spaces have been demonstrated in the literature for analytical detection (not excluding fluorescence-based detections) and they include, but are not limited to CYMK (cyan, yellow, magenta, key),[2,11] CIE,[5,12] hue and saturation,[13–16] and grayscale.[2,3,17,18] Interestingly, it appears in the case of the HSV or HSB (hue, saturation, value) color space, H is the most often used parameter for quantification purposes. Generally, hue is defined as the numerical representation of the color, while saturation is the degree of that particular color, and value is the brightness, [13]

where the actual value of these parameters are derived from the red, green, and blue intensities. While hue and saturation are determined from RGB, CYMK is distinct in being a subtractive color model; conversions between the two color spaces are device-dependent. Because of the nature of how digital cameras are produced, with image processing built in to mimic human perception (and as such, manipulates the original color) but also with CMOS censors containing three bandpass filters in the R-G-B wavelength regions, the color information of each pixel is represented as a RGB triplet.[12] This suggests that regardless of the color space used in image analysis, the images obtained using a phone or digital camera ultimately depends on the processing done and the RGB bandpass filters. CYMK analysis would too depend on the RGB image obtained and the subsequent conversion. However, provided images were obtained and analyzed on the same platform, it may be possible to utilize multiple color spaces to analyze a multiplexed assay imaged simultaneously. The image here would need to be looked at in each color space individually because each model is limited by the number of color channels that the image can be split into and any wavelength situated in the range between two color channels may cause crosstalk.

Apart from fluorescence, other detection methods utilizing the smartphone camera have been demonstrated; for example, Lebiga et al.[18] showed that chemiluminescence (CL) detection of H_2O_2 (reaction with bis(2,4,6-trichlorophenyl)oxalate in the presence of rubrene and imidazole) on a paper-based microfluidic device could be obtained; a video of the CL was recorded and the snapshots were processed in ImageJ. Here, the paper was also situated in a case that was placed in front of the camera to shield light, thereby reducing any influence from ambient lightning, thus improving the detection limit.

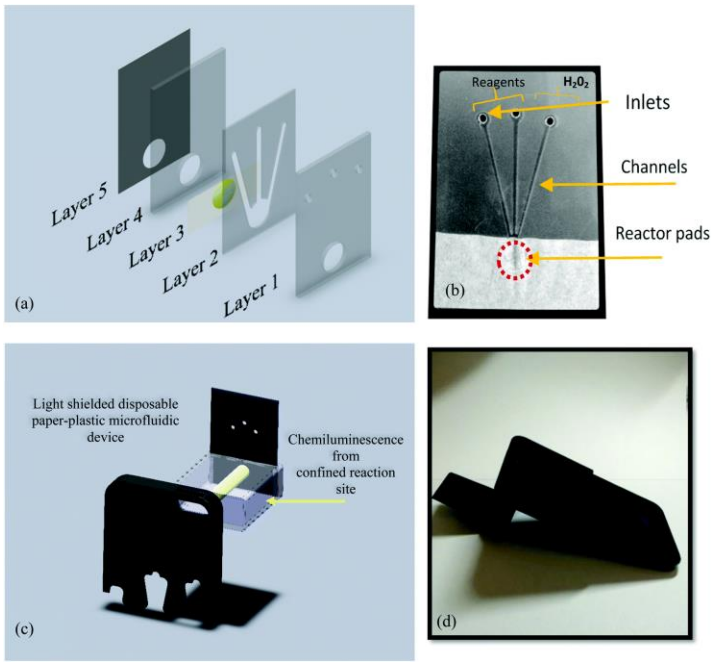

Figure 1.7. Design of plastic-paper disposable microfluidic device for chemiluminescence reactions (a,b). (c) Smartphone accessory to house the microfluidic device for imaging.

Note. Reprinted with permission from Lebiga, E.; Edwin Fernandez, R.; Beskok, A. Confined Chemiluminescence Detection of Nanomolar Levels of H2O2 in a Paper–plastic Disposable Microfluidic Device Using a Smartphone. *Analyst* 2015, 140, 5006–5011. Copyright 2015 The Royal Society of Chemistry.

Such protection in the detection of other chemiluminescence-based detections is common, as seen in case of Delaney et al.[19] who showed that a smartphone can be made to act as a potentiostat used for detecting electrochemiluminescence (ECL). Two pieces of hardware on the phone were exploited for the analytical purpose, namely the camera and the headphone jack. It was demonstrated that by playing an audio clip consisting of square waveforms, a potential could be generated, which in turn was used to initiate ECL from a paper-based microfluidic device adhered to screen printed electrodes that were connected to the audio jack. The output voltage was found to be controlled by the volume setting on the phone, while other potentiostatic functions were controlled through a custom app. While the app was customized to perform all steps required for chemical sensing such as control the number of times the audio clip is played, to record (video) of the process, and analyze the ECL intensities as imaged by the camera, the development of the app itself and how it runs (the processing steps

taken) were not the focus of the publication and therefore not discussed in detail. Despite this, these recent works suggest that most luminescence-based detections can be done via the smartphone camera, while more specialized ones can be done by small modifications to the phone itself, or by addition of accessories fitted onto the phone.

Much research has been done in the area of accessories fitted to improve the performance of the phone. Unlike the work of Lebiga et al.[18] and Delaney et al.[19], where the customized case that is situated in front of the camera only acts to block out background light, the accessories can contain parts that work in addition to the ones already on the phone. One research group that has developed a series of external devices to complement the smartphone camera is the Ozcan group at UCLA. The group has developed, and continues to develop, smartphone attachments to replace traditional laboratory instrumentation. For applications in immunoassays, both for colorimetric- and fluorescence-based detections, the external attachments typically consist of a sample holder, lights (light emitting diodes, LED) and light diffusers, filters and additional lenses, all of which improve the sensitivity and performance of the device.[20,21] Using a commercially available allergen test kit, Coskun et al. demonstrated the ease-of-use and effectiveness of smartphone-based detection.[20] An ELISA test for peanuts, normally quantitated by absorbance readings on a plate reader, was quantitatively analyzed here with a simple set up that simultaneously measures the transmittance intensities of two microtiter plate wells (tubes), with the absorbance of the test well calculated relative to the control well. This is made possible by the additional lens that allows both wells to be in the field of view of the camera and because the samples are illuminated with an external, controlled light source as opposed to ambient lighting, the accurate quantitation are not subject to fluctuations in lightning conditions.

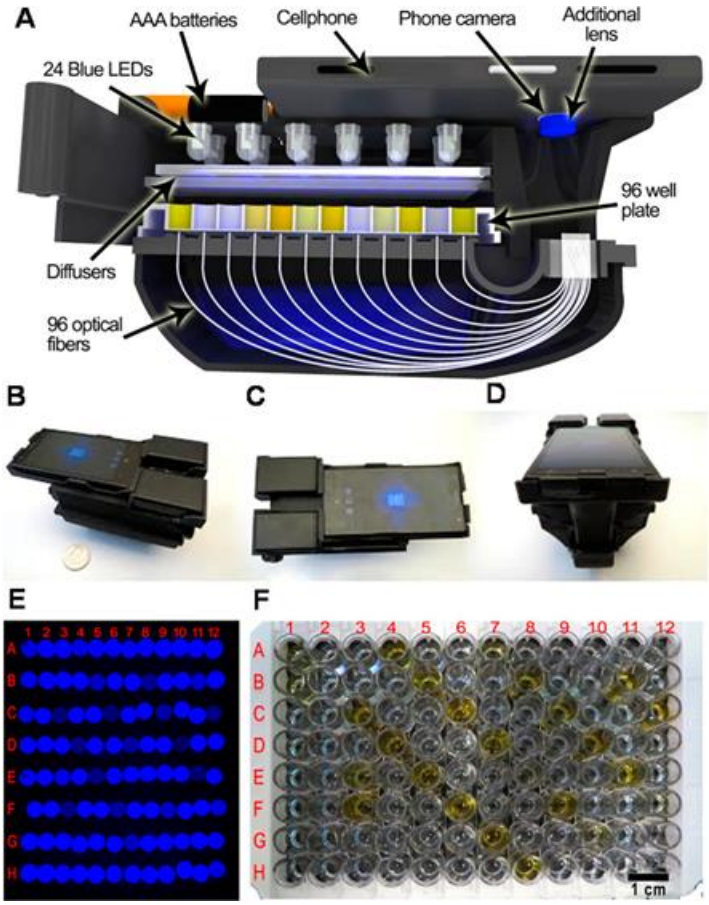

Figure 1.8. (a) Schematic of mobile-based ELISA plate reader (b-d). (e) Image as viewed on the phone by the reader; (f) image by a camera.

Note. Reprinted with permission from Berg, B.; Cortazar, B.; Tseng, D.; Ozkan, H.; Feng, S.; Wei, Q.; Chan, R. Y. L.; Burbano, J.; Farooqui, Q.; Lewinski, M.; et al. Cellphone-Based Hand-Held Microplate Reader for Point-of-Care Testing of Enzyme-Linked Immunosorbent Assays. *ACS Nano* 2015, 9, 7857–7866. ACS AuthorChoice License (Open access). Copyright 2015 American Chemical Society.

Recently, the group introduced a hand-held microplate reader that was shown to be comparable to a benchtop microplate reader in ELISA tests for mumps, measles, and two herpes viruses in clinical samples.[22] Previously, other researchers have published colorimetric, digital methods for analysis of microtiter plates; the methods rely on technological devices such as digital cameras or scanners, or more recently, camera phones, for capturing the images of the wells but required subsequent transferring to a computer for further analysis.[23–26] In the method by Berg et al.[22], a microtiter plate-compatible attachment was 3D printed and further fitted with an additional lens, LEDs,

and 96 individual optical fibers for simultaneous, uniform illumination and image acquisition (Fig. 1.8). Because signal acquisition is from the light directed to the camera via the optical fibers, the method does not suffer from optical aberration from the large field of view, but rather, the image is generated from the collection of illuminated optical fiber ends.[22] The resulting image is then transmitted to an external server for image processing for the blue channel intensity (RGB mode) of each of the wells, which then yields quantitative information when compared with a calibration curve. Interestingly, a machine learning algorithm was also implemented to improve the accuracy of the results as the number of tests increased, made possible by the server-side analysis capabilities; following image processing and analysis, the results were transmitted back to the cell phone used.[22]

Su et al.[27] also developed a colorimetric (based on the HSV color mode) smartphone-microplate reading method, dubbed Bionic e-Eye, which consists of a smartphone camera situated atop a wide-angle lens and dark containment with an illumination source below (Fig. 1.9). The additional wide-angle lens provided the demagnification needed to accommodate the microplate in the image so that aberrations can be reduced compared to some other phone-based methods. Processing of the image from RGB to HSV was accomplished with an app's algorithm and the saturation channel was used in comparison tests of commercially available kits, specifically, bicinchoninic acid (BCA) protein assay and Cell Counting Kit-8.[27] While the two methods are similar in terms of the ability to analyze microplates and the potential for on-site, this setup can be considered to be inherently less portable and is limited in abilities than that of Berg et al.[22] due to various factors including size, ease of use, susceptibility to user error, as well as aberrations from field of view of the microplate (although reduced, it is still present, which can lead to edge effects and lighting inconsistencies that affect the measured signal).

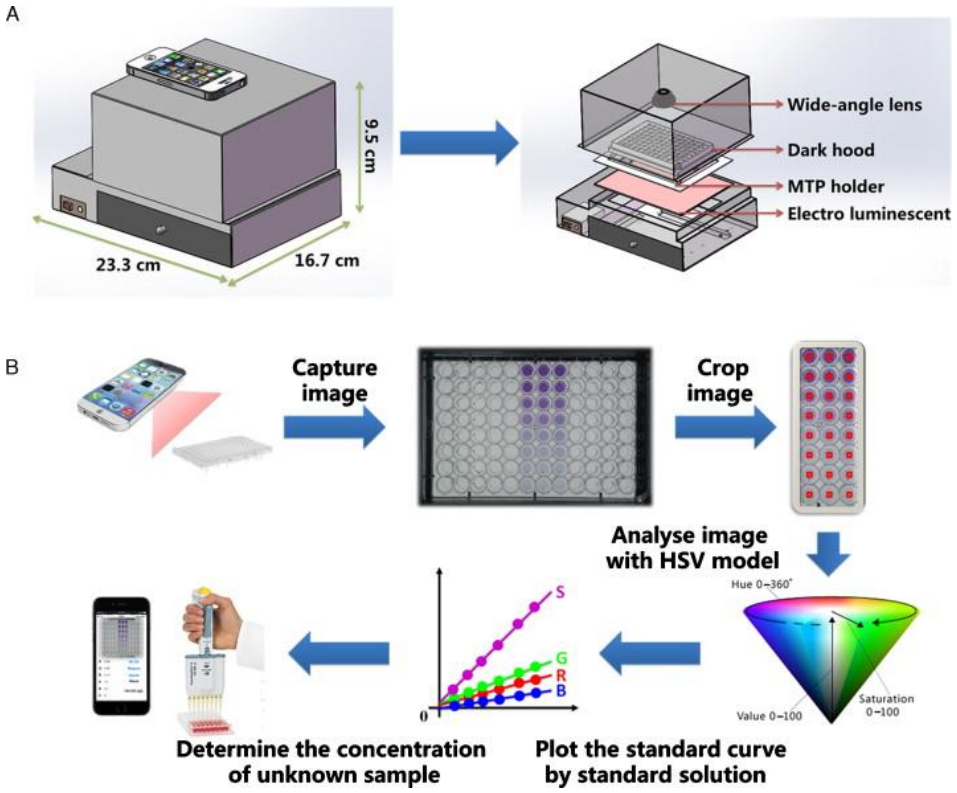

Figure 1.9. (a) Bionic e-Eye set up with smartphone running an app. (b) Processing of the app for HSV color parameters and determination of concentration.

Note. Reprinted with permission from Su, K.; Zou, Q.; Zhou, J.; Zou, L.; Li, H.; Wang, T.; Hu, N.; Wang, P. High-Sensitive and High-Efficient Biochemical Analysis Method Using a Bionic Electronic Eye in Combination with a Smartphone-Based Colorimetric Reader System. *Sens. Actuators, B* 2015, 216, 134–140. Copyright 2015 Elsevier B.V.

It should be noted that in the literature, many other examples of smartphone-based methods for POC or medical diagnostics have been demonstrated. One of these areas is cellphone microscopy, and while the field of research is related, it is not the subject of this thesis. Generally speaking however, these methods typically also involve the use of external attachments that aid or improve upon the hardware already contained in the smartphone. Briefly, microscopic images of fluorescence-based immunoassays to single nanoparticles, viruses, and DNA strands have been shown,[21,28,29] as well as imaging of traditional Giemsa stained blood samples.[30] Even complex samples such as whole blood, dynamic, and label-free microscopy methods have been developed, [31–33] that when combined with customized apps, quantification and

image analysis can be accomplished (both on-site and off-site at remote servers).[29,31,34,35] In an effort to simplify the requirements needed for phone-based microscopy and reduce costs, some researchers added simple lenses (ball or GRIN),[36,37] or inkjet-printed PDMS lenses[38] in front of the built-in camera. In many cases, the resolution and magnification of the phone-based microscope cannot compete with traditional instruments and scanning electron microscopes (SEMs), but the low cost and size certainly make them a practical choice, particularly in the field or in resource-limited settings.

1.2. **Integration of imaging methods with apps**

1.2.1. Commercial tests and assays

Two innovations that have revolutionized the medical diagnostics field (developed prior to the invention of smartphones) by simplifying it greatly are rapid test strip or lateral flow assays, both of which are simple examples of colorimetric tests. Much related, traditionally, these are diagnostic tools that are paper- or polymer-based and have regions that are immobilized with analyte-specific binding or analyte-reacting entities, such as indicator dyes for test strips (Fig. 1.10a) or antibodies for lateral flow immunoassays (Fig. 1.10b). The mechanism of how the lateral flow immunoassay works will be described in greater detail in Chapter 3 (Section 3.3), but as with other colorimetric tests, the appearance or degree of color change is used to indicate the result of the test.

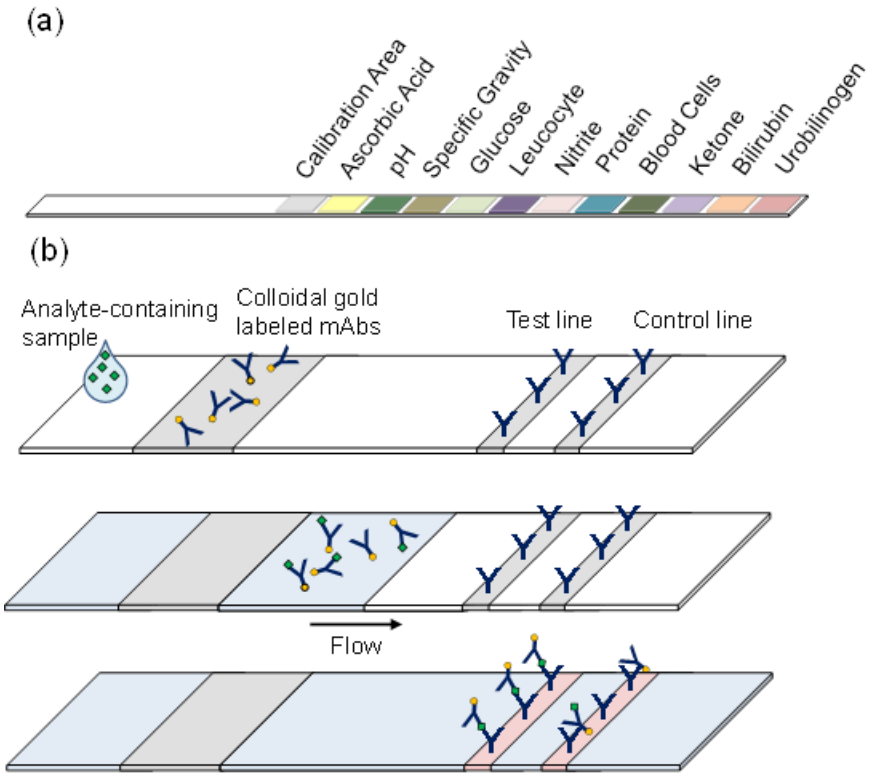

Figure 1.10. POC diagnostic tools in the form of (a) test strip for 11 targets; (b) lateral flow immunoassay.

As these can sometimes be difficult to interpret for users, particularly if the analyte concentrations are low or there is a minor change in color, early research with integration of imaging methods with apps involved these test strips and the automated reading of the results. Mudanyali et al.[39] developed a rapid diagnostic test reader that was mechanically installed directly in front of the smartphone's camera unit and could be used to analyze tests through the use of an app. Containing a lens to demagnify the entirety of the test area into the camera's focal range and an LED array for high contrast illumination purposes (and to allow for both transmittance and reflectance measurements), the reader was adaptable for a series of rapid tests including the lateral flow strips and cassette tests used commonly for pregnancy, parasite, and infectious disease testing by using customized 3D-printed trays. In this particular instance, the authors used the platform with rapid tests of malaria, tuberculosis (TB), and human immunodeficiency virus (HIV). When a user inserts a completed test cartridge into the reader and opens the app to image the test, the captured image is converted to

grayscale and enhanced by an algorithm. The different regions of interest on the test are extracted (removing flow areas to leave lines of interest) and the line intensity (average column pixel intensity) is correlated to the antigen density by further calibrating the test with an unfunctionalized test (minimum intensity) and a saturated test (maximum intensity); the quantified result is relative (indicated as a percent) to these two standards. A unique feature to this platform (enabled by the app) is geo-tagging that allows for real-time statistics on the prevalence of infectious diseases.[39]

A slightly different approach to colorimetric test detection was taken by Erickson's group who also implemented quantification abilities based on a calibration curve of a range of different analyte concentrations into an app. The test substrates in their platforms used range widely, as does the detection mechanism, although the common themes amongst them are its use as a health accessory and the integration of applications (apps) to analyze the test results. As a simpler alternative to the previously discussed accessories that contain many additional parts that requires an initial set up, the "accessories" fitted to the phone in these works primarily act as a sample holder and to provide controlled lighting while imaging, either using an additional LED or a flash diffuser, that can be 3D printed. Colorimetric detection and quantification has been demonstrated by the Erickson group for vitamin D levels, biomarkers in sweat and saliva, and cholesterol.[40–42] While some researchers in the previous section had implemented apps in their works, it was not the focus of the papers and thus, few details were provided. In some works reported in the literature, the app-based analysis method is the focus. Methods that are primarily app-based have the advantage of accessibility since the app can be downloaded to any smartphone (provided an app has been developed for that platform) that is connected to a network and remain installed until use. Particularly important for colorimetric app-based methods are that small differences in color can be better discerned by the CMOS (complementary metal-oxide semiconductor) sensors within the camera and the analysis software than with the human eye, even given that the RGB color space mimics human perception. In many reported examples, commercially available test strips were used to demonstrate the applicability of the method, such as the dry reagent strips for cholesterol and pH indicator strips for sweat and saliva. Low salivary pH has been linked to enamel decalcification, while sweat pH can indicate hydration levels during physical activity.[41,43]

In the work of Oncescu et al., indicator strips of a different pH range for each test were cut to fit a 3D printed cartridge containing the strip, a reference region of white plastic (for white balance correction) and a flash diffuser for uniform illumination across the strip that was inserted in front of the camera.[41] A series of strips were tested with buffer solutions of known pH values to generate a calibration curve that correlated the H (hue) with pH and was stored within the app for future quantification of tests. For each unknown test strip, sweat was applied by touching the strip to sweat, or saliva was applied by spitting on the strip. The cartridge was inserted to the sample holder on the phone and upon acquiring the image, two regions of the test were analyzed; the RGB values in the test strip and the reference area were converted to H values from which they are sorted and the median value taken.[41] The H of the reference area was compared to standard H values and if deemed abnormal (varies by more than 5°, on a scale of 0-360°), the test was considered invalid. For valid tests, the pH was then determined from the calibration curve using the H value of the test region.

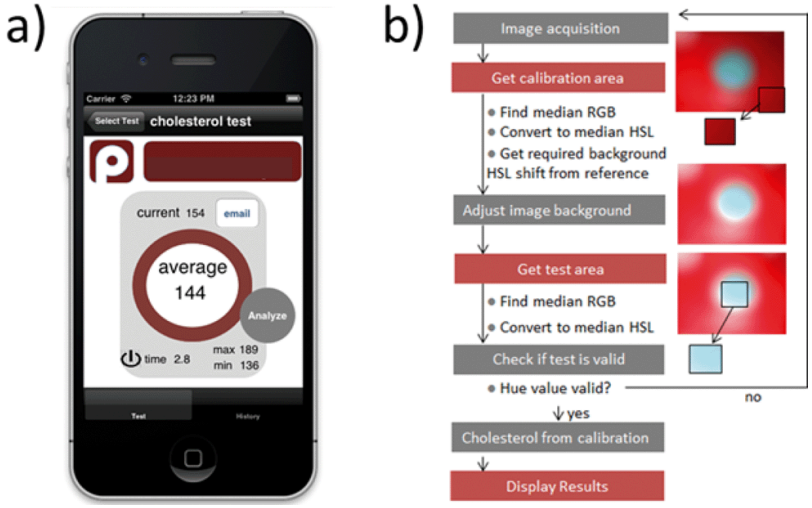

Figure 1.11. Mobile app-based testing of cholesterol. (a) Image showing the working app. (b) Algorithm used for image processing of test strips.

Note. Reprinted with permission from Oncescu, V.; Mancuso, M.; Erickson, D. Cholesterol Testing on a Smartphone. *Lab Chip* 2014, *14*, 759–763. Copyright 2014 The Royal Society of Chemistry.

Similarly in the case of cholesterol, whole blood was tested by application of a drop to the test, which was then filtered through a series of filter papers in the strip to

separate the red blood cells from the plasma.[42] The plasma continued to flow to the reaction pad where the total cholesterol is converted in an enzymatic reaction to produce hydrogen peroxide as a product that subsequently reacted to form a dye. It is the color change as a result of the dye that is imaged and used to indirectly quantify the cholesterol concentration in the blood. After application of a drop of blood to the test strip and allowing a color change to occur (a fixed time between 60-80s), the strips were imaged with the custom app.[42] The app was written to select a calibration area in the image in which the RGB value was converted to the average HSL value (another cylindrical-coordinate representation of the RGB color space, similar to HSV, where lightness is denoted as L) according to

$$H = \begin{cases} \frac{B-R}{C} + 2 \text{ if } M = G \\ \frac{R-G}{C} + 4 \text{ if } M = B \end{cases} \quad (1)$$

$$C = M - m \quad (2)$$

$$S = \frac{M-m}{1-|2L-1|} \quad (3)$$

$$L = \frac{1}{2}(M + m) \quad (4)$$

where M = max(R,G,B) and m = min(R,G,B).[42] The computed value was compared to a reference value and the entire image was subjected to a background adjustment (Figure 1.11). On the adjusted image, the test area was selected and another RGB to HSL value was computed. The authors found that cholesterol concentration could be directly correlated to both saturation (S) and L values, while H acted as a validity test in a similar fashion as the pH tests previously. In this case, H values in tests were found to typically fall within the range of 170-190°; H values outside this range signaled that the tests were considered invalid.[42] As demonstrated in the two examples, user errors were minimal factors in the test results as much of the process was automated. Additionally, the accessory provided guides for the test strips to be inserted and improperly conducted tests or outliers could be easily identified.

At the same time, Yetison et al.[44] reported a similar technique and algorithm using an app that was developed for the Android and iOS operating systems. The authors demonstrated that colorimetric urine strips containing test regions for pH, protein and glucose concentrations could be quantified by testing standard solutions in artificial urine. In their work, Yetison and co-workers did not require the use of an accessory but rather both the calibration using a reference chart and imaging of the test strip were performed under the same conditions by holding the smartphone 5 cm above the sample. The algorithm within the app was written such that there were defined evaluation areas that corresponded to the colorimetric areas of the test strips. Demonstrated using the CIE 1931 color space, both the calibration data and the test data were subjected to the same conversion in color; the RGB values were linearized and converted to the X,Y,Z tristimulus values by[44]

$$\begin{aligned} X &= 0.4124R + 0.3576G + 0.1805B \\ Y &= 0.2126R + 0.7152G + 0.0722B \\ Z &= 0.0193R + 0.1192G + 0.9505B \end{aligned} \tag{5}$$

which were then expressed as chromaticity coordinate values x,y, (which are a function of the tristumulus values)

$$\begin{aligned} x &= \frac{X}{X+Y+Z} \\ y &= \frac{Y}{X+Y+Z} \end{aligned} \tag{6}$$

The test assay results were then determined by interpolating the calibration data with the chromaticity values of the test and displayed to the user as the concentration. While the authors demonstrated the reproducibility of the app in reading test strips, they also acknowledge that accessory-free readers are subject to greater measurement variability from lightning, focus, angle, and shadow effects. Eliminating the need for an additional housing unit, even those that can be 3D printed, may appeal more to those in resource-limited settings. Nonetheless, automation of apps with algorithms to better process images certainly aids in reducing the user dependence and simplifying the method for point-of-care use.

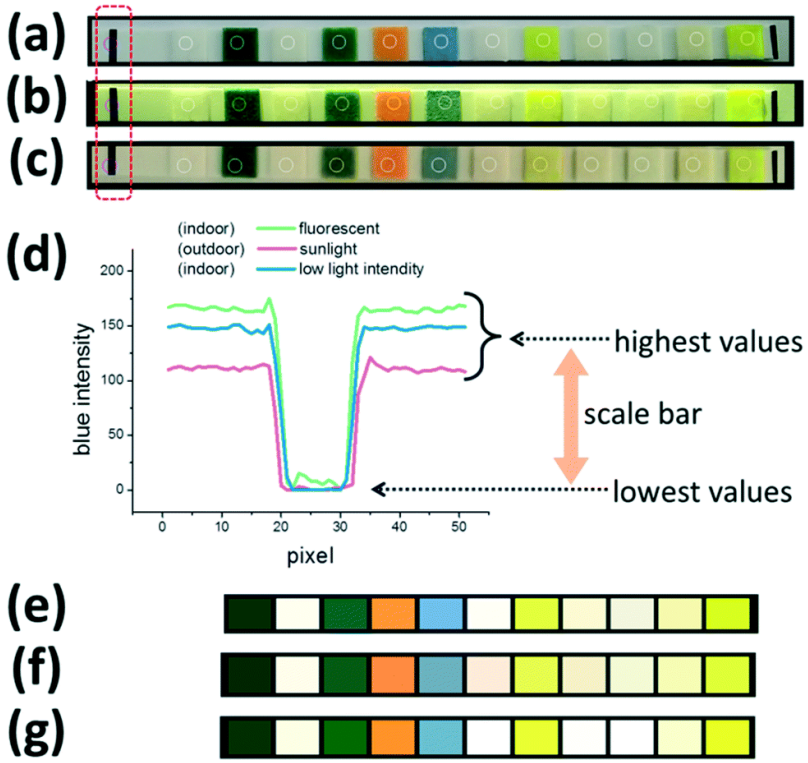

Figure 1.12. Optical images of urine test strips taken under (a) fluorescent lighting; (b) sunlight; (c) low light intensity. (d) Blue intensity profiles of the optical images. (e-g) Corrected colors of the optical images.

Note. Reprinted with permission from Hong, J. I.; Chang, B.-Y. Development of the Smartphone-Based Colorimetry for Multi-Analyte Sensing Arrays. *Lab Chip* 2014, 14, 1725–1732. Copyright 2014 The Royal Society of Chemistry.

Hong and Chang[45] demonstrated in their work with urine test strips such a reduced dependence by incorporating lighting correction and automated detection zone identification algorithms into their app. The latter was determined by adjusting an image of the urine strip to become a highly contrasted monochromatic image upon which a template was projected upon to find each sensing zone on the test strip. A black bar was drawn at each end of the test strip to serve as the recognition elements to aid in determining the exact dimensions of each test. The black bar, along with the white background, also acted as a reference for lighting correction and was used to adjust the RGB values of each pixel in the image according to

$$R_{corr} = \left(\frac{256}{R_W - R_B}\right)(R_{meas} - R_B) \quad (7)$$

where R_{corr} is the corrected value, R_W is the white background value, R_B is the black reference value, and R_{meas} is the measured value in each sensing test zone. The effect of the light source on the image was evaluated by imaging a test under various lightning conditions (indoor fluorescent light, sunlight, and indoor low light) (Fig. 1.12a-c). As shown in Fig. 1.12d, the blue intensity within the black bar varied depending on the lightning, however, using equation 7, the digitized image of the test strip was corrected. A second color space, namely the HSV color space, was used for correlating the changes in color to the concentration of each analyte. In some sensing tests (e.g. pH, glucose), the H displayed more sensitivity while in others (e.g. nitrite, ketone), the S was the better parameter for quantification; each sensing test was expressed as a function of H or S and stored as the calibration curve. For each test, the determined concentration was categorized into three levels of low, medium, and high concentrations of analyte. Testing each sensor numerous times with different concentrations of analyte, the accuracy of the app reading the result of test compared to a commercial test strip analyzer ranged from 72-100%, where the lower accuracies were due to the categorization when a concentration fell between 2 categories. This work demonstrates the potential that app-based POC diagnostics has. Here, regardless of the conditions, all digitized test images can be corrected in order for them to be accurately compared to a stored calibration curve. Hardware and instrument limitations are eliminated since only the app is required and all post-imaging processing is automated.

1.2.2. Specialized tests and assays

While commercial test strips are easy to use and readily available, it is limited by the analytes that can be tested as those already on the market. For example, human epididymis protein 4 (HE4) has been identified as a serum biomarker for ovarian cancer,[46] and has been suggested as a replacement or complement biomarker to CA-125.[47] In studies and clinical testing, HE4 is detected by competitive ELISA or ECL immunoassays,[46–48] which requires the use of specialized instrumentation and personnel

to perform and analyze the data. These laboratory tests have not yet been adapted for easier use on rapid tests as of yet. Some researchers have taken a step forward to integrate the use of apps with immunoassays using specially designed test substrates. Wang et al.[49] demonstrated a microchip ELISA to be used in conjunction with an app for the quantitative measuring of HE4 for POC testing. Microchips fabricated using a non-lithographic technique were assembled from laser cut poly(methyl methacrylate) (PMMA) and double-sided adhesive onto a polystyrene petri dish to create microchannels with inlet and outlets cut at each end (Fig. 1.13a). Sandwich ELISA (Fig. 1.13b) was used capture and detect the HE4 protein before the assay was visualized by a reaction of TMB and H_2O_2, catalyzed by HRP. Unlike conventional ELISA in a microtiter plate, the enzymatic reaction in the microwells was not stopped as addition of H_2SO_4 would displace the solution out of the well; instead, the blue color was imaged quickly by the smartphone (Fig. 1.13c). The authors found that there was an inverse correlation between the red pixel intensity of the solution in the microchannels and the concentration of HE4. It was therefore programmed into the app's searching algorithm to identify regions of continuous low R values (adjustable threshold set to 70) which correspond to the microchannels. For channels with a low concentration of HE4, the color intensity was low and could not be differentiated from the background, the authors facilitated the automated detection with markers in front of the channels. Once located, the image was captured and the RGB pixel values were obtained from these areas. The R values were normalized against that of the background and a calibration curve (obtained prior to imaging the sample) was used to determine the concentration of HE4 in the sample. The results were then displayed on the screen (Fig 1.13d). The colorimetric method had a detection limit of 8.45 nM (19.5 ng/mL) for HE4, which is lower than other reported methods for similar biomarker proteins using electoimmunosensing or a bio-barcode assay, but exhibited high reproducibility and comparable sensitivity to conventional ELISA.

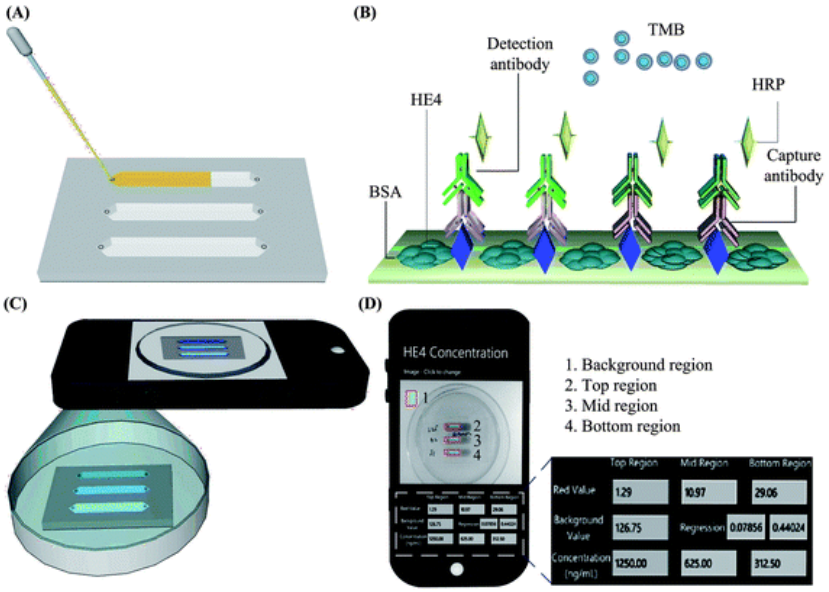

Figure 1.13. (a,c) Schematic of the PMMA-based microchip ELISA. (b) Sandwich ELISA for HE4. (d) Customized app to image and analyze the colorimetric reaction from ELISA; results are displayed on the screen.

Note. Reprinted with permission from Wang, S.; Zhao, X.; Khimji, I.; Akbas, R.; Qiu, W.; Edwards, D.; Cramer, D. W.; Ye, B.; Demirci, U. Integration of Cell Phone Imaging with Microchip ELISA to Detect Ovarian Cancer HE4 Biomarker in Urine at the Point-of-Care. *Lab Chip* 2011, *11*, 3411-3418. Copyright 2011 The Royal Society of Chemistry.

1.3. **Objective of this thesis**

The recent surge in research in this area can be explained by the technological developments surrounding phones. The growing body of works dedicated to smartphone-based detection systems, primarily in the fields of medical diagnostics and POC testing is evidence of this. To satisfy the need in many resource-limited regions of the world and even patients in developed countries, it is ideal that these analytical techniques meet the ASSURED (Affordable, Sensitivity/Specificity, User-friendly, Rapid and Robust, Equipment-free, and Deliverable) characteristics set out by the WHO. In other words, POC devices should be inexpensive, have a low detection limit, easy to use, portable and battery powered, and present results in a short time frame.

In this thesis, the development of a smartphone method for bioanalytical purposes will be discussed. The method will be primarily app-based and utilize a custom plastic biochip. Following the Introduction where various smartphone-based techniques found in the literature are presented, Chapters 2 and 3 focus on the development of an app for grayscale analysis and integration of linear barcodes with immunoassays, respectively, such that we can move towards automated analyte testing and analysis. Finally, Chapter 4 presents the conclusion and suggests future directions for the project.

Chapter 2.

Mobile app-based quantitative scanometric analysis*

This chapter gives a brief introduction into silver enhancement protocols used for the visualization of colorimetric assays and the steps taken to develop an app to analyze these assays. Paper-printed bars of various darknesses were used to determine the correlation between the scanning method and grayscale intensities. This correlation was then used to develop an app with an algorithm that analyzes the test lines automatically without the need to transfer images to a secondary device or the use of additional software. A simple biotin-streptavidin assay was used to demonstrate the practicality of the method.

2.1. State of the art in scanometry

Colorimetric tests make use of a color change to qualitatively determine the presence or absence of an analyte such as in the case of lateral flow test (e.g. dipstick pregnancy tests), but can also be semi-quantitative such as using pH indicator strips and comparing the color to the chart provided. These tests do not necessarily require the use of specialized equipment and in such cases are limited in its quantitative abilities.[50] Even so, the benefit of their ease of use, low cost, minimal waiting time (for results), and lack of need for expensive instrumentation make these types of test a popular choice.[50] More

* Adapted from Wong, J. X. H.; Liu, F. S. F.; Yu, H.-Z. Mobile App-Based Quantitative Scanometric Analysis. *Anal. Chem.* **2014**, *86*, 11966-11971. Copyright 2014 American Chemical Society. Wong designed and carried out the experiments; Liu wrote the customized app; Wong and Yu wrote the manuscript.

accurate quantitative colorimetric tests are possible, as in the case of ELISA where the color change is a result of an enzyme's catalytic conversion on a substrate to a colored product is quantified using absorbance measurements. Inevitably, the ELISA tests require specialized instrumentation (spectrometer-based-plate reader) and trained professionals for the rather cumbersome operations.[51]

A "subcategory" of colorimetry is scanometry that uses a grayscale as opposed to the various color spaces. In scanometry, the gray intensity, usually a result of silver enhancement is the measured signal. Taton et al. initially used the scanometric method on DNA hybridization assays on glass slides, visualizing the signal with silver enhancement solutions and scanning the resulting samples with a desktop scanner for further processing and analysis on a computer using an 8-bit grayscale.[52] While the silver enhancement technique was not considered novel at the time, typically used for cells and tissue staining,[53,54] Taton et al. showed that the method was also applicable to solid substrates; for their target DNA, concentrations as low as 100 pM could be detected, although the grayscale value was dependent on the sequence of oligonucleotides and on the silver amplification conditions.[52] Gupta et al. later developed the scanometric method further and showed that a silver enhanced immunoassay could be considered quantitative by the optical darkness of the reaction regions.[55] The sandwich-format immunoassays used in their work were shown to be highly selective and reproducible,[55] which stimulated a number of studies on various assay systems.[56,57] Our research group recently demonstrated that the scanometric method could also be applied to the detection of proteins (thrombin) and heavy metal ions (Hg^{2+}) using a DNA molecular beacon immobilized on a plastic (polycarbonate) substrate.[58] The scanometric method thus far relies on either a light scattering instrument or desktop scanner, [52,57–60] which limits it applications in point-of-care diagnostics, i.e., providing health care in rural areas and developing countries.

As had been previously discussed in the Introduction, it has been suggested the need for health care be combated by growing infrastructure of mobile networks; this has been supported by current research focusing on the adaptation of smartphones and tablets, their sensors, cameras, and general power supply and functions, particularly those for colorimetric detection.[61] Mobile-based detection has evolved dramatically from

using only the camera to image the assay, both with dyes and enzymatic methods[2,8,62,63] to cell phone camera-based microscopy,[30,36,64] and fluorescence/luminescence detection and imaging.[8,31,65] As demonstrated by a number of researchers very recently,[19,44,49] integrating the imaging and analysis capabilities are possible through the use of custom applications (apps).

2.2. **Method**

2.2.1. Scanning mode and grayscale comparison

Optical densitometry in the form of optical darkness ratio (ODR) has been adapted as standard protocol for analyzing chip-based bioassays,[55,58,66–69] which was initially proposed by Gupta et al., and is given by equation 8.[55]

$$ODR = (I_b - I_s)/I_b \tag{8}$$

where I_b is the grayscale value (intensity) of the background and I_s the grayscale value (intensity) of the signal, thereby giving a normalized ratio of the signal to the background. The key question that has not been addressed is how these grayscale values are determined, and whether they are influenced by the different modes of image acquisition. Herein, a thorough comparison of imaging methods available on desktop scanners and mobile devices was carried out.

On a typical office scanner, there are three modes available for scanning, namely in color, grayscale, or black and white. The black and white mode does not serve well for quantitative purposes as no pixel can have a value that is an intermediate between the two extremes and was not considered further. For images scanned in the color mode, the pixels are presented in three different colors: red (R), green (G) and blue (B), and the grayscale values (I) are calculated in two ways. The average I value is determined according to equation 9,

$$I = (R + G + B)/3 \tag{9}$$

where R, G, B are the pixel intensities in each of those channels. The other measure, the weighted *I* (luminosity) accounts for a human's color perception and is determined by

$$I = 0.30R + 0.59G + 0.11B \quad (10)$$

For images scanned in the grayscale mode, the *I* value can be directly measured. Typically, the scanned images are analyzed using Adobe Photoshop's grayscale mode, however, the way the grayscale value determined from the RGB values in that case was not revealed.[58]

To study the modes, grayscale values ranging from 255 to 0 were printed on white paper (Fig. 2.1) using an HP 2055dn printer (Hewlett-Packard Company) at 300 dpi and subsequently scanned back into a computer using an office scanner (Epson Perfection 1250) in the color or grayscale mode (900 dpi). The images were imported into Adobe Photoshop and a section of each gray region (50,000 pixels) was selected and analyzed.

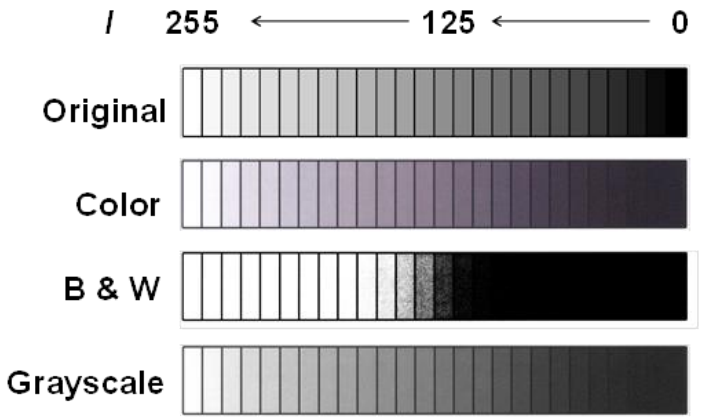

Figure 2.1. Images obtained with different scanning modes on an office scanner; a range of gray value intensities, from 255 (white) to 0 (black), is shown. The original was printed on a white paper, and then scanned using a desktop scanner in the color, black and white (B&W), and grayscale mode, respectively.

The average grayscale was determined in the RGB mode by the mean value of the RGB channels. The weighted average grayscale was determined in the RGB mode

by the mean value of the luminosity channel. The “Photoshop Grayscale” values were determined by converting the scanned color image from RGB to grayscale mode and taking the mean value of the gray channel (direct measure of *I*).

2.2.2. App development and testing

The Mobile ODR app has so far been installed and tested on a Nexus 7 tablet running Android version 4.4.2. It was written using the Android Developer Tools in Java by Frank Liu and can be summarized as described below. When a user launches the app, it opens the rear camera of the mobile device and displays a camera preview with a red box in the center of screen (Fig. 2.2). It has been written to display four bars in the red box that the user aligns with the channels of the sample using the zoom button when positioned in a dark containment (Fig. 2.3) and situated 7 cm from the sample with a single light source above (40W, 120V lightbulb was used here although any light can be used provided it is consistent amongst imaging of all samples). The user captures the image using the capture button, which commands the app to start measuring the ODR values of the test strips. The app captures the raw CMOS data from the camera and converts them into an array of RGB values, where x, y are coordinates of the pixel.

$$\mathrm{Color}_{\mathrm{pixel(x,y)}} = \left(R_{x,y}, G_{x,y}, B_{x,y}\right) \tag{11}$$

For each pixel, the *I* value is calculated using the average grayscale method described below (equation 10), and the mean of the average grayscale values in a particular region (a cluster, 4715 pixels) is determined, along with the standard deviation.

$$C_i = \left\{ pixel_{x,y} \,\middle|\, pixel_{x,y} \in pixel_{(range(x),range(y))} \right\} \tag{12}$$

$$|C_0| = |C_1| = |C_2| = |C_3| \tag{13}$$

$$\overline{I_i} = \frac{\sum I_{x,y}}{|C_i|},\ \sigma_{\mathrm{i}} = \frac{\sum(\bar{I} - \frac{(\bar{I_1}+\bar{I_2}+\bar{I_3})}{3})}{2} \text{ where i} \in [1,3] \tag{14}$$

For each group of pixels from the test strip and the test background(C_0), the app samples 3 clusters (C_1, C_2, C_3) of pixels and calculates their average mean grayscale value and standard deviation. Using the mean grayscale of background ($\overline{I_0}$), the app obtains the ODR value for each test strip by the difference between the mean grayscale of background and mean grayscale of test strip relative to the mean grayscale of *background*, according to equation (8).

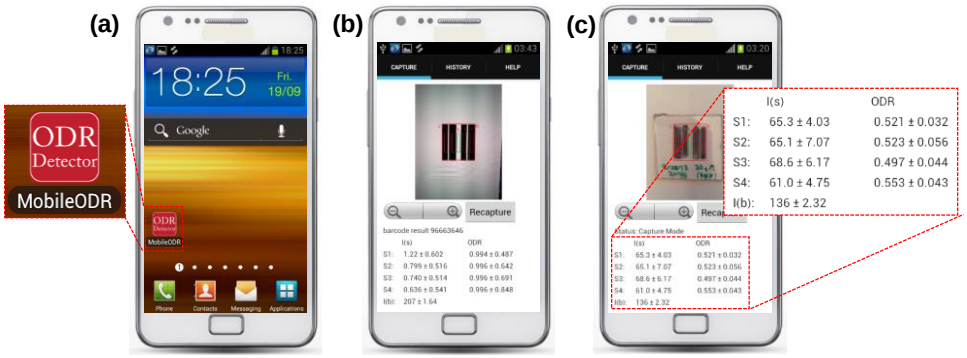

Figure 2.2. **Screen captures of the Android Mobile ODR app. (a) The Mobile ODR app is launched and is used to measure the ODR of (b) printed "channels" on paper; (c) silver stained binding strips of a direct biotin-streptavidin assay on polycarbonate. Results are directly displayed on the screen and saved automatically.**

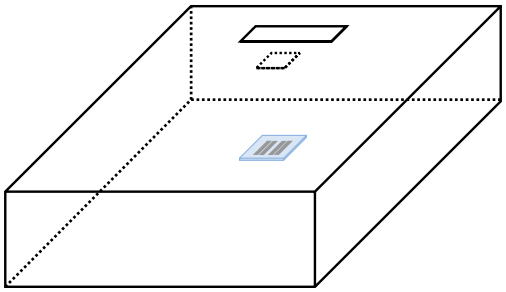

Figure 2.3. **Schematic representation of the containment used to control lighting while samples are imaged or analyzed by the Mobile ODR app. The rectangular opening at the top of the containment is used for the light source, while the smaller, square opening below is for the camera of the smartphone to image the silver stained PC inside the containment.**

2.2.3. Biotin-streptavidin assay

A piece of polycarbonate board (3×3 cm, Fig. 2.4 and 2.5) was rinsed with ethanol and deionized water, and dried with nitrogen gas. The polycarbonate was placed in a UV/Ozone cleaner for 15 min and incubated in the ozone environment for 20 min. A 100 mM EDC (*N*-(3-dimethylaminopropyl)-*N*′-ethylcarbodiimide hydrochloride) and 25 mM NHS (N-hydroxysuccinimide) in 0.1 M MES (2-(*N*-morpholino) ethanesulfonic acid, pH 5.8) solution was placed on the surface of the polycarbonate for 3 hours, rinsed off with deionized water, dried before a PDMS chip with four channels patterned as in Fig. 2.2 and 2.4 was fixed to the surface. The PDMS was prepared by cutting Scotch tape into 3.5x17 mm strips (3.5 µL of solution) that will form the channels. The tape was adhered onto a standard microscope slide that was subsequently placed into a petri dish into which PDMS was poured (mixture of 10:1 Sylgard 184 base and curing agent). The PDMS was cured for 2 h at 60°C in an oven. Into each of the channels of the PDMS-PC chip, NH_2-PEG_2-Biotin (30 µg/mL) was pipetted and incubated for one hour, followed by rinsing with 100 mM phosphate buffer solution (containing 500 mM NaCl, 0.8% bovine serum albumin, 0.1% gelatin, 0.05% Tween 20, and 2 mM NaN_3 at pH 7.4). This was followed by passivation with an 8% solution of bovine serum albumin (BSA) for two hours and further rinsing with the phosphate buffer. Nanogold streptavidin conjugate solution was injected and incubated in the channels for 50 min before rinsing with the phosphate buffer solution. The PDMS chip was removed and the polycarbonate surface was washed with deionized water. The channels were then silver stained to visualize the signal using a 1:1 mixture of 0.048 M silver nitrate and 0.182 M hydroquinone with 4% gelatin in citrate buffer (pH 5.4) for 10 min. The polycarbonate was rinsed once more with deionized water and dried.

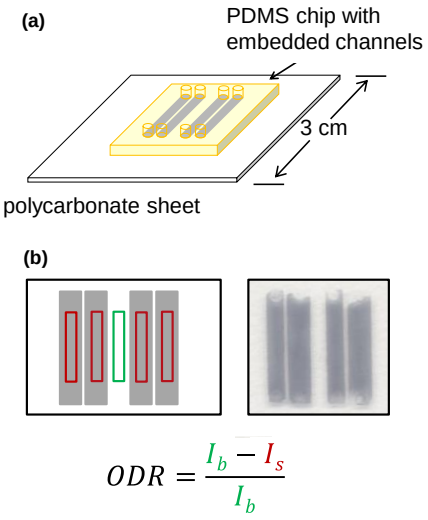

$$ODR = \frac{I_b - I_s}{I_b}$$

Figure 2.4. **Schematic view of the formation of assay lanes with the help of a PDMS channel plate on PC (a) and reading of grayscale intensities of the silver stained assays for the calculation of ODR values with the Mobile app (b). The right side shows a silver stained biotin-streptavidin assay.**

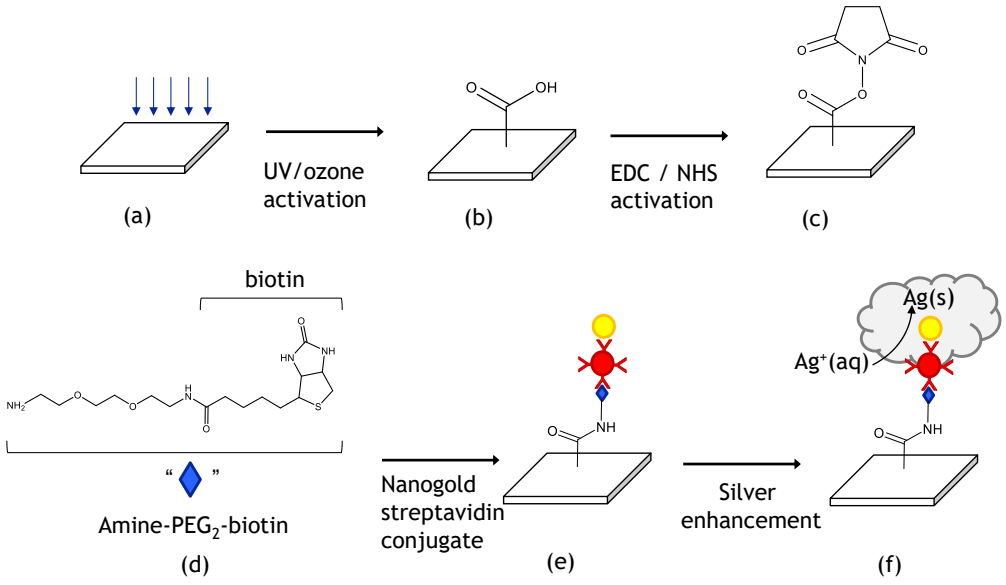

Figure 2.5. **Preparation of a biotin-streptavidin binding assay on polycarbonate (PC). (a) A piece of polycarbonate board (3×3 cm); (b) UV/ozone activated PC plate; (c) EDC/NHS activated PC plate; (d) immobilization of NH2-PEG2-biotin via amide coupling; (e) Binding of Nanogold streptavidin conjugate on the surface; (f) silver staining to enhance the signal.**

2.3. **Results and discussion**

For the initial test, a series of bars of different *I* values in grayscale (Fig. 2.1), ranging from 255 (white) to 0 (black), were printed on plain white paper and scanned using a standard office scanner in the color, black and white, and grayscale modes. As shown in Fig. 2.1, the gray bars scanned in color mode differ from the original in that the bars appear to take on a purple tinge and appear to be not as dark as the original at low *I* values. Using this image, the average and weighted *I* values were calculated and shown in Fig.2.6. The results show that the Photoshop grayscale mode consistently gives ODRs that are higher than theoretical values, while on the other hand, when analyzed in the RGB mode, the ODRs are more consistent with the theoretical ODR. In all cases however, the ODRs at low *I* values level off; this is likely due to the printing quality of the original bars and not the scanning or analysis methods. Figure 2.6b shows the comparison of the theoretical ODR to the ODRs of the analysis methods. The data has only been fitted to a theoretical ODR value of 0.75 whereby after, the ODRs are saturated. In this linear range, the weighted average *I* (luminosity, determined using equation 10) values demonstrates the best correlation with theoretically preset ODRs with an $R^2 = 0.9981$ and a slope of 0.9939 ± 0.0051, though the averaged RGB protocol yields very close results ($R^2 = 0.9985$, slope of 0.9653 ± 0.0046). The other method, the Adobe Photoshop grayscale, deviates slightly, $R^2 = 0.9856$, slope of 1.1537 ± 0.0156. Figure 2.1 can also be scanned using the grayscale mode where the *I* values are directly measured rather than calculated according to any particular formula. In Fig. 2.6, the grayscale deviates further from the theoretical ODR than the average and weighted average ODRs, but is less than that of the Photoshop grayscale. This mode was not used further because the conversion between the color and grayscale modes used by the scanner is unknown. The other scanning mode that was not considered further was the black and white mode.

From the above analysis, it is clear that both the average and weighted grayscales are suitable for *I* value analysis. We then developed an app, “Mobile ODR” that analyzes the weighted average (luminosity) grayscale based on equation (10), which runs on the android platform, both smartphones and tablets (Figure 2.2). The

same grayscale intensities as used in Figure 2.1 were reprinted as a series of four "channels" (for microfluidic microchip applications at a later time) and the ODRs as determined by the app are compared to the theoretical values (as designed) and those determined with a conventional desktop scanner.

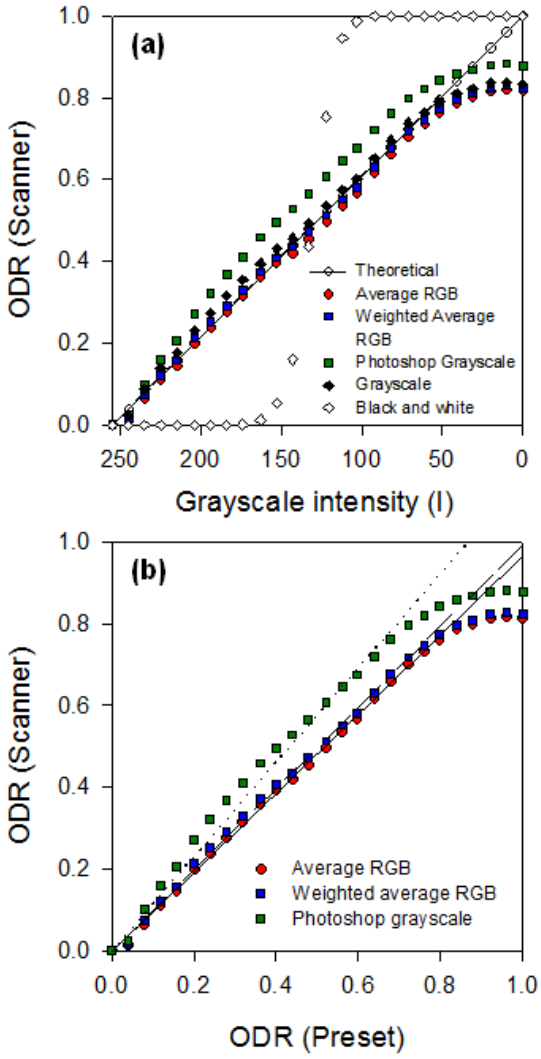

Figure 2.6. **(a) ODRs determined from the scanned image in color, grayscale, and black and white modes, of the gray bars of different grayscale intensities (*I*). The color image was analyzed by the average, weighted (luminosity), and the Adobe Photoshop specific grayscale, respectively. (b) Correlation between experimentally determined ODRs and the theoretical values. The linear fitting has been limited to a maximum ODR value of 0.75 for the average RGB (solid), weighted average RGB (dashed), and Photoshop grayscale (dotted) lines.**

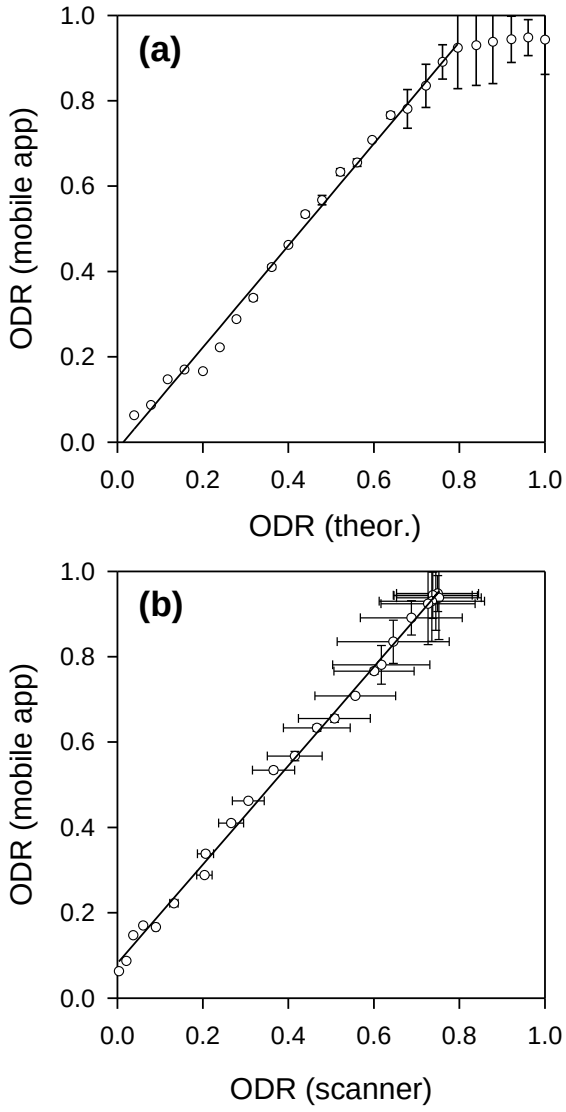

Figure 2.7. ODRs determined by the mobile app as a function of the theoretical values (a) and those determined by an office scanner (b). ODRs are calculated using the weighted average (luminosity) grayscale intensities. Error bars are propagated uncertainties from the different pixel intensities of each selected test region. The solid line shows the best linear fit of all data points.

As shown in Figure 2.7a, with the Mobile ODR app we are able to obtain a series of ODRs of the gray bars show in Figure 2.1 (color mode), which correlates with the theoretical values up to 0.80; the linear fit in this range yields a R^2 value of 0.9968 that is comparable to that obtained for scanners as described above. The slope (1.19 ± 0.02),

though, is slightly higher than unity, indicating the app-determined ODR values are generally higher than the present values. The rather large error bars for the high ODR values (> 0.65) result from the error propagation of the variation in pixel intensities of the test region (dot gain in the printing process); because the high ODRs are from low *I* values, there is a greater relative uncertainty compared to high *I* values with similar variations in pixel intensities. This is only a factor in our printed paper tests (*vide infra*). When we directly compare the ODR values obtained with the mobile app and a standard office printer on the same set of printed gray bars, the correlation between them is also impressive. Figure 2.7b shows that the two sets of ODR values are linearly correlated with each other: the best linear fit yields a slope of 1.16 ± 0.01 and R^2 = 0.9986, confirming the accuracy of the app in determining the ODR values (which is comparable with well-established image processing software, e.g., Adobe Photoshop). It is also evident the uncertainties are smaller for when the mobile app was used, especially for smaller ODR values (e.g., < 0.6). More importantly, with this custom design app, a defined method to obtain grayscale values was implemented.

The mobile app platform was then tested with a direct biotin-streptavidin binding assay and the signals visualized using silver enhancement. The biotin-streptavidin system was chosen because its binding interactions have been well studied, and is known to bind with high affinity and specificity; more importantly, it has been shown to be a suitable model for many biorecognition interactions.[70–73] The assay was prepared on polycarbonate (PC) substrate as previously reported.[66] Briefly, the polycarbonate chip was activated by UV/ozone surface treatment, followed by immobilization of biotin via an amide coupling reaction. Streptavidin conjugated to a gold nanoparticle (Nanogold streptavidin conjugates) was then added before silver enhancement, nucleated by the nanoparticle, was performed to visualize the reaction. The resulting signals were gray in color (Fig. 2.2c), similar to that of the printed channels and are well-suited for grayscale analysis. ODRs are from triplicate samples of each Nanogold streptavidin concentration and were tested using the two platforms.

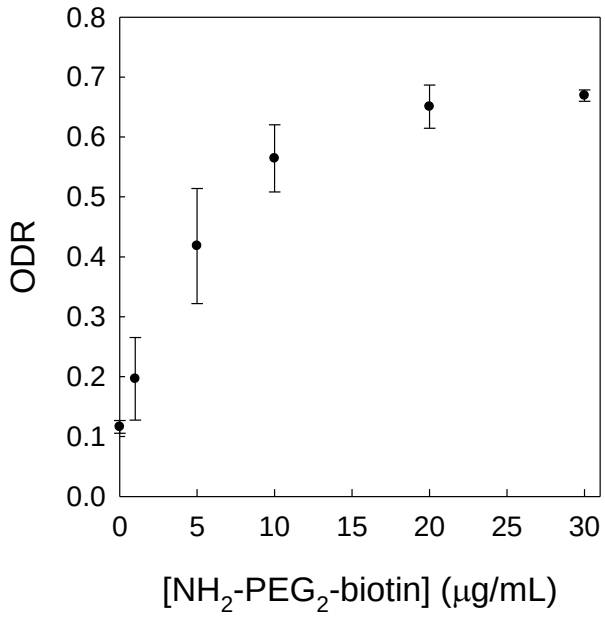

Figure 2.8. ODR as a function of the NH_2-PEG_2- biotin concentration in the initial test of biotin-streptavidin assay.

The concentration of biotin required to saturate the PC was first determined by performing the assay with different concentrations of the amine-terminated biotin molecule. In Fig. 2.8, using the same concentration of Nanogold streptavidin conjugates added prior to silver enhancement, it is clear that the binding signal (ODR) rises initially and then saturates around 20 μg/mL. An excess concentration of 30 μg/mL was used in all biotin-streptavidin assay experiments.

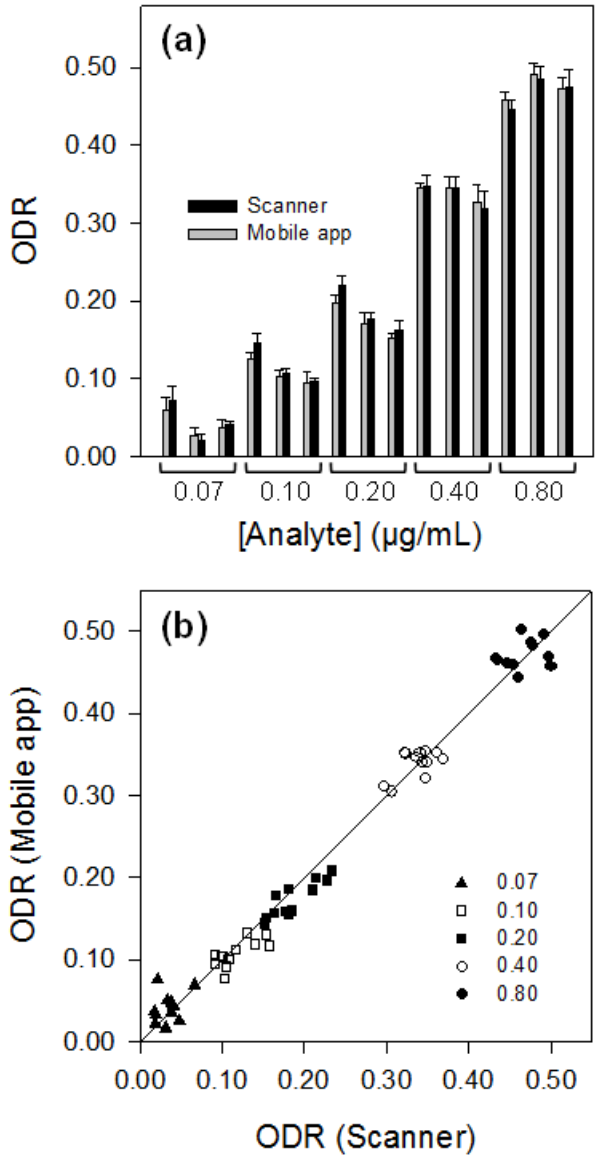

Figure 2.9. **Comparison of ODRs on a biotin-streptavidin assay as determined from the scanner and Mobile ODR app using the averaged grayscale intensities. (a) ODRs as a function of Nanogold streptavidin conjugate (analyte) concentration. Error bars are standard deviations from the four channels of each assay; (b) linear correlation between the ODRs from the scanner and Mobile ODR app. The data points are the individual ODRs of each channel from the three samples in (a).The legend denotes the concentrations of the Nanogold streptavidin conjugate (µg/mL).**

On a surface saturated with biotin, different concentrations of Nanogold streptavidin conjugates were tested. Figure 2.9a reveals that in these experiments, the scanner and app give consistent ODRs at all concentrations of the conjugate. At higher concentrations of Nanogold streptavidin (0.4 – 0.8 µg/mL), the Mobile ODR app provides ODRs that are slightly higher (between 0 and 3%) than those obtained by the scanner; while at lower concentrations (0.07- 0.2 µg/mL), app ODRs are on average 6% lower than scanner ODRs. Aside from this discrepancy, the data shows that not only within each sample is the silver enhanced signal reproducible, as indicated by the small error bars, but also that between samples of the same concentration, the signal can be considered very reproducible. To be more specific, we also generated a correlation plot by plotting the two against each other, i.e., the app ODRs as a function of the scanner ODRs (Figure 2.9b) to demonstrate that the Mobile app and scanner correlate well. The slope of the best linear fit is 0.9980 and R^2 = 0.9847. We must note that scattering of the points is likely not from errors in the ODR measurements (and therefore the grayscale intensities), but rather from variations in experimental parameters such as from the signal enhancement process and the silver particle size growth.

The Mobile ODR app is currently designed for Android platform and is simple to use: the user directs the app to the area of interest and taps the capture button to gain the results of the ODR. Because it can be installed on any user's smartphones or tablets, it makes the quantitative detection portable. Particularly, the results are immediately displayed, both ideal for POC diagnostics and on-site chemical analysis. It has been shown that the app's performance is comparable to that of desktop scanners, without the need for additional software to analyze the results, making it a suitable alternative to the current method of using bulky office scanner in conjunction with advanced image processing software. Although the app has its benefits, like all colorimetric assays, the ODR can be affected by the lighting and ambient conditions. On some level, because equation 8 accounts for the background intensity, the lighting conditions are relatively less significant, though for quantitation purposes, even lighting will be required across all areas of the sample and the results are only applicable if the sample is imaged under the same conditions as the calibration curve. As well, currently the user is required to align the sample to the alignment aids on the screen; the

development of an assay and algorithm for the app to automatically detect and zoom onto the assay region may be pursued in the future.

2.4. **Conclusion**

Mobile devices including smartphones and tablet computers, in conjunction with a custom developed app, have been shown to be an applicable platform for quantitative scanometric analysis, thus supporting its case for application in point-of-care diagnostics and on-site chemical analysis. Using the scanometric method of grayscale analysis, it is discovered that the ODRs determined from average and weighted grayscales are comparable to the traditional methods of using office scanners; however, the weighted (luminosity) grayscale approach provides better results with respect to the originally printed chart of different grayscale values, which was adapted in the development a mobile app for the data processing. The app yielded consistent ODRs to the office scanner for printed assays and when applied to a direct assay on a plastic substrate. Applying the app to immunoassays is demonstrated in Chapter 3.

Chapter 3.

Direct reading of bona fide barcode assays for diagnostics with smartphone apps*

This chapter reports the design and development of an assay that is formatted in the form of a linear barcode such that the results of the test can be scanned using a smartphone. Standard barcodes are briefly introduced and a sandwich immunoassay for human chorionic gonadotropin (hCG) is used to demonstrate practical applications of the method. Although barcode-reading abilities were added to the Mobile ODR app previously discussed, in the initial works, a freely available barcode app is used. In the case of a commercially available app, quantitative means are determined using the Mobile ODR app or other software.

3.1. Point-of-care medical diagnostics

Medical diagnostic tools (e.g., biosensors) respond to biochemical and physiological signals of interest and relay this information in the form of electrical or optical output, and thereby reliably diagnose diseases and illnesses.[74] As previously discussed in Chapter 1, these devices, however, while readily accessible in developed countries, are often costly and complex to the average untrained person, and not easily accessible in all regions of the world.[36] To aid in reducing global health care costs, point-

* Adapted from Wong, J.X.H.; Liu, F.S.F.; Li, X.; Yu, H.-Z. Direct reading of bona fide barcode assays for diagnostics with smartphone apps. *Sci. Rep*. **2015**, *5*, 11727. (CC BY 4.0, https://creativecommons.org/licenses/by/4.0/). Yu conceived the research; Wong designed and carried out the experiments; Li designed and conducted some preliminary experiments; Liu wrote the customized app; Wong and Yu wrote the manuscript.

of-care (POC) diagnostics aims to provide patients with rapid real-time clinical testing and treatment, primarily in developing countries which lack medical facilities. Diagnostic systems of this caliber must be inexpensive, easy to use and disposable due to limitations in trained personnel, infrastructure, medical instruments, and operational funds.[2,49] The trend toward low-cost instrumentation has led to the integration of apps with POC abilities, having been adapted for diseases detection;[2,36,49] the wireless system can relay patient information and test results to health professionals for further analysis if necessary. To date, POC devices already in use include glucose meters, pregnancy tests, and infectious disease tests which commonly employ strip testing using colorimetric, fluorescence, or electrochemical detection methods.[75,76] Detection methods employing mobile devices have been adapted to the traditional approaches; of these, colorimetric detection has been studied most thoroughly.[2,20,39,44,49,77–79] There is no doubt that the amount of interest in furthering this area of research, in colorimetric assays and other areas, is expected to rise substantially in coming years.[80]

Software development for mobile devices has also grown rapidly in recent years, with readily available public apps ranging from games, news to first aid guidance.[81] One such type of app that utilizes the phone cameras is the barcode scanner, commonly marketed for price comparisons and product review purposes. The barcode scanners decipher a series of bars and spaces to read the encoded data within. Conceptually different from the bio-barcode assays that utilize nanoparticle probes functionalized with encoding DNA or other specific binding components (i.e., antibodies),[82–87] herein, a barcode-formatted assay protocol that integrates the smartphone camera in reading the assay with standard barcode scanning apps is described. The objective is to design a *bona fide* barcode assay capable of both qualitative and quantitative analysis with a regular smartphone (no hardware and software driver modifications). In particular, the assay used is for the detection of analytes primarily of biomedical relevance (e.g., protein biomarkers), in which the pattern of the assay binding strips is styled in the manner of a common linear barcode such that it can be detected both visually by the naked eye and by a smartphone barcode scanner. The “data” in the barcode is the qualitative portion of the test, and the presence or absence of the analyte is determined by a barcode scanner app. Quantitation can be achieved directly on the same assay

using a scanometric method with the aid of the Mobile app of Chapter 2 or computer-based image analysis software.

3.1.1. Standard barcodes

Barcodes are optical representations of data; they consist of a series of bars and spaces, with varying widths, which can be scanned and deciphered by readers or scanners. Each character to be encoded within a barcode has a unique pattern of bars and spaces that is recognizable to the reader. Linear barcodes are available in many different types; in retail, the most commonly used is the U.P.C. (Universal Product Code), libraries prefer to use the Interleaved 2 of 5 system, and the E.A.N. 8 or 13 systems that is used in both retail and on books. Some barcode systems have yet to find widespread public usage, such as Code 39. Different elements are incorporated into different types of barcodes; some are limited to encoding of numbers, others are able to encode more characters, while some can encode more information within a particular area than others. There are two formats of encoding data into linear barcodes. In one method, the encoding of data is done so continuously; in other words, the pattern of each character in the barcode begins with a bar and ends with a space, with the next character's pattern beginning immediately after the last character's space. A discrete barcode on the other hand, begins and ends with a bar. A space is an added element used to separate between the last bar of one character and the first bar of the next, and is ignored by the scanner if it can read this particular barcode type. In order to encode the numerous possibility of characters (e.g., letters, numbers and special characters), barcodes, as previously mentioned, operate under a system of variable bars and widths; the patterns are not such that one letter has a single bar and another letter has two bars. Each character in a single barcode type have the same number of elements; for example, Code 39 (or Code 3 of 9) characters all have 5 bars and 4 spaces (9 elements, 3 of which are wide elements) that make up the code and it is the variation in the width of the bars and spaces in a particular pattern that codes for a character. The variation in patterns between characters allows for the design of a test such that depending on the result of the test, a different character can be generated.

Code 39 demonstrates a discrete barcode system where the widths of the bars and spaces are either narrow or wide. It can encode only the upper case letters (A-Z) of the Latin alphabet and the Arabic digits (0-9), in addition to 7 special characters (space, -, +, ., $, /, %). Of the 5 bars and 4 spaces, three of the nine elements are wide, and the remaining six are narrow. The concept of wide and narrow is defined by the relative widths of the bars and spaces to other bars and spaces; the ratio can be set between 2:1 and 3:1. The space between each character's first and last bars is typically narrow so as to not "end" the barcode as it appears to the scanner. At each end of the barcode is the symbol "*" which acts as the start and stop character to indicate to the scanner the direction of reading. A disadvantage of the 39 coding system is that it requires a greater area to encode a particular set of data compared to some of the previously mentioned linear coding types. As well, the system can be considered simplified as it does not employ a check character (that changes depending on the data encoded) as a method of checking the barcode in the event of the introduction of error during the barcode's transmission or storage. Although appearing to be slightly disadvantageous in this manner, the coding system still allows for a checking mechanism in that single misprint of a bar or space will not result in an erroneous reading because it would not encode for any characters; the scanner will act as if no barcode is present.

For the purpose of our assay development, Code 39 does have an advantage over some other linear systems, e.g., it offers two characters having almost identical barcodes, apart from 4 elements, as a result of not employing an individual checking character. The barcode encoding for the "-" and "+" symbols have the same start and stop characters, and are identical in the first 5 elements of the code; the differences are the last 4 elements where one has two narrow spaces neighboring two wide bars whereas the other has two wide spaces between the two narrow bars (Figure 3.1a).

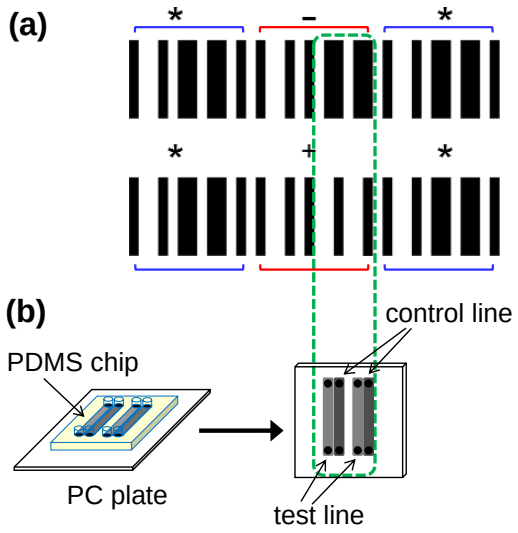

Figure 3.1. **(a) Barcodes of "-"and "+" symbols as created using Code 39. The two characters (highlighted with the red brackets above and below the barcodes) are identical apart from the 4 elements of each character (dashed green box); start and stop characters are denoted by "*" (highlighted with the blue brackets). (b) The design of the assay strips, as patterned using a microfluidic PDMS chip. The wide bars of the "-" character have been "divided" into four separate binding strips. The first and third serve as test lines while the second and fourth serve as control lines for the test. Barcodes are scanned by placing the PC plate atop a piece of paper with printed barcode, apart from the strips indicated in the green dash-line box. In a positive test, all channels will produce a visible signal that can be scanned, reading as "-", while in a negative test, only channels two and four will produce a signal, reading as "+".**

3.1.2. Barcode-formatted assay design

Using this Code 39 coding system, an assay can be designed to be in the exact format of a barcode and to elicit a color change such that upon binding (or lack of) an analyte, the species of interest, a different barcode symbol will be read. These barcode symbols in this case are the above-mentioned "-" and "+". Because the rest of the barcode is identical, rather than waste reagents, only the two bars, represented with 4 binding strips (Figure 3.1b), are used as the test platform and the remainder is printed on white paper using an office printer, creating a paper-hybrid assay. The brightness of the

paper will slightly alter the ODRs determined, therefore the paper with the start and stop characters used for reading the barcodes of the standards (used to generate the calibration curve) should be consistent with that of the unknown samples. A benefit of printing the additional bars is that the printed sections can act as a color (or grayscale) reference in the quantitative function of the test. Similar to lateral flow assays, the barcode assay here is conducted only in the test region where each of the two wide bars of "-" are "separated" into two narrow entities (Figure 3.1b) in which the first acts as a test line and the second as control line. In the control line, regardless of whether the intended antigen binds, a signal will appear and can be read by barcode scanner. The control serves as validity test; the absence of signal indicates that the test is invalid and the result is void. In the test region, a particular antibody is immobilized in the test line to capture the analyte; the presence of analyte will result in a visible signal following addition of the detection antibody and signal enhancement, thus allowing the scanner to read the barcode, provided the test is valid. Therefore, in the case of a positive test where both the test and control lines produce visible signals (represented as a wide bar), the reader will scan the test as "-". In the case of a valid negative test, "+" will appear due to signals only in the control lines (represented as a narrow bar). The test and control regions can then undergo quantitative analysis where measurements of antigens or analyte can be determined colorimetrically or scanometrically; that is, the intensity of the color or grayscale change as a result of the binding reactions of the second antibody to the analyte and signal enhancement process (silver staining) is compared to the intensity of the background color. This can be accomplished by scanning the samples (using a desktop scanner in the reflectance mode) into the computer as a RGB image for further processing using software (e.g., ImageJ). From the RGB image, the weighted averaged grayscale intensities are found and used to determine the ODR (equation 8).

I (grayscale)	255	245	235	225	215	204	194	184	174	163	153	143	133	122	112	103	92
ODR (preset)	0	0.04	0.08	0.12	0.16	0.20	0.24	0.28	0.32	0.36	0.40	0.44	0.48	0.52	0.56	0.60	0.64
ODR (measured)	0	0.03	0.10	0.16	0.22	0.25	0.25	0.29	0.33	0.38	0.43	0.45	0.49	0.51	0.53	0.56	0.58
Barcoding (+)	×	×	×	×	~	~	✓	✓	✓	✓	✓	✓	✓	✓	✓	✓	✓
Barcoding (-)	×	×	×	×	×	×	×	~	~	~	~	✓	✓	✓	✓	✓	✓

False negative region

Figure 3.2. Correlation between the preset grayscale values, the preset ODR, the measured ODR, and the reading capability by the barcode app. The test and control lines (Figure 3.1b, the four differential elements) were printed at the preset grayscale values and scanned to determine whether the barcode app could read the result; the remaining bars of the barcode (start, stop, and other elements of the "+" and "-" characters) are printed in black (I = 0).

To determine the detection range that the barcodes can encompass, a range of darkness intensities of barcodes for "-" and "+", with ODRs from 0-1 (grayscale values between 255 and 0 on an 8-bit grayscale), were printed (Figure 3.2) and tested with the mobile app XZing Barcode Scanner[88] (other free barcode reading apps can also be employed). It was found that when reading "+", the barcode with an ODR as low as 0.24 can be scanned, while with ODRs of approximately 0.16-0.20, successful barcode reading was intermittent or required longer time focusing and decoding. When trying to read "-", slightly higher ODRs are required (0.44). Similar to reading "+", there exists a range (ODRs between 0.28-0.40) where sporadic correct results occurred. As can be interpreted from the data, "-" is more difficult to decipher, creating a region of ODRs below 0.44 that can be considered as the false negative region due to the possibility of a positive assay having a low concentration of analyte that cannot produce a detectable signal by the barcode reading app.

3.2. **Proof of concept: biotin-streptavidin binding assay reading**

The biotin-streptavidin binding assay that was used to develop the app in Chapter 2, was used as a model system to evaluate the barcode assay principle because of its well-studied binding interactions; it is known to bind with high affinity ($K_a \approx 10^{15}$ M^{-1}) and specificity, thereby making it a suitable model for many bio-recognition interactions.[70–73]

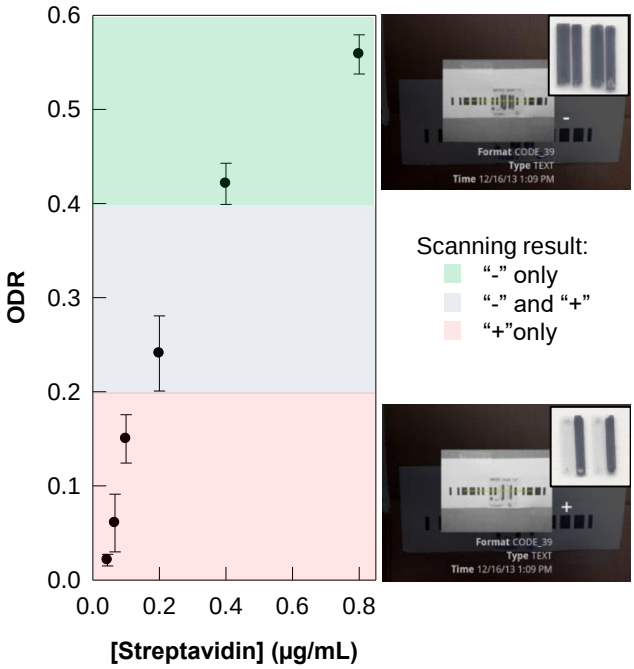

Figure 3.3. **Dependence of ODR on concentration of Nanogold streptavidin conjugate following silver enhancement for biotin-streptavidin assays prepared as "-" and "+." Scanning by the barcode app is done by placing the PC plate atop a sheet of white paper with the remainder of the barcode printed on it. The different highlighting colors in the plot indicate their feasibility to be scanned by the barcode app: the "-" character can be readily scanned in the green zone, "+"is readable in the pink, and neither is read by the app in the gray zone.**

The particular pattern of lines in Chapter 2 was designed with the barcode pattern in mind. Figure 3.3 shows how the particular ODRs at particular concentrations scan using a barcode app. Here, the increasing ODR trend is evident, with the signal reaching saturation between an ODR of 0.50-0.60, which corresponds to high concentrations (0.8 µg/mL) of the conjugate. At concentrations at or above 0.40 µg/mL of the conjugate, both "-" and "+" barcodes can be read by the scanner app. For the "+" barcode, as predicted from previous results, even low concentrations down to 0.20 µg/mL, "+" can be read; concentrations below 0.20 µg/mL can still be analyzed, but cannot be read by the scanner app for its encoded character.

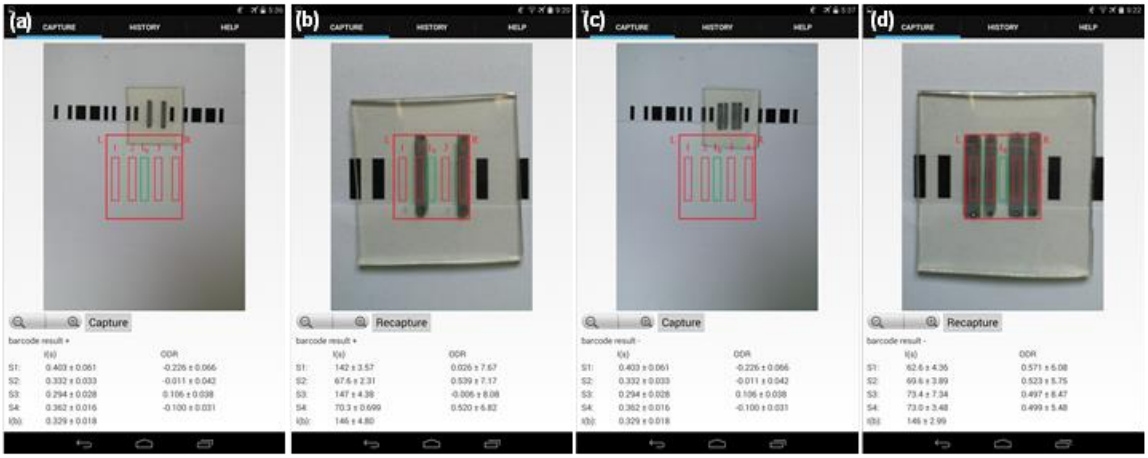

Figure 3.4. Scanning of the assays with the customized app for (a) the encoded barcode result of "+" before (b) ODR analysis; and (c) the result of the "-" assay and the (d) ODR analysis of the four binding strips. The assays presented here are for hCG at 20 mIU/mL.

To improve the general analysis method, particularly the ability to read the barcodes, the developed an app in Chapter 2 was modified to scan barcodes in addition to analyzing the darkness intensities of the channels (Figure 3.4). This revised, customized app is more versatile than the free app because it is capable of obtaining both qualitative and quantitative information. Specifically, the app first scans the barcode for the encoded data, providing live feedback (Figure 3.4a, c). The user then positions the channels to obtain the ODR values (Figure 3.4b, d). By encoding the assays, this also introduces the possibility of multiplexing (*vide infra*).

3.3. Real-world application: hCG detection and potential multiplexing

3.3.1. Human chorionic gonadotropin

Human chorionic gonadotropin, or hCG, is a hormone produced mainly during pregnancy, with low levels present as well in males and non-pregnant women (0.5 IU/L). It consists of two non-covalently linked subunits, hCGα and hCGβ (Fig. 3.5a, b). As a pregnancy progresses, hCG levels in the blood and in urine vary (Fig. 3.5c). When qualitatively detected, hCG identifies a patient as pregnant, and when concentrations are quantitatively determined, this may also indicate anomalies in the pregnancy.[89–92] Quantitative hCG tests have the advantage of being more sensitive and being so allows it to be used to identify false positive serum hCG tests in non-pregnant women (that are exposed to interfering anti-animal antibodies), to detect biochemical pregnancies (pregnancies where implantation occurs briefly before it fails), and to detect normal pregnancies earlier than with qualitative tests.[93]

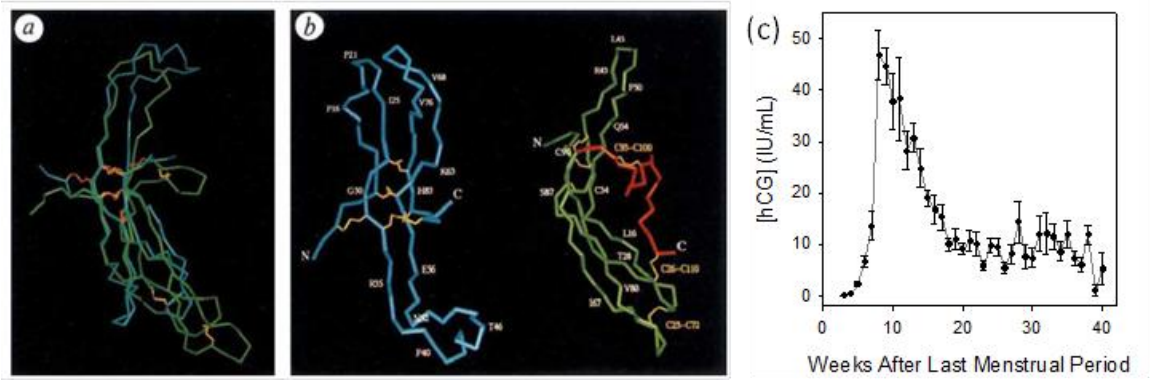

Figure 3.5. Structure of hCG shown as (a) heterodimer; (b) hCG α (blue) and hCGβ (green) subunits. (c) hCG levels over the pregnancy period.

Note. (a) and (b) Reprinted with permission from Lapthorn, A. J.; Harris, D. C.; Littlejohn, A.; Lustbader, J. W.; Canfield, R. E.; Machin, K. J.; Morgan, F. J.; Isaacs, N. W. *Nature* 1994, 369, 455-461. Copyright 1994 Nature Publishing Group.

The most commonly used hCG test is found in home pregnancy test kits and is the lateral flow immunoassay previously shown in Fig. 1.10b (Section 1.2.2), which consists of three sets of antibodies. In the reaction zone, analyte-binding monoclonal antibodies (mouse anti-hCG antibodies) are labeled with colloidal gold. In the presence of the target, the antibodies in the reaction zone bind to the target and the complexes flow to the test line where the antibody immobilized there also binds to the analyte at a different epitope, forming a sandwich structure with the complex. Any free antibodies, either excess antibodies that did not bind to the target or those that were not captured at the test line, are captured by anti-mouse antibodies immobilized at the control line. For a positive test, two pink lines appear due to the aggregation of the colloidal gold nanoparticles at both the test and control lines. For a negative test, the colloidal gold labels are only found at the control line; the control line therefore serves as a validity test for the assay and appears regardless of the test result. This type of POC test is purely qualitative; therefore there is a need for the development of a quantitative hCG assay.

3.3.2. hCG assay method

A schematic representation of the assay is shown in Fig. 3.6. As with the previously described biotin-streptavidin assay protocol in Section 2.2.3, the PC plate was activated before a PDMS chip with microfluidic channels was adhered to the surface. Into each of the channels, anti-αhCG antibody (50 µg/mL, in 10 mM phosphate buffer with 150 mM NaCl, 5% glycerol, at pH 7.4) was added and allowed to immobilize on the surface for an hour. The surface was then passivated with 10 mM PBS buffer containing 2% BSA and 0.5% Tween 20 at pH 6.0 for 2 h to prevent non-specific binding. Channels were then rinsed with 10 mM PBS buffer (with 0.5% Tween 20); the introduction of an hCG-containing solution to the channels (incubation period of an hour at room temperature, diluted with 10 mM PBS buffer) would allow binding between hCG and the antibody immobilized on the surface. The second antibody required in the sandwich assay is biotinylated anti-βhCG (0.1 µg/mL) which was added to the channels of the PDMS and remained for one hour at room temperature before rinsing. Nanogold streptavidin conjugates (0.8 µg/mL) were then added and incubated for 50 min, before the silver staining treatment. The same concentrations of solutions and staining time are used for

the hCG assay as the biotin-streptavidin assay (the stain begins to appear between 5-6 min in this case). The signal detection and analysis were also performed in a same way as the biotin-streptavidin assay using the same smartphone app and/or scanner. The concentration of the analyte was determined by obtaining an image of the barcode and an analysis of the optical density ratio relative to that of a standard curve.

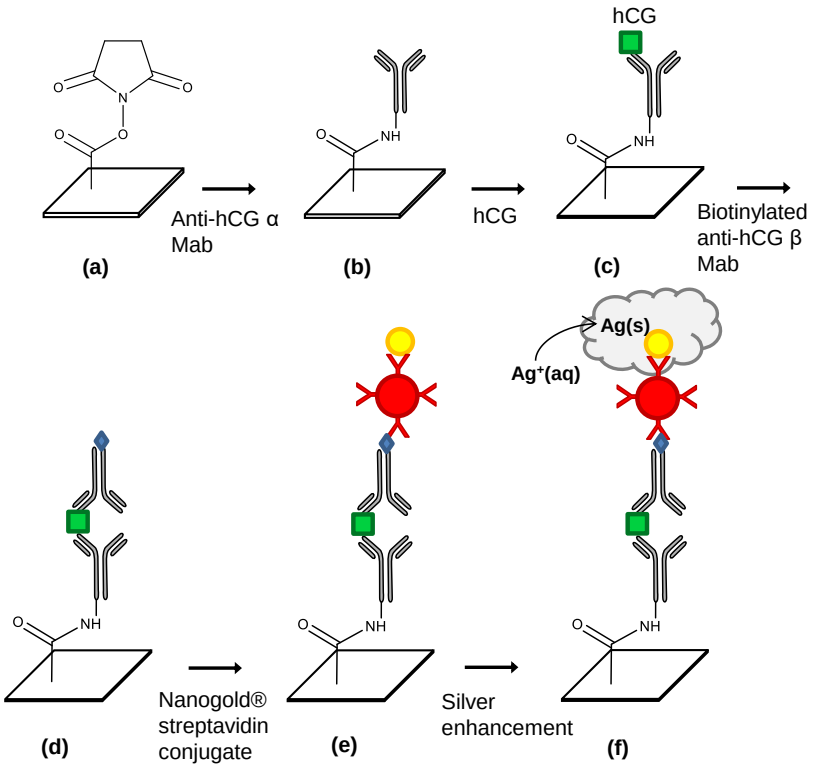

Figure 3.6. **Preparation of the sandwich immunoassay for hCG performed on the polycarbonate (PC) substrate. On an activated PC (a), a monoclonal antibody specific for the α subunit of hCG is immobilized on the surface (b). The target, hCG, binds (c) and another monoclonal antibody, conjugated to biotin, and specific for the β subunit of the hCG is added (d). The Nanogold streptavidin conjugate is added (e) before silver enhancement is used to visualize the signal (f). In the case of the direct biotin-streptavidin assay, NH_2-PEG_2-biotin is added after the surface activation steps; no antibodies are added. Nanogold streptavidin and silver enhancement is also used.**

3.3.3. Barcode assays of hCG

The preparation of the hCG assay on the PC substrate is similar to a standard sandwich-format immunoassay (Figure 3.6), with gold nanoparticle-promoted silver deposition used to visualize the signal. As expected, the ODR increases as the concentration of hCG increases, reaching saturation at 15 mIU/mL (Figure 3.7). Using the free barcode app, hCG assays as low as 5 mIU/mL for a positive test ("-") can be scanned, while using the custom app, no limitations apply, i.e. low ODRs provide enough contrast between the bars and spaces to be scanned by the app. Therefore, even concentrations below 2.0 mIU/mL can be detected.

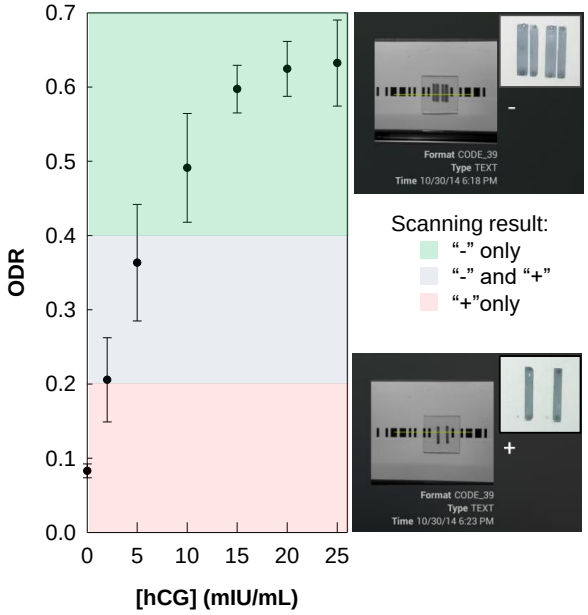

Figure 3.7. Quantitation of hCG with the barcode assay protocol; ODR as a function of hCG concentration. Tests are performed in triplicate; the errors are the standard deviations of the repeated.

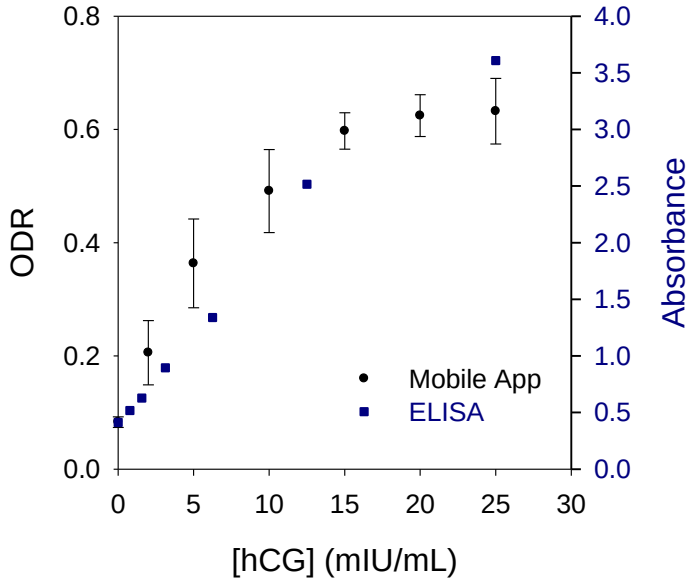

Figure 3.8. Comparison of hCG assay with Mobile App and ELISA (blue).

As it was previously shown in Chapter 2 that the performance of the app for a bioassay is comparable to the scanner, the ODR results of the hCG assay from the app was also compared to the standard testing method of ELISA (Fig. 3.8). In both cases, there is a slight signal associated with the background, but for the app-based ODR method, the signal begins to saturate early (10-15 mIU/mL) and levels off by 25 mIU/mL, while for ELISA the linear region expands a slightly greater range of concentrations (up to 15-20 mIU/mL). At the tested concentrations, the absorbance is nears saturation but has not completely leveled off. (As we continue to work to improve the range of the method by optimization of various conditions, particularly in the silver enhancement protocol, one possible alternative could be the use of the app-based method as a screening tool for low concentrations of hCG before an ELISA test is performed. Another alternative is simply diluting samples that exceed the detectable signal range such that the ODR result fits within the calibration range of the app; the actual concentration can then be determined from the dilution factor. Nonetheless, it should be noted that even with the lower sensitivity, regardless of the app used for detection, hCG concentrations up to 25 mIU/mL can be quantitated, which is comparable with the rapid, lateral flow pregnancy tests ("pee on a stick" tests) whose limits of detection are usually between 5.5 and 100 mIU/mL,[94,95] although as technology evolves, this detection limit will surely decrease. These low concentrations can be used as early indicators of pregnancy.

Another aspect of the system that has been tested is its specificity, which has been tested preliminarily with two hormones related to hCG, namely, thyroid-stimulating hormone (TSH) and follicle-stimulating hormone (FSH). TSH and FSH share an essentially identical α subunit with hCG,[96] but vary in the β subunits. This suggests that while each can bind to the capture antibody, the detection antibody would not bind, and therefore no signal should be observed. The results support this hypothesis as when the two hormones were tested, the obtained ODRs for TSH (0.07 ± 0.02) and FSH (0.05 ± 0.02) were not much different from that of the blank signal (no hCG, 0.04 ±0.01). TSH and FSH concentrations in the experiments were chosen to be on the high end of the normal range, at 15 μIU/mL and 25 mIU/mL, respectively.

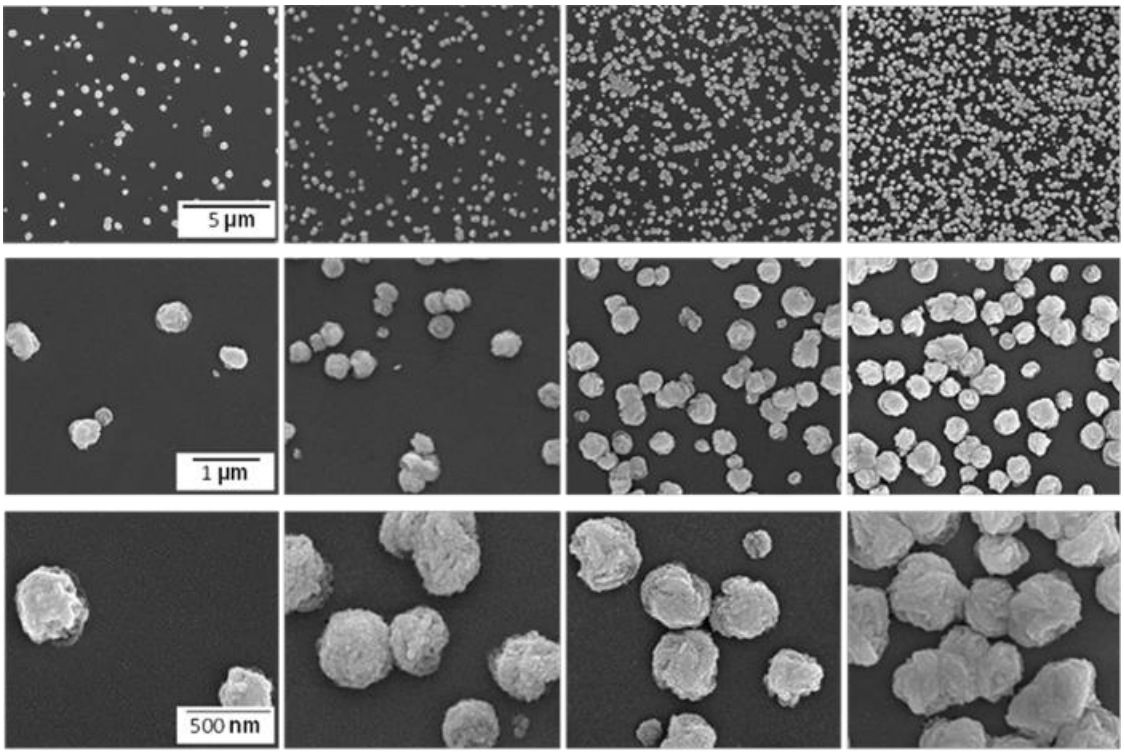

Figure 3.9. SEM images of hCG assay at different concentrations of hCG (from left to right: 0, 3.5, 10, 20 mIU/mL) and at different magnifications. The scale bar applies to the images within the row.

When the samples were imaged under a scanning electron microscope (SEM), the result of the silver deposition was observed. The PC surface was covered with small, uneven particles of approximately 300 nm in size. The particle surfaces were textured

(i.e. not smooth) and as expected, as the concentration of hCG increased (from 0 to 20 mIU/mL), there was an increase in both particle density and a general decrease in particle size. At low concentrations, the particles were distributed across the surface, while at higher concentrations, the particles tended to form aggregations, thereby increasing the total particle size.

3.3.4. Multiplexing barcodes

Typically, a test for a single marker is considered insufficient, or multiple markers can lead to early clinical diagnosis of diseases and disorders since numerous markers are usually indicative of issues.[97–99] For example, a combination of 4 markers, namely hCG, alpha-fetoprotein (AFP), unconjugated estriol (uE_3), and inhibin A, is currently used to screen for Down Syndrome during pregnancy using sera from the mother.[90,97] A multiplexing system is possible for the barcode assay protocol. Due to the nature of Code 39, we can extend the barcode to test for more than one analyte. Apart from the "-" and "+" characters, "$" and "F" also share a similar format (Fig.3.10). To multiplex, a test for one analyte is done using the -/+ characters, while another analyte would use the $/F characters. It is possible to test further for an increasing number of analytes with repetition of any of these characters, or addition of different ones with similar formatting.

An alternative multiplexing possibility would be to use two (or more) characters for each analyte in series, whereby the first character (e.g. a letter) would designate the target, while the second character would use the "+/-" system to indicate the presence or absence of the analyte. These pairs of characters would be scanned by the barcode app as "A+", "B-", which would allow users to easily determine the results, particularly if a highly multiplexed test was conducted. In that case, users would be able to identify the test result of the n^{th} target simply based on the first character's designation, without having to track the results of which assay corresponded to the n^{th} test.

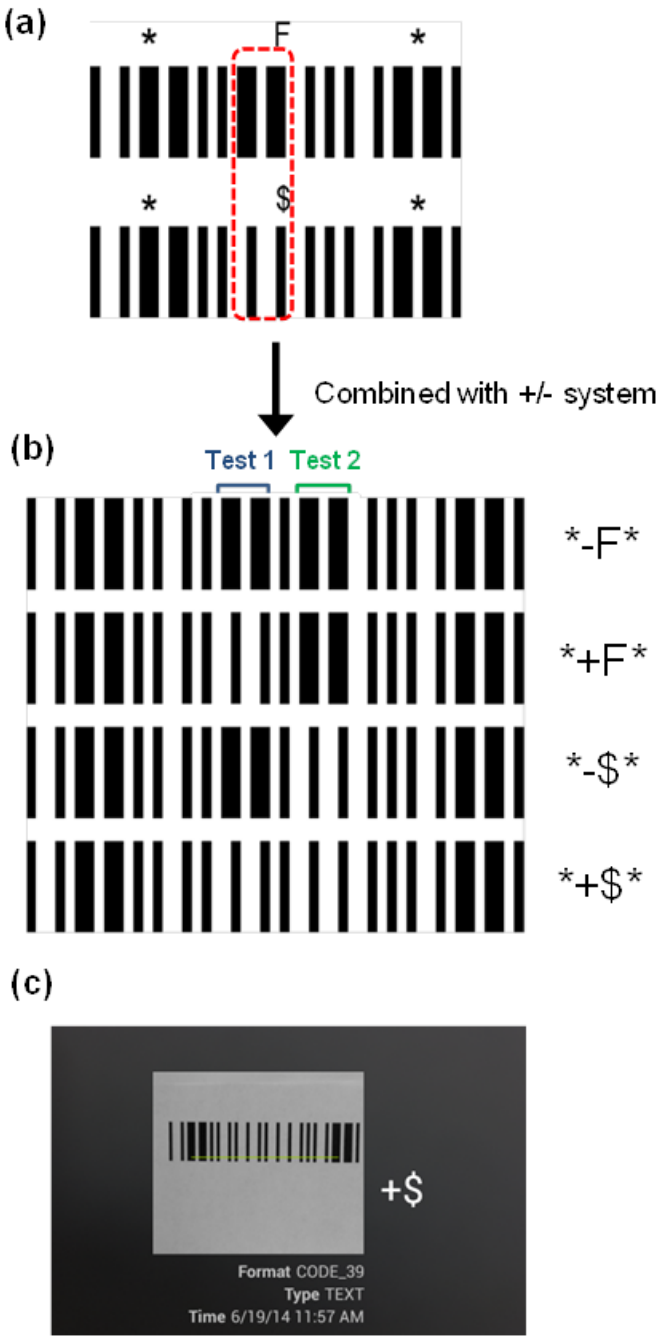

Figure 3.10. **(a) Similarities between the "F" and "$" codes. (b) Possible combinations of the − /+ and $/F barcodes. One analyte is tested with the + /− (Test 1, blue bracket) characters, another one with the F/$ (Test 2, green bracket) characters. Additional analytes require further extension of the barcode using the same − /+ , $/F codes or others. (c) Reading of the combined barcode for "+ $" with a free app.**

3.4. **Conclusion**

The app we have developed can both scan the barcodes for the encoded character and quantify the binding strips after signal enhancement based on the ODR, albeit in two separate steps. A multiplexing version, is in a preferred form, would allow the user to indicate the number of assays to be analyzed by the app. The current system, however, has first been employed on a PC plate for a single test, but along with the app, other substrates (e.g., paper, glass, and other polymeric materials) are being studied as future perspectives for the work. While the PC barcode assay test now is relatively low cost (approximately $0.20 per test, including all reagents and PC), substrates such as paper can be considered more ideal in that they are readily available, inexpensive, disposable, and simpler to work with. With colorimetric tests, the contrast between the white background and the colored portions of the reactions can easily be observed, providing for easier color intensity analysis after imaging with the camera on mobile phone.[2]

Because the assay shown here for hCG is a proof-of-concept, only a single analyte was used. For different targets, even in low multiplexed assays of our barcode sort, it may be simpler to count the number of channels, similar to that of a lateral flow pregnancy test strip. At highly multiplexed assays however, scanning for the encoded data offers a more practical approach. For multiplexed assays, we would be able to test a series of related targets (e.g. different pregnancy hormones in urine) and obtain results simultaneously. An advantage of this method, whether they be a single assay or highly multiplexed, is that the app can immediately quantify the amount of target present in the sample based on the ODR, which has been shown previously to be comparable to standard scanometric methods.[100] The scanometric method by desktop scanner and ODR, particularly for hCG, has also been shown here and via an alternative disc-based method, to be consistent with the ELISA method.[101] When compared to these, the barcode-smartphone approach is considerably more portable, commonly available, and lower cost (since it does not require any specialized instrumentation such as a plate reader), and has similar assay preparation time as ELISA.

It should be mentioned that at the same time that this barcode-formatted hCG assay was published, a research group independently reported a microfluidic-based test, also for bioassays and patterned in the form of a linear barcode.[102] Using the Codabar coding system, Zhang et al. designed a PDMS channel plate with microfluidic channels capable of conducting 20 tests in parallel, which is analogous to the proposed multiplexing. The assay principle for barcode reading is predominantly based on the same logic as the Code 39 barcode assays, although in the work of Zhang et al.,[102] no additional lines are required to be printed; the 6 channels make up the entirety of the test, with 2 lines used as the test lines and the remaining 4 as the control. As it turns out, the coding system the authors opted for is simpler than that of Code 39. Nevertheless, as the two works were published at the same time, this undoubtedly demonstrates that other researchers are too striving to develop app-based POC devices.

Chapter 4.

Concluding remarks and future work

In summary, a smartphone-readable, *bona fide* barcode assay has been demonstrated. Using a custom app, the assay was first shown using a direct biotin-streptavidin assay before being applied to the pregnancy hormone, hCG. The linear barcode assay is both qualitative and quantitative when scanned and imaged using a smartphone-app combination, and requires no external accessories, thereby highlighting its potential to boost the research and development of POC devices, particularly by minimizing the need for specialized instrumentation and providing instant testing results on-site.

The presented method meets the ASSURED characteristics set by the WHO in that both the device and tests are affordable and portable. The assay and app are easy to use and the results for each test are available within a short timeframe. While the method is not necessarily equipment-free, WHO notes that the target specification of this characteristic is to be compact, battery powdered and be able to provide on-site data analysis of tests, all of which accomplished by barcode assays. In terms of sensitivity and specificity, for the particular case of hCG analysis, the assay has been shown to be specific and have specificity that is on the same order of magnitude as ELISA.

Even so, further improvements of the app can be done in the future, particularly for it to be an all-in-one, single scan, qualitative and quantitative platform on a smartphone. For example, an additional feature can be implemented into the app to reduce confusion to users surrounding the positive and negative results of a tests scanning as “-” and “+” characters respectively; users would be able to select the test type (e.g., positive or negative assay) and the corresponding result would be displayed.

Additional improvements include the tuning of the minimum detectable ODR such that the barcode scanning is possible while still maintaining low detection limits. An alternative color space may be one possibility to expand the detectable range of the analyte as others have reported previously owing to the one dimensionality of grayscale as opposed to, for example, HSL, which has better correlation to colorimetric changes as a result of concentration changes.

Another inconvenience currently is the need for consistent lighting to be provided across all assay strips as any inconsistencies such as glare or preferential lighting (i.e. from left or right sides instead of directly from the top) can lead to errors in the ODR reading. As equation 8 takes into account the intensity of the background, variable lighting is reduced to some extent. An additional option is to implement a lighting-correction algorithm to the app, such as that reported by Hong and Chang.[45] This and other improvements that aid the user (e.g. alignment aids on the PC to help the app self-recognize signal strips) are future directions that could be implemented in an improved version of the app.

One major future direction for the project would be the design of the barcode-readable assays with two-dimensional, or matrix, barcodes (the most commonly known is the QR code). Two-dimensional (2D) barcodes implement an error correction element (typically the Reed-Solomon error correction algorithm). The barcode assay method used in this thesis, where the test line and control lines are independent of each other, would be difficult to use in the 2D barcodes. That is not to say that it is impossible however; the error correction element may be used advantageously by deleting elements (intentionally “damaging” the 2D barcode) such that the assay relies on fewer elements in the code. Furthermore, as 2D barcodes can be generated with different levels of error correction capability, selecting the lowest level of error correction would help in the design of the assay.

References

(1) Smartphone Ownership and Internet Usage Continues to Climb in Emerging Economies | Pew Research Centre http://www.pewglobal.org/2016/02/22/smartphone-ownership-and-internet-usage-continues-to-climb-in-emerging-economies/ (accessed May 10, 2016).

(2) Martinez, A. W.; Phillips, S. T.; Carrilho, E.; Thomas III, S. W.; Sindi, H.; Whitesides, G. M. Simple Telemedicine for Developing Regions: Camera Phones and Paper-Based Microfluidic Devices for Real-Time, Off-Site Diagnosis. *Anal. Chem.* **2008**, *80*, 3699–3707.

(3) Lu, Y.; Shi, W.; Qin, J.; Lin, B. Low Cost, Portable Detection of Gold Nanoparticle-Labeled Microfluidic Immunoassay with Camera Cell Phone. *Electrophoresis* **2009**, *30*, 579–582.

(4) Veigas, B.; Jacob, J. M.; Costa, M. N.; Santos, D. S.; Viveiros, M.; Inácio, J.; Martins, R.; Barquinha, P.; Fortunato, E.; Baptista, P. V. Gold on Paper-Paper Platform for Au-Nanoprobe TB Detection. *Lab Chip* **2012**, *12*, 4802–4808.

(5) Shen, L.; Hagen, J. A.; Papautsky, I. Point-of-Care Colorimetric Detection with a Smartphone. *Lab Chip* **2012**, *12*, 4240–4243.

(6) Noor, M. O.; Krull, U. J. Camera-Based Ratiometric Fluorescence Transduction of Nucleic Acid Hybridization with Reagentless Signal Amplification on a Paper-Based Platform Using Immobilized Quantum Dots as Donors. *Anal. Chem.* **2014**, *86*, 10331–10339.

(7) Noor, M. O.; Hrovat, D.; Moazami-Goudarzi, M.; Espie, G. S.; Krull, U. J. Ratiometric Fluorescence Transduction by Hybridization after Isothermal Amplification for Determination of Zeptomole Quantities of Oligonucleotide Biomarkers with a Paper-Based Platform and Camera-Based Detection. *Anal. Chim. Acta* **2015**, *885*, 156–165.

(8) Petryayeva, E.; Algar, W. R. Multiplexed Homogeneous Assays of Proteolytic Activity Using a Smartphone and Quantum Dots. *Anal. Chem.* **2014**, *86*, 3195–3202.

(9) Melton, L. Protein Arrays: Proteomics in Multiplex. *Nature* **2004**, *429*, 101–107.

(10) Vignali, D. A. A. Multiplexed Particle-Based Flow Cytometric Assays. *J. Immunol. Methods* **2000**, *243*, 243–255.

(11) Klasner, S. A.; Price, A. K.; Hoeman, K. W.; Wilson, R. S.; Bell, K. J.; Culbertson, C. T. Paper-Based Microfluidic Devices for Analysis of Clinically Relevant Analytes Present in Urine and Saliva. *Anal. Bioanal. Chem.* **2010**, *397*, 1821–1829.

(12) Cheng, X.; Dai, D.; Yuan, Z.; Peng, L.; He, Y.; Yeung, E. S. Color Difference Amplification between Gold Nanoparticles in Colorimetric Analysis with Actively Controlled Multiband Illumination. *Anal. Chem.* **2014**, *86*, 7584–7592.

(13) Cantrell, K.; Erenas, M. M.; De Orbe-Payá, I.; Capitán-Vallvey, L. F. Use of the Hue Parameter of the Hue, Saturation, Value Color Space as a Quantitative Analytical Parameter for Bitonal Optical Sensors. *Anal. Chem.* **2010**, *82*, 531–542.

(14) Lopez-Ruiz, N.; Curto, V. F.; Erenas, M. M.; Benito-Lopez, F.; Diamond, D.; Palma, A. J.; Capitan-Vallvey, L. F. Smartphone-Based Simultaneous pH and Nitrite Colorimetric Determination for Paper Microfluidic Devices. *Anal. Chem.* **2014**, *86*, 9554–9562.

(15) Zhou, G.; Mao, X.; Juncker, D. Immunochromatographic Assay on Thread. *Anal. Chem.* **2012**, *84*, 7736–7743.

(16) Doeven, E. H.; Barbante, G. J.; Kerr, E.; Hogan, C. F.; Endler, J. A.; Francis, P. S. Red-Green-Blue Electrogenerated Chemiluminescence Utilizing a Digital Camera as Detector. *Anal. Chem.* **2014**, *86*, 2727–2732.

(17) Mentele, M. M.; Cunningham, J.; Koehler, K.; Volckens, J.; Henry, C. S. Microfluidic Paper-Based Analytical Device for Particulate Metals. *Anal. Chem.* **2012**, *84*, 4474–4480.

(18) Lebiga, E.; Edwin Fernandez, R.; Beskok, A. Confined Chemiluminescence Detection of Nanomolar Levels of H2O2 in a Paper–plastic Disposable Microfluidic Device Using a Smartphone. *Analyst* **2015**, *140*, 5006–5011.

(19) Delaney, J. L.; Doeven, E. H.; Harsant, A. J.; Hogan, C. F. Use of a Mobile Phone for Potentiostatic Control with Low Cost Paper-Based Microfluidic Sensors. *Anal. Chim. Acta* **2013**, *790*, 56–60.

(20) Coskun, A. F.; Wong, J.; Khodadadi, D.; Nagi, R.; Tey, A.; Ozcan, A. A Personalized Food Allergen Testing Platform on a Cellphone. *Lab Chip* **2013**, *13*, 636–640.

(21) Zhu, H.; Sikora, U.; Ozcan, A. Quantum Dot Enabled Detection of Escherichia Coli Using a Cell-Phone. *Analyst* **2012**, *137*, 2541–2544.

(22) Berg, B.; Cortazar, B.; Tseng, D.; Ozkan, H.; Feng, S.; Wei, Q.; Chan, R. Y. L.; Burbano, J.; Farooqui, Q.; Lewinski, M.; *et al.* Cellphone-Based Hand-Held Microplate Reader for Point-of-Care Testing of Enzyme-Linked Immunosorbent Assays. *ACS Nano* **2015**, *9*, 7857–7866.

(23) Soldat, D. J.; Barak, P.; Lepore, B. J. Microscale Colorimetric Analysis Using a

Desktop Scanner and Automated Digital Image Analysis. *J. Chem. Educ.* **2009**, *86*, 617–620.

(24) P, D. A.; Sankaran, K.; Muttan, S. An Image Based Microtiter Plate Reader System for 96-Well Format Fluorescence Assays. **2013**, *9*, 58–68.

(25) McGeough, C. M.; O'Driscoll, S. Camera Phone-Based Quantitative Analysis of c-Reactive Protein Elisa. *IEEE Trans. Biomed. Circuits Syst.* **2013**, *7*, 655–659.

(26) Vashist, S. K.; van Oordt, T.; Schneider, E. M.; Zengerle, R.; von Stetten, F.; Luong, J. H. T. A Smartphone-Based Colorimetric Reader for Bioanalytical Applications Using the Screen-Based Bottom Illumination Provided by Gadgets. *Biosens. Bioelectron.* **2015**, *67*, 248–255.

(27) Su, K.; Zou, Q.; Zhou, J.; Zou, L.; Li, H.; Wang, T.; Hu, N.; Wang, P. High-Sensitive and High-Efficient Biochemical Analysis Method Using a Bionic Electronic Eye in Combination with a Smartphone-Based Colorimetric Reader System. *Sens. Actuators, B* **2015**, *216*, 134–140.

(28) Wei, Q.; Qi, H.; Luo, W.; Tseng, D.; Ki, S. J.; Wan, Z.; Gorocs, Z.; Bentolila, L. A.; Wu, T.-T.; Sun, R.; *et al.* Fluorescent Imaging of Single Nanoparticles and Viruses on a Smart-Phone. *ACS Nano* **2013**, 130909100631007.

(29) Wei, Q.; Luo, W.; Chiang, S.; Kappel, T.; Mejia, C.; Tseng, D.; Chan, R. Y. L.; Yan, E.; Qi, H.; Shabbir, F.; *et al.* Imaging and Sizing of Single DNA Molecules on a Mobile Phone. *ACS Nano* **2014**, *8*, 12725–12733.

(30) Breslauer, D. N.; Maamari, R. N.; Switz, N. A.; Lam, W. A.; Fletcher, D. A. Mobile Phone Based Clinical Microscopy for Global Health Applications. *PLoS One* **2009**, *4*, e6320.

(31) Zhu, H.; Mavandadi, S.; Coskun, A. F.; Yaglidere, O.; Ozcan, A. Optofluidic

Fluorescent Imaging Cytometry on a Cell Phone. *Anal. Chem.* **2011**, *83*, 6641–6647.

(32) Switz, N. A.; D'Ambrosio, M. V.; Fletcher, D. A. Low-Cost Mobile Phone Microscopy with a Reversed Mobile Phone Camera Lens. *PLoS One* **2014**, *9*, e95330.

(33) Phillips, Z. F.; D'Ambrosio, M. V.; Tian, L.; Rulison, J. J.; Patel, H. S.; Sadras, N.; Gande, A. V.; Switz, N. A.; Fletcher, D. A.; Waller, L. Multi-Contrast Imaging and Digital Refocusing on a Mobile Microscope with a Domed LED Array. *PLoS One* **2015**, *10*, 1–13.

(34) Skandarajah, A.; Reber, C. D.; Switz, N. A.; Fletcher, D. A. Quantitative Imaging with a Mobile Phone Microscope. *PLoS One* **2014**, *9*.

(35) D'Ambrosio, M. V.; Bakalar, M.; Bennuru, S.; Reber, C.; Skandarajah, A.; Nilsson, L.; Switz, N.; Kamgno, J.; Pion, S.; Boussinesq, M.; *et al.* Point-of-Care Quantification of Blood-Borne Filarial Parasites with a Mobile Phone Microscope. *Sci. Transl. Med.* **2015**, *7*, 286re4.

(36) Smith, Z. J.; Chu, K.; Espenson, A. R.; Rahimzadeh, M.; Gryshuk, A.; Molinaro, M.; Dwyre, D. M.; Lane, S.; Matthews, D.; Wachsmann-Hogiu, S. Cell-Phone-Based Platform for Biomedical Device Development and Education Applications. *PLoS One* **2011**, *6*, e17150.

(37) Bogoch, I. I.; Andrews, J. R.; Speich, B.; Utzinger, J.; Ame, S. M.; Ali, S. M.; Keiser, J. Short Report: Mobile Phone Microscopy for the Diagnosis of Soil-Transmitted Helminth Infections: A Proof-of-Concept Study. *Am. J. Trop. Med. Hyg.* **2013**, *88*, 626–629.

(38) Sung, Y.-L.; Jeang, J.; Lee, C.-H.; Shih, W.-C. Fabricating Optical Lenses by Inket Printing and Heat-Assited in Situ Curing of Polydimethylsiloxane for Smartphone

Microscopy. *J. Biomed. Opt.* **2015**, *20*, 047005.

(39) Mudanyali, O.; Dimitrov, S.; Sikora, U.; Padmanabhan, S.; Navruz, I.; Ozcan, A. Integrated Rapid-Diagnostic-Test Reader Platform on a Cellphone. *Lab Chip* **2012**, *12*, 2678–2686.

(40) Lee, S.; Oncescu, V.; Mancuso, M.; Mehta, S.; Erickson, D. A Smartphone Platform for the Quantification of Vitamin D Levels. *Lab Chip* **2014**, *14*, 1437–1442.

(41) Oncescu, V.; O'Dell, D.; Erickson, D. Smartphone Based Health Accessory for Colorimetric Detection of Biomarkers in Sweat and Saliva. *Lab Chip* **2013**, *13*, 3232–3238.

(42) Oncescu, V.; Mancuso, M.; Erickson, D. Cholesterol Testing on a Smartphone. *Lab Chip* **2014**, *14*, 759–763.

(43) Fosdick, L. S.; Starke, a. C. Solubility of Tooth Enamel in Saliva At Various pH Levels. *J. Dent. Res.* **1939**, *18*, 417–430.

(44) Yetisen, A. K.; Martinez-Hurtado, J. L.; Garcia-Melendrez, A.; da Cruz Vasconcellos, F.; Lowe, C. R. A Smartphone Algorithm with Inter-Phone Repeatability for the Analysis of Colorimetric Tests. *Sens. Actuators, B* **2014**, *196*, 156–160.

(45) Hong, J. Il; Chang, B.-Y. Development of the Smartphone-Based Colorimetry for Multi-Analyte Sensing Arrays. *Lab Chip* **2014**, *14*, 1725–1732.

(46) Helistrom, I.; Raycraft, J.; Hayden-Ledbetter, M.; Ledbetter, J. A.; Schummer, M.; McIntosh, M.; Drescher, C.; Urban, N.; Hellstrom, K. E. The HE4 (WFDC2) Protein Is a Biomarker for Ovarian Carcinoma. *Cancer Res.* **2003**, *63*, 3695–3700.

(47) Molina, R.; Escudero, J. M.; Augé, J. M.; Filella, X.; Foj, L.; Torné, A.; Lejarcegui, J.; Pahisa, J. HE4 a Novel Tumour Marker for Ovarian Cancer: Comparison with CA 125 and ROMA Algorithm in Patients with Gynaecological Diseases. *Tumor Biol.* **2011**, 1–9.

(48) Chang, X.; Ye, X.; Dong, L.; Cheng, H.; Cheng, Y.; Zhu, L.; Liao, Q.; Zhao, Y.; Tian, L.; Fu, T.; *et al.* Human Epididymis Protein 4 (HE4) as a Serum Tumor Biomarker in Patients with Ovarian Carcinoma. *Int. J. Gynecol. Cancer* **2011**, *21*, 852–858.

(49) Wang, S.; Zhao, X.; Khimji, I.; Akbas, R.; Qiu, W.; Edwards, D.; Cramer, D. W.; Ye, B.; Demirci, U. Integration of Cell Phone Imaging with Microchip ELISA to Detect Ovarian Cancer HE4 Biomarker in Urine at the Point-of-Care. *Lab Chip* **2011**, *11*, 3411–3418.

(50) Tucker, S.; Robinson, R.; Keane, C.; Boff, M.; Zenko, M.; Batish, S.; Street, K. W. Colorimetric Determination of pH. *J. Chem. Educ.* **1989**, *66*, 769–771.

(51) Chareonsirisuthigul, T.; Khositnithikul, R.; Intaramat, A.; Inkomlue, R.; Sriwanichrak, K.; Piromsontikorn, S.; Kitiwanwanich, S.; Lowhnoo, T.; Yingyong, W.; Chaiprasert, A.; *et al.* Performance Comparison of Immunodiffusion, Enzyme-Linked Immunosorbent Assay, Immunochromatography and Hemagglutination for Serodiagnosis of Human Pythiosis. *Diagn. Microbiol. Infect. Dis.* **2013**, *76*, 42–45.

(52) Taton, T. A.; Mirkin, C. A.; Letsinger, R. L. Scanometric DNA Array Detection with Nanoparticle Probes. *Science* **2000**, *289*, 1757–1760.

(53) Danscher, G.; Nørgaard, J. O.; Baatrup, E. Autometallography: Tissue Metals Demonstrated by a Silver Enhancement Kit. *Histochemistry* **1987**, *86*, 465–469.

(54) Christensen, M. M.; Danscher, G.; Ellermann-Eriksen, S.; Schionning, J. D.; Rungby, J. Autometallographic Silver-Enhancement of Colloidal Gold Particles

Used to Label Phagocytic Cells. *Histochemistry* **1992**, *97*, 207–211.

(55) Gupta, S.; Huda, S.; Kilpatrick, P. K.; Velev, O. D. Characterization and Optimization of Gold Immunoassays. *Anal. Chem.* **2007**, *79*, 3810–3820.

(56) Yang, M.; Wang, C. Label-Free Immunosensor Based on Gold Nanoparticle Silver Enhancement. *Anal. Biochem.* **2009**, *385*, 128–131.

(57) Ma, S.; Tang, Y.; Liu, J.; Wu, J. Visible Paper Chip Immunoassay for Rapid Determination of Bacteria in Water Distribution System. *Talanta* **2014**, *120*, 135–140.

(58) Shi, X.; Wen, J.; Li, Y.; Zheng, Y.; Zhou, J.; Li, X.; Yu, H.-Z. DNA Molecular Beacon-Based Plastic Biochip: A Versatile and Sensitive Scanometric Detection Platform. *ACS Appl. Mater. Interfaces* **2014**, *6*, 21788–21797.

(59) Lee, J. S.; Mirkin, C. A. Chip-Based Scanometric Detection of Mercuric Ion Using DNA-Functionalized Gold Nanoparticles. *Anal. Chem.* **2008**, *80*, 6805–6808.

(60) Kim, D.; Daniel, W. L.; Mirkin, C. A. A Microarray-Based Multiplexed Scanometric Immunoassay for Protein Cancer Markers Using Gold Nanoparticle Probes. **2009**, *81*, 1–3.

(61) Komatireddy, R.; Topol, E. J. Medicine Unplugged: The Future of Laboratory Medicine. *Clin. Chem.* **2012**, *58*, 1644–1647.

(62) Vaher, M.; Borissova, M.; Seiman, A.; Aid, T.; Kolde, H.; Kazarjan, J.; Kaljurand, M. Automatic Spot Preparation and Image Processing of Paper Microzone-Based Assays for Analysis of Bioactive Compounds in Plant Extracts. *Food Chem.* **2014**, *143*, 465–471.

(63) Cai, L.; Wang, Y.; Wu, Y.; Xu, C.; Zhong, M.; Lai, H.; Huang, J. Fabrication of a

Microfluidic Paper-Based Analytical Device by Silanization of Filter Cellulose Using a Paper Mask for Glucose Assay. *Analyst* **2014**, *139*, 4593–4598.

(64) Tseng, D.; Mudanyali, O.; Oztoprak, C.; Isikman, S. O.; Sencan, I.; Yaglidere, O.; Ozcan, A. Lensfree Microscopy on a Cellphone. *Lab Chip* **2010**, *10*, 1787–1792.

(65) Delaney, J. L.; Hogan, C. F.; Tian, J.; Shen, W. Electrogenerated Chemiluminescence Detection in Paper-Based Microfluidic Sensors. *Anal. Chem.* **2011**, *83*, 1300–1306.

(66) Li, Y.; Ou, L. M. L.; Yu, H.-Z. Digitized Molecular Diagnostics: Reading Disk-Based Bioassays with Standard Computer Drives. *Anal. Chem.* **2008**, *80*, 8216–8223.

(67) Gupta, S.; Andresen, H.; Stevens, M. M. Single-Step Kinase Inhibitor Screening Using a Peptide-Modified Gold Nanoparticle Platform. *Chem. Commun.* **2011**, *47*, 2249–2251.

(68) Wang, H.; Ou, L. M. L.; Suo, Y.; Yu, H.-Z. Computer-Readable DNAzyme Assay on Disc for Ppb-Level Lead Detection. *Anal. Chem.* **2011**, *83*, 1557–1563.

(69) Wen, J.; Shi, X.; He, Y.; Zhou, J.; Li, Y. Novel Plastic Biochips for Colorimetric Detection of Biomolecules. *Anal. Bioanal. Chem.* **2012**, *404*, 1935–1944.

(70) Guesdon, J.; Ternynck, T.; Avrameas, S. The Use of Avidin-Biotin Interaction in Immunoenzymatic Techniques. *J. Histochem. Cytochem.* **1979**, *27*, 1131–1139.

(71) Wilchek, M.; Bayer, E. A.; Livnah, O. Essentials of Biorecognition: The (strept)avidin-Biotin System as a Model for Protein-Protein and Protein-Ligand Interaction. *Immunol. Lett.* **2006**, *103*, 27–32.

(72) Laitinen, O. H.; Marttila, A. T.; Airenne, K. J.; Kulik, T.; Livnah, O.; Bayer, E. A.;

Wilchek, M.; Kulomaa, M. S. Biotin Induces Tetramerization of a Recombinant Monomeric Avidin. A Model for Protein-Protein Interactions. *J. Biol. Chem.* **2001**, *276*, 8219–8224.

(73) Guo, S.; Ray, C.; Kirkpatrick, A.; Lad, N.; Akhremitchev, B. B. Effects of Multiple-Bond Ruptures on Kinetic Parameters Extracted from Force Spectroscopy Measurements: Revisiting Biotin-Streptavidin Interactions. *Biophys. J.* **2008**, *95*, 3964–3976.

(74) Jones, D. *Biomedical Sensors*; Momentum Press, 2010.

(75) Prasad, P. V; Chaube, S. K.; Shrivastav, T. G.; Kumari, G. L. Development of Colorimetric Enzyme-Linked Immunosorbent Assay for Human Chorionic Gonadotropin. *J. Immunoassay Immunochem.* **2006**, *27*, 15–30.

(76) Kristensen, G. B. B.; Sandberg, S. Self-Monitoring of Blood Glucose with a Focus on Analytical Quality: An Overview. *Clin. Chem. Lab. Med.* **2010**, *48*, 963–972.

(77) You, D. J.; Park, T. S.; Yoon, J. Y. Cell-Phone-Based Measurement of TSH Using Mie Scatter Optimized Lateral Flow Assays. *Biosens. Bioelectron.* **2013**, *40*, 180–185.

(78) Gupta, R.; Reifenberger, R. G.; Kulkarni, G. U. Cellphone Camera Imaging of a Periodically Patterned Chip as a Potential Method for Point-of-Care Diagnostics. *ACS Appl. Mater. Interfaces* **2014**, *6*, 3923–3929.

(79) Wang, H.; Li, Y. J.; Wei, J. F.; Xu, J. R.; Wang, Y. H.; Zheng, G. X. Paper-Based Three-Dimensional Microfluidic Device for Monitoring of Heavy Metals with a Camera Cell Phone. *Anal. Bioanal. Chem.* **2014**, *406*, 2799–2807.

(80) Liu, L.; Liu, J. Biomedical Sensor Technologies on the Platform of Mobile Phones. *Front. Mech. Eng.* **2011**, *6*, 160–175.

(81) Lifesaver https://life-saver.org.uk/#/GET_THE_APP (accessed Jun 20, 2004).

(82) Nam, J.-M.; Thaxton, C. S.; Mirkin, C. A. Nanoparticle-Based Bio-Bar Codes for the Ultrasensitive Detection of Proteins. *Science* **2003**, *301*, 1884–1886.

(83) Thaxton, C. S.; Elghanian, R.; Thomas, A. D.; Stoeva, S. I.; Lee, J.-S.; Smith, N. D.; Schaeffer, A. J.; Klocker, H.; Horninger, W.; Bartsch, G.; *et al.* Nanoparticle-Based Bio-Barcode Assay Redefines "Undetectable" PSA and Biochemical Recurrence after Radical Prostatectomy. *Proc. Natl. Acad. Sci. U. S. A.* **2009**, *106*, 18437–18442.

(84) Kim, E.-Y.; Stanton, J.; Korber, B. T.; Krebs, K.; Bogdan, D.; Kuntsman, K.; Wu, S.; Phair, J. P.; Mirkin, C. A.; Wolinsky, S. M. Detection of HIV-1 p24 Gag in Plasma by a Nanoparticle-Based Bio-Barcode Amplification Method. *Nanomedicine* **2008**, *3*, 293–303.

(85) Georganopoulou, D. G.; Chang, L.; Nam, J.-M.; Thaxton, C. S.; Mufson, E. J.; Klein, W. L.; Mirkin, C. A. Nanoparticle-Based Detection in Cerebral Spinal Fluid of a Soluble Pathogenic Biomarker for Alzheimer's Disease. *Proc. Natl. Acad. Sci. U. S. A.* **2005**, *102*, 2273–2276.

(86) Ding, C.; Zhang, Q.; Zhang, S. An Electrochemical Immunoassay for Protein Based on Bio Bar Code Method. *Biosens. Bioelectron.* **2009**, *24*, 2434–2440.

(87) Zhu, D.; Zhou, X.; Xing, D. Ultrasensitive Aptamer-Based Bio Bar Code Immunomagnetic Separation and Electrochemiluminescence Method for the Detection of Protein. *Anal. Chim. Acta* **2012**, *725*, 39–43.

(88) XZing Project http://zxing.org/w/decode.jspx (accessed Apr 1, 2016).

(89) Braunstein, G. D.; Rasor, J.; Adler, D.; Danzer, H.; Wade, M. E. Serum Human Chorionic Gonadotropin Levels Throughout Normal Pregnancy. *Am. J. Obstet.*

Gynecol. **1976**, *126*, 678–681.

(90) Bogart, M. H.; Pandian, M. R.; Jones, O. W. Abnormal Maternal Serum Chorionic Gonadotropin Levels in Pregnancies with Fetal Chromosome Abnormalities. *Prenat. Diagn.* **1987**, *7*, 623–630.

(91) Wald, N. J.; Cuckle, H. S.; Densem, J. W.; Nanchahal, K.; Royston, P.; Chard, T.; Haddow, J. E.; Knight, G. J.; Palomaki, G. E.; Canick, J. A. Maternal Serum Screening for Down's Syndrome in Early Pregnancy. *Bmj* **1988**, *297*, 883–887.

(92) Wolf, G. C.; Byrn, F. W.; McConnell, T. S.; Khazaeli, M. B. Amniotic Fluid Levels of Human Chorionic Gonadotropin and Its Alpha and Beta Subunits in Second-Trimester Chromosomally Abnormal Pregnancies. **1992**, *12*, 93–101.

(93) Cole, L. A.; Khanlian, S. A. The Need for a Quantitative Urine hCG Assay. *Clin. Biochem.* **2009**, *42*, 676–683.

(94) Cole, L. A. The Utility of Six over-the-Counter (home) Pregnancy Tests. *Clin. Chem. Lab. Med.* **2011**, *49*, 1317–1322.

(95) Cole, L. A.; Sutton-Riley, J. M.; Khanlian, S. A.; Borkovskaya, M.; Rayburn, B. B.; Rayburn, W. F. Sensitivity of over-the-Counter Pregnancy Tests: Comparison of Utility and Marketing Messages. *J. Am. Pharm. Assoc.* **2005**, *45*, 608–615.

(96) Pierce, J. G.; Parsons, T. F. Glycoprotein Hormones: Structure and Function. *Annu. Rev. Biochem.* **1981**, *50*, 465–495.

(97) Dugoff, L.; Hobbins, J. C.; Malone, F. D.; Vidaver, J.; Sullivan, L.; Canick, J. A.; Lambert-Messerlian, G. M.; Porter, T. F.; Luthy, D. A.; Comstock, C. H.; *et al.* Quad Screen as a Predictor of Adverse Pregnancy Outcome. *Obstet. Gynecol.* **2005**, *106*, 260–267 8p.

(98) An, S.-A.; Kim, J.; Kim, O.-J.; Kim, J. K.; Kim, N.-K.; Song, J.; Oh, S.-H. Limited Clinical Value of Multiple Blood Markers in the Diagnosis of Ischemic Stroke. *Clin. Biochem.* **2013**, *46*, 710–715.

(99) Yang, H.; Xia, B. Q.; Jiang, B.; Wang, G.; Yang, Y. P.; Chen, H.; Li, B. S.; Xu, A. G.; Huang, Y. B.; Wang, X. Y. Diagnostic Value of Stool DNA Testing for Multiple Markers of Colorectal Cancer and Advanced Adenoma: A Meta-Analysis. *Can. J. Gastroenterol.* **2013**, *27*, 467–475.

(100) Wong, J. X. H.; Liu, F. S. F.; Yu, H.-Z. Mobile App-Based Quantitative Scanometric Analysis. *Anal. Chem.* **2014**, *86*, 11966–11971.

(101) Li, X.; Weng, S.; Ge, B.; Yao, Z.; Yu, H.-Z. DVD Technology-Based Molecular Diagnosis Platform: Quantitative Pregnancy Test on a Disc. *Lab Chip* **2014**, *14*, 1686–1694.

(102) Zhang, Y.; Sun, J.; Zou, Y.; Chen, W.; Zhang, W.; Xi, J. J.; Jiang, X. Barcoded Microchips for Biomolecular Assays. *Anal. Chem.* **2015**, *87*, 900–906.

Appendix.

Smartphone-readable barcode assay for the detection and quantitation of pesticide residues

In collaboration with Juan Guo in Dr. Xiaochun Li's lab at Taiyuan Institute of Technology in Shanxi, China, this work was performed, demonstrating a test for pesticide residues using the same working principle as Chapter 3. Guo designed the chip assembly method and performed all of the experiments, while I performed the data analysis, prepared the manuscript and several figures, as well as made revisions to the manuscript before the work was published. This appendix is therefore reproduced with permission of The Royal Society of Chemistry from

Guo, J.;† Wong, J. X. H.;† Cui, C.; Li, X.; Yu, H.-Z. *Analyst* **2015**, *140*, 5518-5525. (†co-first authors)

Abstract

In this paper, we present a smartphone-readable barcode assay for the qualitative detection of methylparathion residues, a toxic organophosphorus pesticide that is popularly used in agriculture worldwide. The detection principle is based on the irreversible inhibition of the enzymatic activity of acetylcholinesterase (AchE) by methyl parathion; AchE catalytically hydrolyzes acetylthiocholine iodine to thiocholine that in turn dissociates dithiobis-nitrobenzoate to produce a yellow product (deprotonated thio-nitrobenzoate). The yellow intensity of the product was confirmed to be inversely dependent on the concentrationof the pesticide. We have designed a barcode-formatted assay chip by using a PDMS (polydimethylsiloxane) channel plate (as the reaction reservoir), situated under a printed partial barcode, to complete the whole barcode such that it can be directly read by a barcode scanning app installed on a smartphone. The app is able to qualitatively present the result of the pesticide test; the absence or a low concentration of methyl parathion results in the barcode reading as "−", identifying the test as negative for pesticides. Upon obtaining a positive result (the app reads a "+" character), the captured image can be further analyzed to quantitate the methyl parathion concentration in the sample. Besides the portability and simplicity, this mobile-app based colorimetric barcode assay compares favorably with the standard spectrophotometric method.

1. Introduction

Methyl parathion is an organophosphorus pesticide (OP) largely used in agriculture and fish hatcheries, and is toxic for both vertebrates and invertebrates by the inhibition of the acetylcholinesterase enzyme in nerve tissue.[1] As with most other pesticides, traditional methods for detecting methyl parathion include gas chromatography (GC) with electron

capture, nitrogen-phosphorus, or flame photometric detection, and more recently, coupled with mass spectrometry (MS),[2-3] high performance liquid chromatography (HPLC-MS),[2,4-5] and capillary electrophoresis (CE-MS).[6] As of their high accuracy and sensitivity, these traditional methods are most suitable for centralized laboratory settings, but less effective for rapid, on-site tests, especially in resource-limited situations. Meanwhile, the abuse of pesticide is an increasingly serious problem around the world; therefore, cost-effective, easily operated pesticide detection assays are highly desirable. Among many newly developed protocols, enzyme inhibition-based colorimetric determination of OPs has been the most successful and has attracted significant attention since Ellman et al. first reported the colorimetric determination of acetylcholinesterase (AChE) activity in 1961.[7-9]

Due to the powerful imaging function of the modern smartphone cameras, mobile phone-based colorimetric detection and quantitation has attracted increasingly greater attention.[10-20] For example, Intaravanne et al. developed a method to analyze and estimate the ripeness of bananas by imaging the fruit under both white and UV lights; the red-green ratio (from their respective color channels) of the white light image is compared to the blue-green fluorescence of the UV image to produce a two-dimensional ripeness concept.[10] Meanwhile, Sumriddetchkajorn et al. presented a method to quantitate the chlorine concentration in water simply by imaging the sample and a reference together; the color intensities from the red, green, and blue channels of the sample are averaged relative to the reference image in order to correlate the chlorine concentration to the color ratio.[11] One major limitation to mobile phone-based imaging methods, as in the above, is the influence of lighting conditions on the observed color intensities. To combat this (as well as other limitations, e.g., sample positioning while capturing the image), researchers have turned to the use of external accessories or mobile-based software (applications or apps) to analyze and correct the image).[12-20] Erickson and co-workers have developed innovative smartphone accessories (for use with test strips) for testing vitamin D ,[16] cholesterol,[17] and biomarkers in sweat or saliva.[18] In each case, the test strip is inserted into the accessory and imaged by the phone's camera under controlled lighting by using either the flash or an LED embedded in the accessory. The color intensity was analyzed using custom apps and used to quantitate the target.[16-18] Independently, Ozcan and coworkers have expanded from simple colorimetric reactions (e.g., using an allergy test kit for peanuts)[12] to the development of accessories that are compatible with fluorescence detection (albumin in urine) and blood cell density measurements.[14,19] These tests also use mobile apps to analyze the samples that are solution-based, contained in test tubes, cuvettes, or microplate wells.[12,14,19] Hong and Chang reported a different approach to smartphone-based colorimetry; a correction algorithm was employed with their app to account for variations in lighting, particularly in indoor, outdoor, and low lighting conditions. The app was applicable to paper-based multi-purpose urine test strips as it is programmed to auto-detect the background and test regions.[15]

Here, we demonstrate a colorimetric barcode assay that can be used with free apps for the detection and quantitation of pesticide residues without any modifications to either the mobile device or app coding. The colorimetric reaction utilizes the reaction of thiol with 5,5'-dithio-bis-2-nitrobenzoate) (DTNB, Ellman's reagent) to produce 2-nitro-5-thiobenzoate (TNB), which has a distinct yellow color. In the absence of pesticides,

acetylcholinesterase catalyzes the hydrolysis of acetylthiocholine, yielding thiocholine which then reacts with DTNB; pesticides however, inhibit the enzyme, prohibiting the production of the thiol and thus resulting in a colorless (or less colored) solution. The barcode assay presented herein is based on the patterning of the assay strips in the style of a common barcode.[21] The absence or presence of the target pesticide will result in the changing of the data encoded on the barcode, as read by a standard barcode scanning app, and as such, provides qualitative information on the test. Quantification of the assay can be subsequently performed using Adobe Photoshop or ImageJ software. The colorimetric reaction was first confirmed by spectrophotometric methods and then adapted to the barcode assay protocol.

2 Results and Discussion

2.1 Detection principle and spectrophotometric analysis.

As mentioned above, the colorimetric barcode assay for the detection of organophosphorus pesticides (methyl parathion) was based on the irreversible inhibition of the activity of acetylcholinesterase (AChE, the enzyme) on the hydrolysis of acetylthiocholine iodide (ATCh, the substrate)[7-9] (Scheme S1).The intermediate (thiocholine) then reacts with DTNB (dithio-bis-nitrobenzoate, a chromogenic reagent) to generate TNB (thionitrobenzoate) which has a strong absorbance peak centered at 412 nm with a high extinction coefficient (14,150 M^{-1} cm^{-1}) in dilute buffer solutions.[22]

We firstly studied the UV-vis absorbance spectroscopic characteristics of the above reaction in the absence and presence of methyl parathion, respectively, over an extended period of reaction time. Fig. 1a shows the obtained spectra of the reaction in the absence of methyl parathion. From the spectra, two peaks are observed; the absorbance at 320 nm that corresponds to the maximum absorption by DTNB decreases with increasing time, while the peak at 412 nm increases.[23] The absorbance band at 412 nm corresponds TNB and reflects its production during the reaction;[7] increased concentrations of TNB results in an increased, higher yellow intensity of the solution. After 50 min, this peak becomes stable, indicating the completion of the reaction. In the presence of 4 μg/mL methyl parathion (Fig. 1b), no significant changes can be observed to the position and overall trend of the two peaks over reaction time. However, the time needed to reach the completion is prolonged to upwards of >70 min, indicating that methyl parathion has significant inhibitory effect on the reaction. For the purpose of quantitation, we further evaluate the influence of the methyl parathion concentration on the reaction by monitoring the 412 nm absorption peak (Fig. 1c). The absorbance at 412 nm at all concentrations of methyl parathion increases with time and eventually reaches saturation, however, as the concentration increases, the reaction rate apparently decreases. In the early stages (within the first 20 min), the absorbance at 412 nm almost linearly increases over time; and the absorbance decreases with increasing the pesticide concentration. The relationship between the absorbance (at 15 min) and the methyl parathion concentration is presented in Fig. 1d; clearly the absorbance monotonically decreases in the concentration range from 0 to 5 μg/mL. This result confirms the inhibition of AChE activity by methyl parathion, and provides a measure for the

quantitation of methyl parathion in the unknown samples by determining either the absorbance or the yellow color intensity (*vide infra*).

2.2 Design and testing smartphone-readable barcode assay for methyl parathion.

Barcodes are commonly used for product identification, and the U.P.C. (Universal Product Code) is one of the many types of linear barcodes (E.A.N. 8 or 13, and Code39, to name a few). Each different type has its own set of rules for encoding characters, and there are many free apps are available for reading the different types of linear barcodes (Fig. 2a). In Code 39, the coding system chosen here, the barcode consists of wide and narrow bars in solid colors (typically black) and white spaces, and the ratio of the wide bar/space to the narrow one can be set as 1.5:1, 2:1 or 3:1. Each Code 39 barcode consists of three sections: the start, data, and stop characters, where the start and stop character is always the same as a "*" character. This character is used to instruct the scanner in which direction the barcode should be read. For the data characters, each consists of 5 bars and 4 spaces; three of these elements are wide and the other six are narrow. The reason for choosing Code 39 as the format to be used, as opposed to the other available types, was because it was found that two characters in this system have "correlated" barcodes (Fig. 2b).The data characters for "-" and "+"are identical in the first section of the data code, differing only in the section highlighted by the red dash lines. This allows a detection system to be designed such that upon the presence or absence of a target analyte, there will be a colorimetric conversion of the barcode (e.g., from "+" to "–", or *vice versa*) by simply changing the narrow space to narrow bar. To make the barcode readable, all identical elements of the two barcodes are printed on paper, leaving the two bars responsible for the barcode conversion to be "filled" with the reaction solution (Scheme 2). The barcode can be therefore divided into reference and detection regions (Fig. 3a).

As the principle of decoding a barcode is based on the different reflectance between the spaces and bars, and for the common barcode the reading result is secure because of this unequivocal contrast between the black bar and white space. However, for the methyl parathion barcode assay, the final reaction solution is yellow, and the yellow intensity decreases with increasing the concentration of methyl parathion. When the yellow intensity decreases to a particular value, the reflectance difference between the "yellow bar" and white space might be too small to be differentiated by the barcode scanner. Therefore, it is essential to determine the minimum yellow intensity of the bars for the barcode-formatted assay in order to be read by the mobile apps.

For this purpose, we designed a barcode for the"+" character in Code 39 where the bars of the code were yellow using the CMYK color mode (by setting the values of C, M, and K to 0%), while the Y intensity was varied from 20% to 100%, in both the background and detection areas (Fig. 3b). The barcode was then printed on white paper using an inkjet printer. The scanning results of the barcode when the bars of the background and detection area have different yellow intensities (as shown in Fig. 3b) have four possibilities ("+", "–", "+/–", and "×"). The "+" and "–" results indicate the QuickMark barcode app were able to read these characters.[24] When the yellow intensity of the

detection region is low (< 40 %), the barcode reads as “+”; upon increasing the yellow intensity of the detection area (> 60%), the scanning results changes from “+” to “–”. A“×” symbol in Fig. 3b denotes that the barcode scanning app was unable to read the barcode because the bars of either the detection or background areas were too light (low contrast between the white paper and yellow ink printing) to be recognized by the scanner. A “+/–” in the table means the scanning result is not reliable as both “+” and “–” results can be obtained upon repeated reading; this was particularly true for the yellow intensity between 40% and 60%.

The effects of the light source and the imaging mode on the colorimetric analysis was subsequently studied by printing the yellow barcode, of which the bars were set to CMYK values of 0% for C, M, and K, while Y was set at 50% . The yellow intensity was then experimentally measured from the pictures taken under different illumination using two imaging modes available on the smartphone: the camera and screen capture functions. Fig. 4a shows the images taken under a light (1549 lux) by a smartphone using the camera and screen capture function, both with and without flash. Comparing the images, it can be observed that without the additional lighting from the flash, the resulting images appeared dark; the image obtained by the screen capture method with flash has the lowest background darkness (highest white intensity), followed next by the camera photo with flash .The yellow intensity in the region-of-interest (ROI) was then determined from each of these images by using the histogram tool in Adobe Photoshop. As shown in Fig. 4b, all of the Y values in images are found to be higher than the preset yellow intensity of 50%; the Y values of the pictures taken by the screen capture with flash is closest to the preset values, and appears to be relatively constant, despite the different lighting conditions. A camera picture taken under flash also results in a stable Y values, however, the resulted values are substantially larger than the preset data. With the camera function, the image is stored in a JPEG format, which reduces the quality of the original image.[25] Conversely, when saving an image using the screen capture function on a smartphone running Android system, the image is stored in a PNG format, a lossless image compression method. While the resulting file would be greater in size, the lossless compression has no effect on the colors in the image, thereby maintaining the image quality. It should be noted that in the aforementioned experiments (Fig. 3 and Fig. 4) for testing the barcode assay principle, both the background and detection regions are printed on paper with yellow ink; no colorimetric reactions were involved.

With the validated barcode scanning principle and preferred imaging method, we then fabricated and carried out the methyl parathion assay in the barcode format. For these assays, the yellow intensity of the background area was set at 50%. Standards were prepared as described in the Experimental section and scanned using the QuickMark app. Fig. 5a shows an image of the app scanning the 4.0 µg/mL methyl parathion assay using the barcode format and the scanning result “+”. A series of concentrations of methyl parathion solutions was tested in this manner and the results presented. As shown in Fig. 5b, in scanning the barcodes, at low concentrations of methyl parathion (00.1 µg/mL) that have high Y values (≥60%), the detection region of the barcode appears as a wide bar, resulting in the app reading the assay as the negative result “-”. At higher concentrations of methyl parathion (≥ 0.5 µg/mL), the Y value became low (<50%), thus the detection region appears as a single narrow bar and the app scans as “+”, i.e., a positive result was reported. It is evident that the threshold value to produce a

positive result, which indeed reads as a "+" character, was in between 0.2 to 0.5 μg/mL. Beyond the qualitative aspect of the barcode assay, we further determined the yellow intensity of the samples based on the screen capture image to quantitate the pesticide concentration in standard or unknown samples. The yellow intensities determined in Fig. 2b were found to decrease monotonically with increasing methyl parathion concentrations (up to a concentration of 4.0 μg/mL), based on which a non-linear calibration curve can be constructed.

To validate the barcode assay approach, we have directly compared with the standard spectrophotometry method. Fig. 5c depicts the color intensity as a function of the absorbance for each of the standard solutions tested; the linear relationship ($R^2 = 0.966$), with the exception of the blank, illustrates the direct correlation between color intensity and absorbance. This result not only confirms the accuracy of the colorimetric protocol but also constitute the validated calibration curve (Fig. 2b) for the analysis of unknown samples (*vide infra*).

2.3 Real-world sample testing and comparison with traditional methods.

To evaluate this method for the detection of OP residues in food products, apple samples were sprayed with different concentrations (0, 20, 60, and 100 μg/mL) of methyl parathion. The methyl parathion was extracted and the amount on the apple peels was quantitated by both the barcode assay and spectroscopic methods for a direct comparison. For the samples sprayed with methyl parathion (20-100 μg/mL), the barcode scanning app all produced positive responses (i.e., "+" characters were shown on the smartphone). As the tested concentrations are much lower than that employed in the real-world application (15 to 25 g in 100 L of water, equivalent to 15-25 mg/mL),[26] the above experiment demonstrates the merits and sensitivity of the barcode assay approach. As shown in Fig. 6, the quantification of the three concentrations of methyl parathion pesticide residues and the blank colorimetrically correlates well with the spectroscopically determined results. Although the extraction process has not been optimized and may not be sufficient, it is noted that the residual amount of pesticide detected shows a clear increase proportional to the amount of methyl parathion sprayed onto the apple samples.

In addition to the spectrophotometry method which we have compared with, the traditional methods of methyl parathion detection by the WHO include gas chromatography (GC) are high performance liquid chromatography (HPLC).[26] These chromatographic techniques no doubts provide great sensitivity and selectivity, however they require sophisticated sample preparation and advanced instrumentation.[2-6] The method developed herein is more suitable for on-site detection due to its simple procedure and low cost. Particularly, the initial screening capability demonstrated above (Fig. 5b) provides either a positive or negative confirmation with a regular smartphone and a free app. Without further optimization, a detection limit of 0.2 μg/mL (~200 ppb, also as the threshold value for qualitative detection) was achieved with this smartphone-compatible colorimetric assay, meeting the requirements of the FAO and WHO.[27] The low cost, sufficient sensitivity and ease of use allow the adaption of this colorimetric

method for point-of-collection screening, where traditional analytical instrumentation is not readily accessible.

3 Conclusions

In this study, a simple and low-cost colorimetric assay method based on smartphone app and digital image analysis was demonstrated for the rapid detection of methyl parathion. In the presence of the pesticide residues, the enzyme-catalyzed colorimetric reaction is inhibited, resulting in decreasing yellow intensities. An assay was designed to take advantage of this principle; qualitative analysis of the assay was accomplished using a free app by stylizing the assay in a barcode pattern encoded with two characters that indicate the presence or absence of organophosphorus residues. The yellow color intensity from images captured using the smartphone was found to be inversely proportional to the concentration of methyl parathion, consistent with the traditional spectroscopic method. The barcode assay method offers a unique approach to increase the availability and accessibility of screening testing, especially in remote locations that lack of advanced instrumentation and laboratory facilities.

4 Experimental

4.1 Reagents and apparatus.

A pesticide rapid detection kit was purchased from Nuoya Wei Biotechnology Co., Ltd. (Shijiazhuang, China), which includes the substrate (acetylthiocholine iodide, ATCh), the hydrolytic catalyst (acetylcholinesterase, AChE), the chromogenic reagent (dithiobis-nitrobenzoate, DTNB), and phosphate buffer (pH = 8.0, used to elute methyl parathion residues in fruits and vegetables). Methyl parathion (100 μg/mL in acetone) was purchased from the National Standard Substance Information Center (China). Transparent polycarbonate (PC) with 0.1 mm thickness was purchased from Rijia Paste Product Co., Ltd.(Dongguan, China). Sylgard 184 silicone elastomer (PDMS) was purchased from Dow Corning (Midland, MI).

A Xiaomi2 smartphone was used to scan the barcode assay and utilizes a 1.5 GHz quad-core (Qualcomm Adreno320) processor and an 8 MP color camera with a built-in lens that has a F/2.0 aperture and focal length of 27 mm. UV-Vis absorption spectra were obtained on a UV-3100 spectrophotometer (Mapada Ltd., China).

4.2 Fabrication and reading of barcode assay chip.

A traditional one dimensional barcode consists of a series of bars and spaces with different widths, arranged in a particular pattern according to certain encoding rules. The barcode used in this study is based on the Code 39 encoded “+” and “-” characters. As shown in Scheme 2 and Fig. 3, the “+” barcode was printed on paper in yellow ink and two areas, noted as the detection region was cut out. The detection chip consists of a PDMS channel plate placed between the cover and base PC plates. The channels on

the PDMS plate were cut so that they directly corresponded to the detection region as noted in Fig. 3 and, were used to hold the reaction solution. The PC plates were treated in an UV/ozone cleaner for 20 min to improve the surface hydrophilicity; all plates were then pieced together to form a seal, thereby preventing solution leakage. The barcode was completed by aligning the printed barcode directly above the PDMS channels.

The methyl parathion barcode-formatted assay was scanned using a free barcode scanning app, QuickMark;[24] the barcode is scanned and the result is automatically shown. The image of the working area and the result can be captured by the phone's screen capture function with or without the flash enabled which saved as a PNG format. The flash acts as a stable light source for imaging the barcode with the app. The image is then transferred to a system running Adobe Photoshop CS6 to analyze the image by reading the color (yellow intensity) information within the detection area. The average yellow intensity and the associated uncertainties in each detection region were obtained from at least three replicate measurements.

4.3 Sample preparation.

Fresh apples were purchased from the local supermarket and were washed with ultrapure water. The apples were prepared according to a previously published method, with some modifications.[28] Apples were cut into four pieces. A different concentration of methyl parathion (20, 60, 100 µg/mL) was sprayed onto the skin of three pieces using a sprayer, while the forth piece was used as a control sample. After 3-hour air drying at room temperature, each piece was peeled using a fruit peeler, and then the peel was further cut into smaller pieces; a total of 5 g of apple peel was added to 10 mL of phosphate buffer. The mixture was shaken fiercely by a stirrer for 3 min and centrifuged for 5 min at 10,000 rpm. The supernatant was collected from this mixture as the extracted solution for subsequent pesticides detection.

Standard solutions of methyl parathion (200 µL of different concentrations, ranging from 0-6 µg/mL) or the extracted solutions were prepared in centrifuge tubes, followed with the addition of 10 µL each of the chromogenic reagent and the enzyme (acetylcholinesterase). The mixture was incubated at 37 °C for 30 min before 10 µL of the substrate (acetylthiocholine iodide) was added, mixed well, and injected into the PDMS microchannels or cuvettes for colorimetric and spectroscopic analysis, respectively.

References

[1] D. Silva, C. M. Cortez, J. Cunha-Bastos and S. R. W. Louro, *Toxicol. Lett.*, 2004, **147**, 53–61.

[2] L. Alder, K. Greulich, G. Kempe, and B. Vieth, *Mass Spectrom. Rev.*, 2006, **25**, 838–865.

[3] P. Pugliese, J. C. Molto, P. Damiani, R. Marin, L. Cossignani and J. Manes, J. Chromatogr. A., 2004, **1050**, 185–191.

[4] J. S. Aulakh, A. K. Malik, V. Kaur and P. Schmitt-Kopplin, *Anal. Chem.*, 2005, **35**, 71–85.

[5] L. D. Betowski and T. L. Jones, *Environ. Sci. Technol*., 1988, **22***,* 1430–1434.

[6] L. M. Ravelo-Perez, J. Hernández-Borges and M. A. Rodriguez-Delgado, *J. Sep. Sci*., 2006, **29***,* 2557–2577.

[7] G. L. Ellman, K. D. Courtney, V. Andres and R. M. Featherstone, *Biochem. Pharmacol*., 1961, **7**, 88–95.

[8] C. S. Pundir and N. Chauhan, *Anal. Biochem*., 2012, **429**, 19–31.

[9] S. Andreescu, S. Avramescu, C. Bala, V. Magearu and J. L. Marty, *Anal. Bioanal. Chem*., 2002, **374**, 39–45.

[10] Y. Intaravanne, S. Sumriddetchkajorn and J. Nukeaw, *Sens. Actuators B*, 2013, **168**, 390–394.

[11] S. Sumriddetchkajorn, K. Chaitavon and Y. Intaravanne, *Sens Actuators B*, 2013, **182**, 592–597.

[12] A. F. Coskun, J. Wong, D. Khodadadi, R. Nagi, A. Tey and A. Ozcan, *Lab Chip*, 2013, **13**, 636–630.

[13] M. Mancuso, E. Cesarman and D. Erickson, *Lab Chip*, 2014, **14**, 3809–3816.

[14] H. Zhu, I. Sencan, J. Wong, S. Dimitrov, D. Tseng, K. Nagashima and A. Ozcan, *Lab Chip*, 2013, **13**, 1282–1288.

[15] J. I. Hong and B.-Y. Chang, *Lab Chip*, 2014, **14**, 1725–1732.

[16] S. Lee, V. Oncescu, M. Mancuso, S. Mehta and D. Erickson, *Lab Chip*, 2014, **14**, 1437–1442.

[17] V. Oncescu, M. Mancuso and D. Erickson, *Lab Chip*, 2014, **14**, 759–763.

[18] V. Oncescu, D. O'Dell and D. Erickson, *Lab Chip*, 2013, **13**, 3232–3238.

[19] A. F. Coskun, R. Nagi, K. Sadeghi, S. Phillips and A. Ozcan, *Lab Chip*, 2013, **13**, 4231–4238.

[20] S. Sumriddetchkajorn, K. Chaitavon, and Y. Intaravanne, *Sens. Actuators B*., 2014, **191**, 561–566.

[21] Y. Zhang, J. Sun, Y. Zou, W. Chen, W. Zhang, J. J. Xi and X. Y. Jiang, *Anal. Chem*., 2015, **87**, 900–906.

[22] P. W. Riddles, R.L. Blakeley and B. Zerner, *Methods Enzymol.*, 1983, **91**, 49–60.

[23] T. L. Kirley, L. K. Lane and E. T. Wallick, *J. Biol. Chem*., 1986, **261**, 4525–4528.

[24] QuickMark QR Code Reader – Barcode Scanner. http://www.quickmark.com.tw/ (accessed April 22, 2015).

[25] R. N. J. Graham, R. W. Perriss and A. F. Scarsbrook, *Clin. Radiol*., 2005, **60**, 1133–1140.

[26] IPCS International programme on chemical safety: methyl parathion health and safety guide, http://www.inchem.org/documents/hsg/hsg/hsg75_e.htm (accessed April 22, 2015).

[27] CODEX Online pesticide details for parathion-methyl, http://www.codexalimentarius.net / pestres/data/pesticides/details.html?id=59 (accessed April 22, 2015)

[28] E. Cieslik, A. Sadowska-Rociek, J. M. M. Ruiz and M. Surma-Zadora, *Food Chem*., 2011, **125**, 773–778.

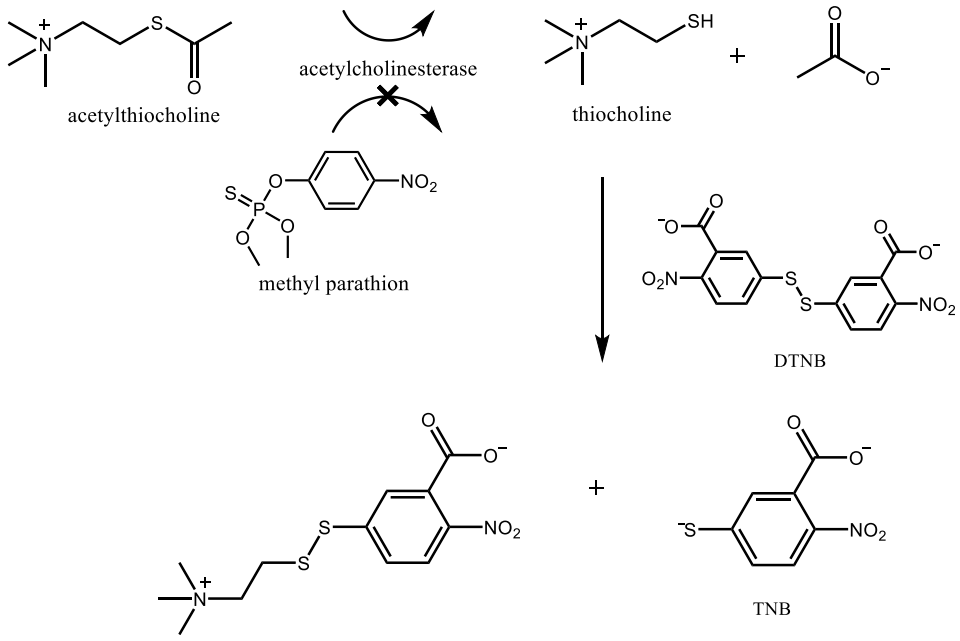

Scheme 1. Detection of methyl parathion based on the irreversible inhibition of the activity of acetylchlinesterase (AchE). AchE catalytically hydrolyzes acetylthiocholine iodide (ATCh) in phosphate buffer (pH = 8.0) to thiocholine that in turn dissociates dithio-bisnitrobenzoate (DTNB) to produce a yellow colored product (TNB).

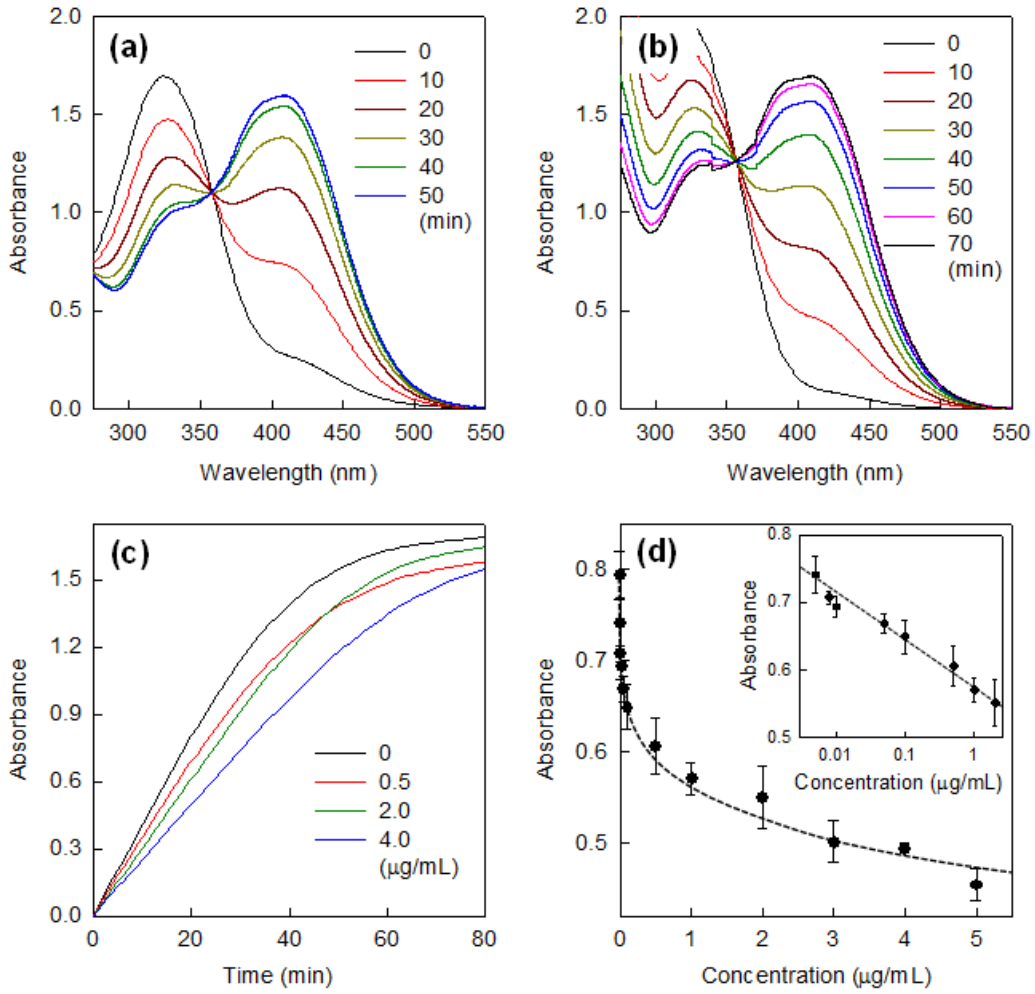

Fig. 1. UV-vis spectra of the colorimetric detection solution (a mixture of chromogenic reagent, substrate, and enzyme) in the absence (a) and presence (b) of 4.0 μg/mL methyl parathion. (c) The absorbance of the peak at 412 nm for different concentrations of methyl parathion solutions are plotted as a function of time; (d) The absorbance at 15 min of reaction time, as a function of methyl parathion concentration. The inset shows the data at lower concentrations, i.e., from 5.0 ng/mL to 2.0 μg/mL. The dashed lines in (d) are trend-lines, meant as guides for the eyes only.

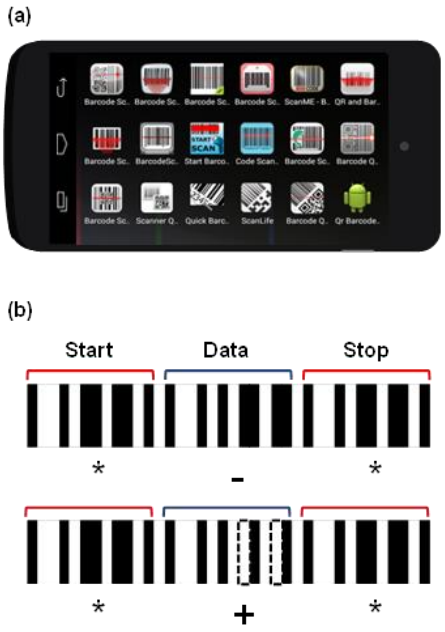

Fig. 2. Barcode scanning apps and barcodes. (a) A set of free barcode scanning apps available for the Android system. (b) Barcodes of the "–" and "+" characters in Code 39. The start and stop character is denoted by "*". The two data characters are other identical, except for the region highlighted by the dashed lines.

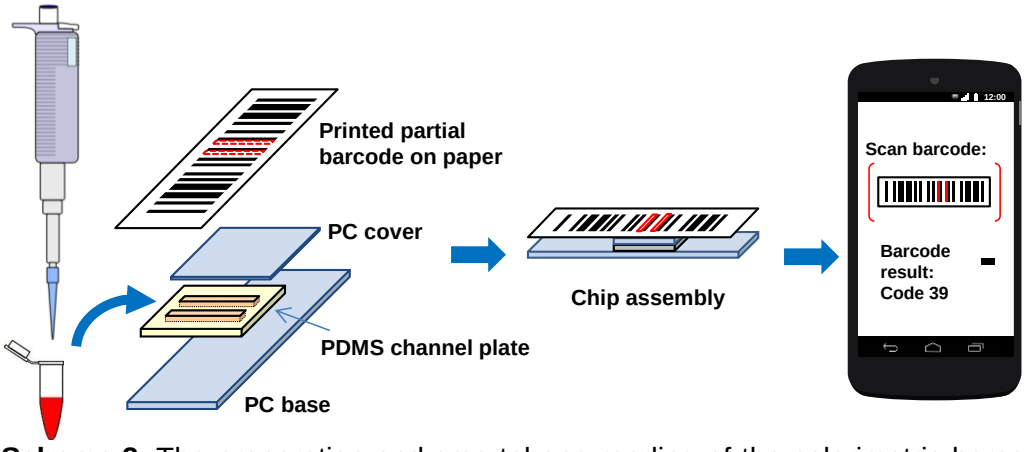

Scheme 2. The preparation and smartphone reading of the colorimetric barcode assay. Solutions are prepared in a micro-centrifuge tube and transferred to a PDMS channel plate attached to a polycarbonate (PC) base. The PDMS chip with two cut-out windows (highlighted in light orange color) is sealed with a second PC plate (the cover) and the paper-printed barcode is positioned above the PDMS channels. The assembled device can then be scanned by a barcode scanner.

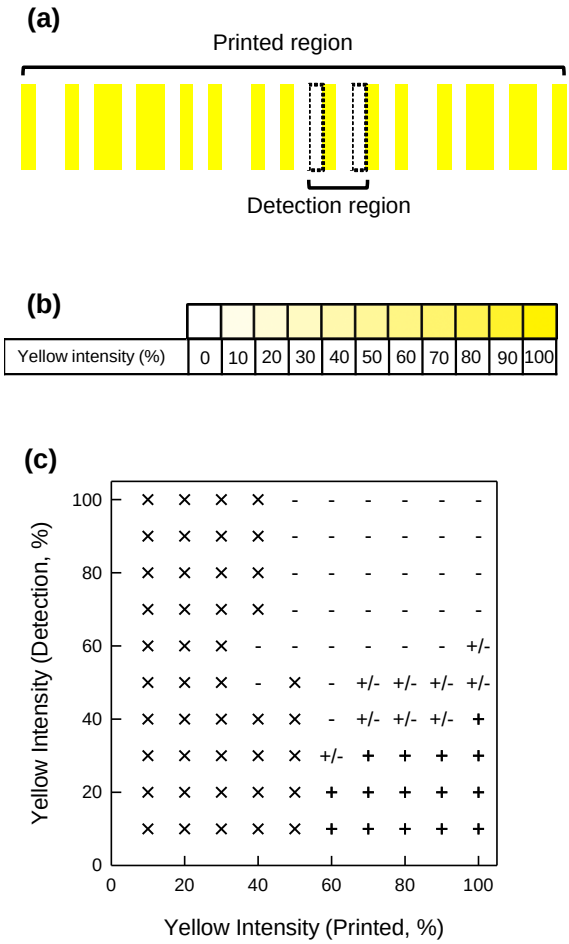

Fig. 3. Design of the barcode assay for methyl parathion detection. There are two distinct regions in the barcode: the printed and detection regions. The printed area is encodes the entire "+" barcode, while the detection area consists of two bars, that when printed or contains a yellow solution, is encoded to read the "–" barcode. (b) Different yellow intensities in the printed and background regions used to determine the scanning ability. (c) Barcodes designed at different yellow intensities of the detection and printed regions. "×" indicates the app could not scan the barcode; "+" and "–" means the app read these particular characters; "+/–" means both characters appear upon repeated reading.

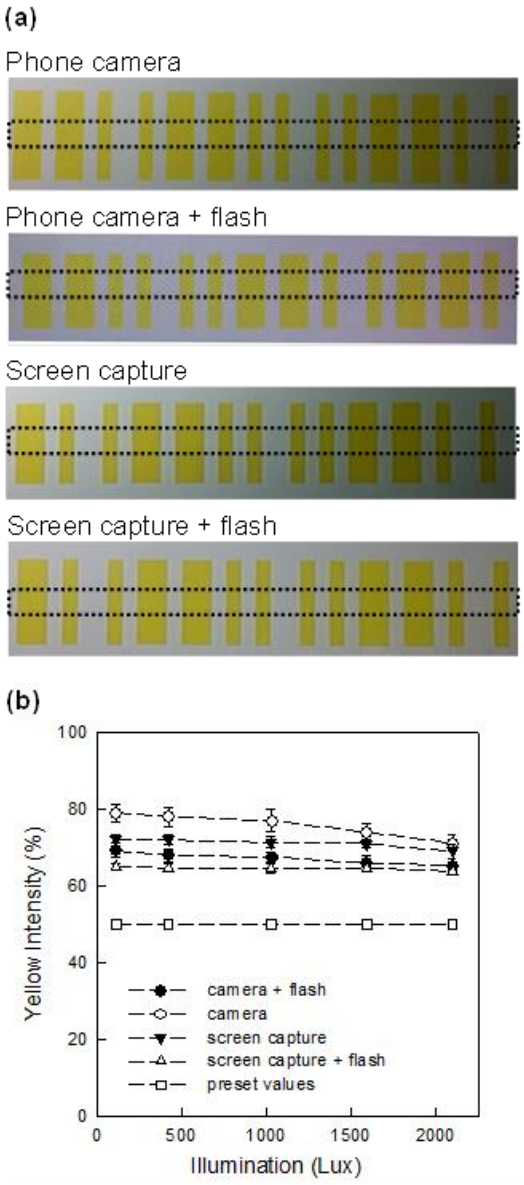

Fig. 4. Comparison of images obtained from a smartphone in different image mode. (a) Images saved from the phone by taking a picture with the camera or screen capture functions, both in the presence and absence of flash under a light (1549 Lux). (b) Relationship between the yellow intensity of the images in the region-of-interest (ROI, dashed lines) with the illumination (based on images shown in (a)).

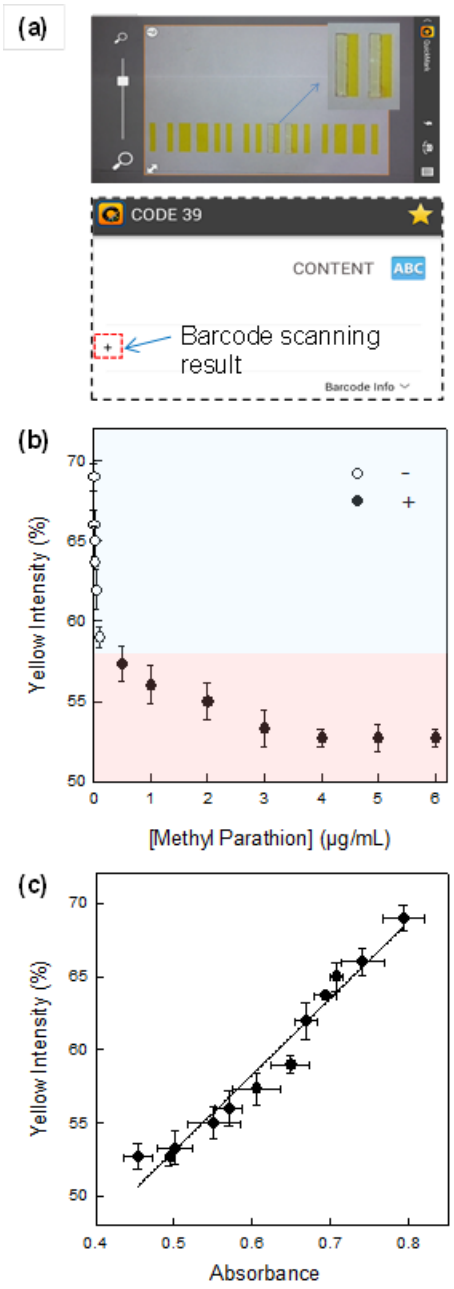

Fig. 5. Methyl parathion assay using the smartphone-readable barcode method. (a) Screen captured images of the app scanning the barcode and a cropped image of the scanning result; top left inset: enlarged image of the detection area with 4 µg/mL methyl parathion solution. (b) The analyzed yellow intensity as a function of the methyl parathion concentration; "+" (highlighted in light red) and "–" (highlighted in light blue) indicates these characters were scanned at these Y values and concentrations. (c) Correlation between the yellow intensity and the absorbance for the set of standards.

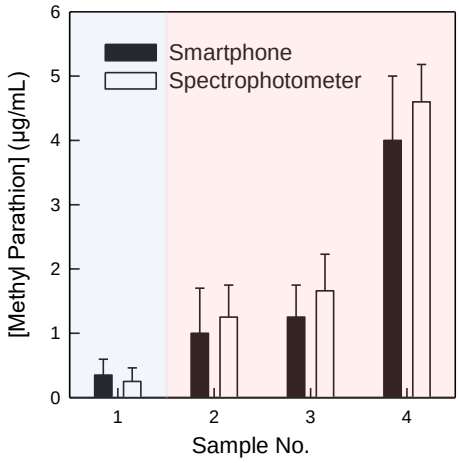

Fig. 6. Comparison of spectrophotometric and colorimetric methods for the detection of methyl parathion pesticide residues extracted from apples. Samples 1-4 represent apples sprayed with 0, 20, 60, and 100 µg/mL of methyl parathion, respectively. The light red region indicates the app scanned as "+", while the region in light blue indicates the app scanned as "–".